8-2018

Uncertainty Quantification and Sensitivity Analysis of Multiphysics Environments for Application in Pressurized Water Reactor Design

Cole David Blakely
Utah State University

UNCERTAINTY QUANTIFICATION AND SENSITIVITY ANALYSIS OF MULTIPHYSICS ENVIRONMENTS FOR APPLICATION IN PRESSURIZED WATER REACTOR DESIGN

by

Cole David Blakely

A dissertation submitted in partial fulfillment
of the requirements for the degree

of

DOCTOR OF PHILOSOPHY

in

Mechanical Engineering

Approved:

Heng Ban, Ph.D. Major Professor	Hongbin Zhang, Ph.D. Committee Member
Robert Spall, Ph.D. Committee Member	Tadd Truscott, Ph.D. Committee Member
Michael Johnson, Ph.D. Committee Member	Richard S. Inouye, Ph.D. School of Graduate Studies

UTAH STATE UNIVERSITY
Logan, Utah

2018

ABSTRACT

Uncertainty Quantification and Sensitivity Analysis of Multiphysics Environments for Application in Pressurized Water Reactor Design

by

Cole David Blakely, Doctor of Philosophy

Utah State University, 2018

Major Professor: Heng Ban, Ph.D.
Department: Mechanical and Aerospace Engineering

In order to aid in the development of new emerging technologies for pressurized water reactors (PWR) within the U.S nuclear fleet, the LOCA Toolkit for US light water reactors (LOTUS) is being developed at Idaho National Laboratory (INL). LOTUS allows for an integration of a variety of codes spanning the nuclear design disciplines of of neutronics, system analysis, and fuel performance. LOTUS is able to produce large random samplings from said integrations, which allows post processing tools to perform uncertainty quantification (UQ) and sensitivity analysis (SA) for specific outputs .

This work includes the first known integration of VERA-CS developed by CASL with the PNWL code FRAPCON for a quasi-steady state, three fuel cycle depletion case. SA results showed linear and consistent behavior for the minimum departure from nucleate boiling point ratio, linear but time dependent results for maximum fuel centerline temperature, and nonlinear, temporally dependent interactions for the gap conductance at peak power (GCPP). In the case of GCPP, new insights were gained through the use of higher order variance and density based SA measures. This work also contains the first known SA of a VERA-CS and BISON integration using higher order methods. SA results were

comparable to the VERA-CS and FRAPCON integration, with slight differences in specific calculation biases (i.e. fission gas release biasing).

Lastly, a loss of coolant accident failure scenario was investigated with an integration of the neutronics code PHISICS and system analysis code RELAP5-3D, both developed at INL, with FRAPCON. This work was unique in its use of the integration to perform a Wilks' based UQ on the ratios of equivalent cladding reacted (ECR) and peak cladding temperature (PCT) to their corresponding cladding hydrogen content based limits. These metrics are only obtainable through a union of a fuel performance code with a system analysis code, thus providing an example of the need for interdisciplinary, multiphysics calculations. The UQ revealed the PCT ratio to be relatively well behaved, with fresh fuel assemblies being of greatest concern. The ECR ratio behaved as a threshold variable, with once burned fuel assemblies being the most limiting.

(190 pages)

PUBLIC ABSTRACT

Uncertainty Quantification and Sensitivity Analysis of Multiphysics Environments for Application in
Pressurized Water Reactor Design
Cole David Blakely

The most common design among U.S. nuclear power plants is the pressurized water reactor (PWR). The three primary design disciplines of these plants are system analysis (which includes thermal hydraulics), neutronics, and fuel performance. The nuclear industry has developed a variety of codes over the course of forty years, each with an emphasis within a specific discipline. Perhaps the greatest difficulty in mathematically modeling a nuclear reactor, is choosing which specific phenomena need to be modeled, and to what detail.

A multiphysics computational environment provides a means of advancing simulations of nuclear plants. Put simply, users are able to combine various physical models which have commonly been treated as separate in the past. The focus of this work is a specific multiphysics environment currently under development at Idaho National Labs known as the LOCA Toolkit for US light water reactors (LOTUS).

The ability of LOTUS to use uncertainty quantification (UQ) and sensitivity analysis(SA) tools within a multihphysics environment allow for a number of unique analyses which to the best of our knowledge, have yet to be performed. These include the first known integration of the neutronics and thermal hydraulic code VERA-CS currently under development by CASL, with the well established fuel performance code FRAPCON by PNWL. The integration was used to model a fuel depletion case.

The outputs of interest for this integration were the minimum departure from nucleate boiling ratio (MDNBR) (a thermal hydraulic parameter indicating how close a heat flux is to causing a dangerous form of boiling in which an insulating layer of coolant vapour is

formed),the maximum fuel centerline temperature (MFCT) of the uranium rod, and the gap conductance at peak power (GCPP). GCPP refers to the thermal conductance of the gas filled gap between fuel and cladding at the axial location with the highest local power generation.

UQ and SA were performed on MDNBR, MFCT, and GCPP at a variety of times throughout the fuel depletion. Results showed the MDNBR to behave linearly and consistently throughout the depletion, with the most impactful input uncertainties being coolant outlet pressure and inlet temperature as well as core power. MFCT also behaves linearly, but with a shift in SA measures. Initially MFCT is sensitive to fuel thermal conductivity and gap dimensions. However, later in the fuel cycle, nearly all uncertainty stems from fuel thermal conductivity, with minor contributions coming from core power and initial fuel density. GCPP uncertainty exhibits nonlinear, time-dependent behaviour which requires higher order SA measures to properly analyse. GCPP begins with a dependence on gap dimensions, but in later states, shifts to a dependence on the biases of a variety of specific calculation such as fuel swelling and cladding creep and oxidation.

LOTUS was also used to perform the first higher order SA of an integration of VERA-CS and the BISON fuel performance code currently under development at INL. The same problem and outputs were studied as the VERA-CS and FRAPCON integration. Results for MDNBR and MFCT were relatively consistent. GCPP results contained notable differences, specifically a large dependence on fuel and clad surface roughness in later states. However, this difference is due to the surface roughness not being perturbed in the first integration. SA of later states also showed an increased sensitivity to fission gas release coefficients.

Lastly a Loss of Coolant Accident was investigated with an integration of FRAPCON with the INL neutronics code PHISICS and system analysis code RELAP5-3D. The outputs of interest were ratios of the peak cladding temperatures (highest temperature encountered by cladding during LOCA) and equivalent cladding reacted (the percentage of cladding oxidized) to their cladding hydrogen content based limits. This work contains the first known UQ of these ratios within the aforementioned integration. Results showed the PCT

ratio to be relatively well behaved. The ECR ratio behaves as a threshold variable, which is to say it abruptly shifts to radically higher values under specific conditions. This threshold behaviour establishes the importance of performing UQ so as to see the full spectrum of possible values for an output of interest.

The SA capabilities of LOTUS provide a path foward for developers to increase code fidelity for specific outputs. Performing UQ within a multiphysics environment may provide improved estimates of safety metrics in nuclear reactors. These improved estimates may allow plants to operate at higher power, thereby increasing profits. Lastly, LOTUS will be of particular use in the development of newly proposed nuclear fuel designs.

I dedicate this work to my family. My loving and encouraging mother and father. My sisters who are always there for me. My new brother-in-law Sam and his family, for providing a home away from home. My awesome nephews Max and David. And as always, the gravitational singularity around which this work has revolved, Stefan Alexander.

ACKNOWLEDGMENTS

My journey to completing this dissertation was unconventional. As an undergrad, I never envisioned myself as a PhD someday. Indeed it is still surreal to be submitting this dissertation.

Thankfully I stuck around one sunny summer in Logan nearly five years ago. My plans that summer did not revolve around research, so it was a surprise when Dr. Byard Wood called me up with an amazing opportunity to work on fluid dynamics research. During that summer and the subsequent fall, I fell in love with research. Dr. Wood served as an incredible first mentor, built my confidence, and sent me on this path.

I then began work with Dr. Aaron Katz, who took me on as a PhD candidate. Dr. Katz gave me chance to work on an in house, higher order CFD code. I myself got to focus on making a combustion simulation come to life. Unfortunately, that time in my life coincided with some intense darkness. I will be forever grateful to Dr. Katz, Oisin Tong, and Dalon Work for their patience with me, and aid during that time.

My life took a radical turn again nearly two years ago when I checked my email. Dr. Katz announced that he was taking his life in a new direction, specifically south, towards Costa Rica. In my search for a new major professor I came to know Dr. Heng Ban. I have never gotten to know a professor who is more focused on the big picture then Dr. Ban. Within a week or two of talking with Dr. Ban, he offered me the opportunity to gut my research, and begin anew at Idaho National Labs.

This led me to my fourth mentor, Dr. Hongbin Zhang. Dr. Zhang had a monumental task ahead of him, teach me how to publish multiple journal and conference papers in a field I had started to study two months ago. It goes without saying, that without his guidance, patience, and friendship, this dissertation would not exist.

Along this journey my friends Anton, Ryan, Trevor, Ethan, and many others kept me happy and sane. I cannot put into words what my family has done for me, so I am not going to attempt to. Lastly, I am grateful to my God, I use no floury language when I state,

without His guidance, I would not be at Idaho National Labs submitting this dissertation.

Cole Blakely

CONTENTS

LIST OF TABLES

LIST OF FIGURES

ACRONYMS

BA	Burnable Absorber
BEPU	Best Estimate Plus Uncertainty
BOC	Beginning of Cycle
CASL	Consortium for Advanced Simulation of Light Water Reactors
CD-A	Core Design Automation
CD-O	Core Design Optimization
CFD	Computational Fluid Dynamic
CIPS	Crud Induced Power Shift
COBRA-TF	Coolant-Boiling in Rod Arrays-Two Fluids
ECCS	Emergency Core Coolant System
ECR	Equivalent Cladding Reacted
ECRR	Equivalent Cladding Reacted Ratio
EOC	End Of Cycle
FOM	Figure Of Merit
FP	Fuel Performance
GCPP	Gap Conductance at Peak Power
HPC	High Performance Computers
IFBA	Integral Fuel Burnable Absorber
INL	Idaho National Laboratory
LB-LOCA	Large Break Loss Of Coolant Accident
LOCA	Loss Of Coolant Accident
LOTUS	LOCA Toolkit for U.S. Light Water Reactors
MCNP	Monte Carlo N-Particle
MDNBR	Minimum Departure from Nucleate Boiling Ratio
MFCT	Maximum Fuel Centerline Temperature
MOOSE	Multiphysics Object Oriented Simulation Environment
MPACT	Michigan Parallel Characteristics Transport Code

MP-BEPU	Multiphysics Best Estimate Plus Uncertainty
NEAMS	Nuclear Energy Advanced Modeling and Simulation
NEM	Nodal Expansion Method
NFFSP	Neutron Fast Flux per Specific Power
NRC	Nuclear Regulatory Commission
OAT	One-at-A-Time
ORNL	Oak Ridge National Laboratory
PCT	Peak Cladding Temperature
PCTR	Peak Cladding Temperature Ratio
PDF	Probability Distribution Function
PHISICS	Parallel and Highly Innovative Simulation for the INL Code System
PPM	Parts Per Million
PWR	Pressurized Water Reactor
RA	Risk Assessment
RELAP	Reactor Excursion and Leak Analysis Program
RIA	Reactivity Insertion Accident
SA	Sensitivity Analysis
UQ	Uncertainty Quantification
VERA-CS	Virtual Environment for Reactor Analysis - Core Simulator
WPPM	Weighted Parts Per Million

CHAPTER 1

Introduction

The recent lowering of natural gas prices as well as the increasing presence of alterative energies necessitate improvements to the U.S. LWR fleet. Two purposed advancements are higher burnup fuel and accident tolerant fuel which would both increase safety while decreasing operation cost. Implementation of new technologies within LWR is facilitated through modeling. Two of the primary means of increasing predictive capability is through multiphysics and best estimate plus uncertainty (BEPU) methodology. A new multihpysics environment currently under development at INL, known as LOTUS, will combine these enhancements creating a mutlitphysics best estimate plus uncertainty (MP-BEPU) methodology. LOTUS will also include extensive sensitivity analysis (SA) capabilities, in the interests of determining the sources output uncertainties.

Special emphasis will be placed on including codes within LOTUS which allow for testing of technologies relating to accident tolerant fuel and higher burnup fuel. Furthermore, in calculating reactor safety margins, the USA Code of Federal Regulation (CFR) 10 CFR 50.46 permits either the conservative methodology presented in Appendix K of the CFR, Title 10, Part 50 or the BEPU methodology [1]. The latter may be improved further by performing UQ with a Monte Carlo sampling in a multiphysics environments. A conceptual representation of the potential gains of using LOTUS MP-BEPU in setting reactor safety margins is shown in Fig. 1.1. The increase in accuracy of LOTUS MP-BEPU has the potential to raise operational safety margins, thereby allowing for greater power generation for LWR plants.

1.1 Key Concepts

The key concepts of this work are Light Water Reactors (LWR) design, multiphysics environments, uncertainty quantification, and sensitivity analysis.

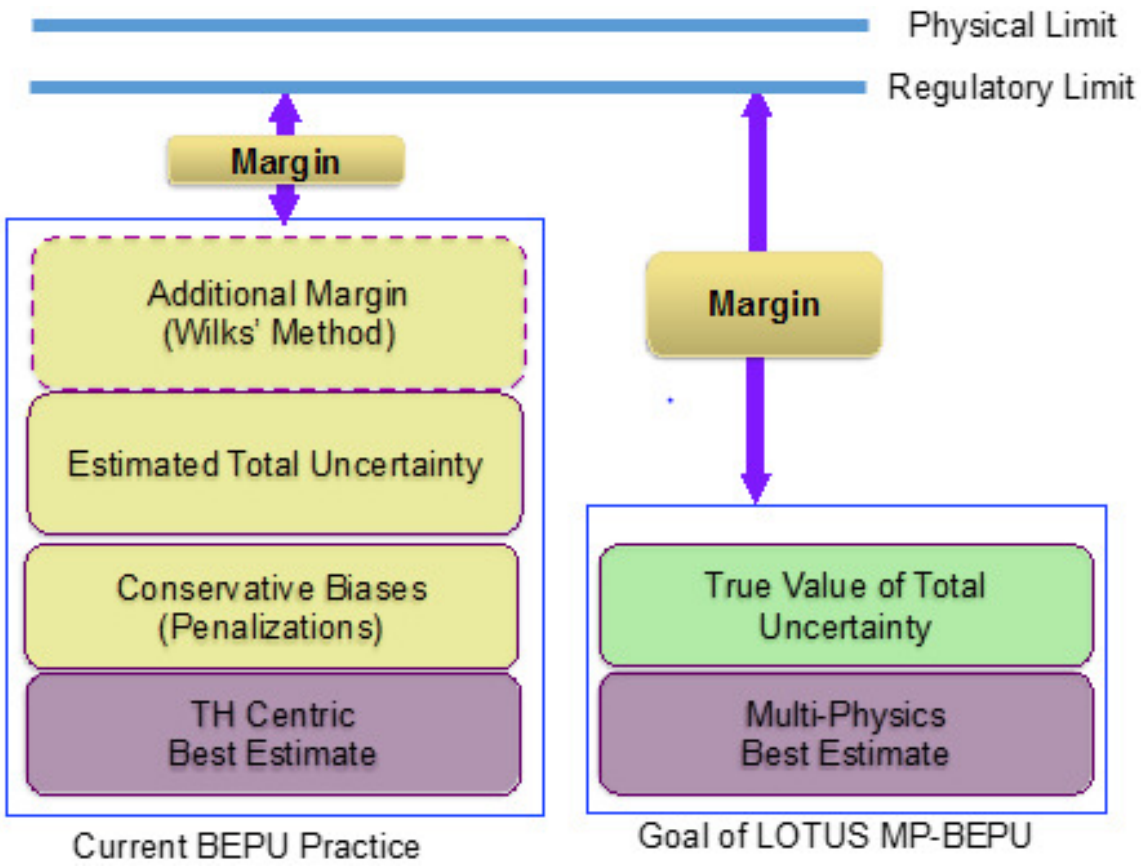

Fig. 1.1: Conceptual Representation of Potential Margin Reductions from LOTUS MP-BEPU over Traditional BEPU.

1.1.1 Light Water Reactor Design

A pressurized water reactor is the most common nuclear reactor design in the U.S. nuclear fleet and remains an active research topic for the purpose of sustainability within the national energy infrastructure. An PWR reactor core can be primitively described as an arrangement of nuclear fuel rods within flowing water. The water acts as both a coolant and moderator and is pressurized to prevent boiling despite temperatures in excess of 300°C under normal operating conditions. This configuration allows for significant heat generation due to fission. This heat is transferred primarily via convection to the coolant within the core. The heated coolant then deposits the gained energy into secondary coolant loops at lower pressure. Water within the secondary loop is converted to steam, which powers turbines, thereby supplying massive amounts of electrical power on the order of Gigawatts. Simulations of PWR are performed either under quasi-steady state operating conditions, or under transient failure scenarios such as loss of coolant accident (LOCA). Areas of study relevant to this process include System Analysis (SA), fuel performance (FP), and neutronics. System analysis (SA) focuses on the thermal hydraulics of the coolant system. Fuel performance (FP) analyzes the thermomechanics, irradiative effects, and fission gas release of the fuel rods themselves. Neutronics deals with the generation, absorption, and scattering of neutron fluxes within the reactor.

1.1.2 Multiphysics Environment

Due to the fact that attempting to model all of the interrelated physical phenomena within an LWR is unreasonable, development teams tend to focus on a particular discipline with simplifications of other models outside the field of study as needed. A large variety of codes are available within nuclear industry, each with a particular emphasis. This siloed approach to modeling has permitted numerous advancement within PWR simulations, however it can lead to inaccuracies when there is strong feedback between cross disciplinary phenomena, which unfortunately is often the case in nuclear reactors. A multiphysics environment allows for a coupling between multiple models. The subject of this work is the multiphysics environment known as the LOCA Toolkit for U.S. light water reactors (LO-

TUS) currently under development at Idaho National Labs (INL). A conceptual schematic of LOTUS is shown in Fig. 1.2.

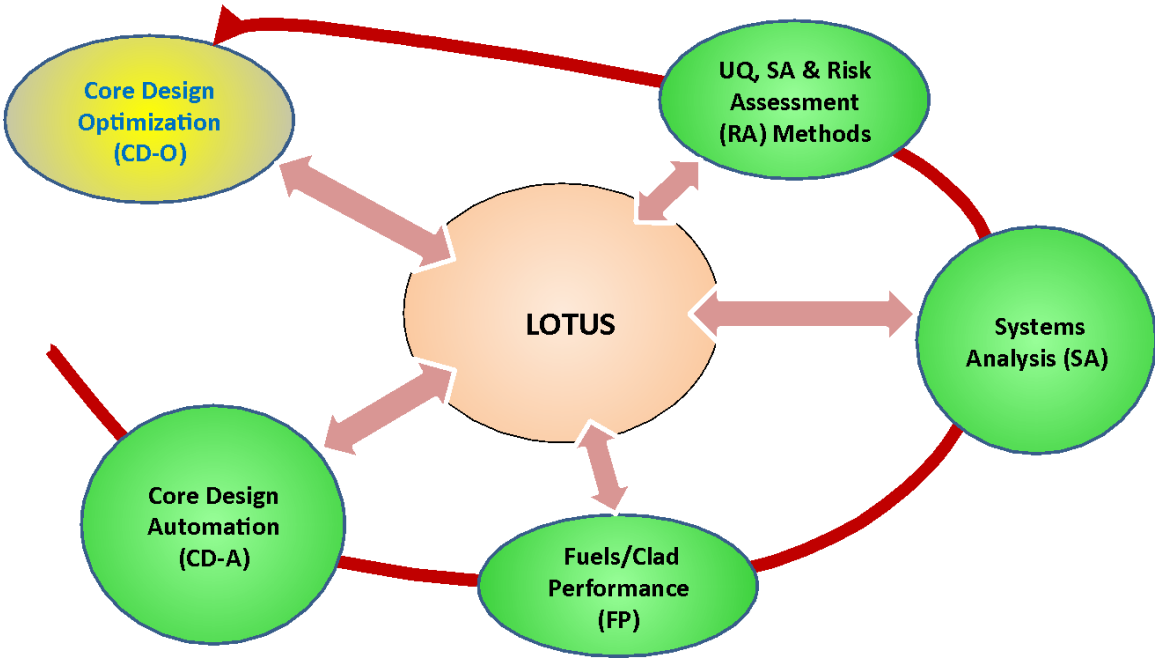

Fig. 1.2: Conceptual Schematic of LOTUS.

As it currently stands, LOTUS provides an interface between core design automation (CD-A) which focuses on neutronics, SA codes, and FP codes. LOTUS also contains uncertainty quantification (UQ) and Sensitivity Analysis (SA) (see sections 1.1.3 and 1.1.4) capabilities. Risk assessment (RA) and core design automation (CD-A) are to be implemented in the future.

1.1.3 Uncertainty Quantification

Decisions makers in the nuclear community must be privy to not only the estimates of mathematical models, but also their associated level of fidelity. For this reason, the Best Estimate Plus Uncertainty (BEPU) methodology has become the de facto industry standard within the nuclear community. As the name suggests, BEPU dictates that any reported calculation must also contain the corresponding uncertainty, a guideline similar to

standard procedure for physically measured values. The uncertainty of a numerical estimate is calculated via an uncertainty quantification (UQ) study.

UQ consists of perturbing the inputs of a code, executing the code for each perturbation, and analyzing the resulting sample of outputs. The most commonly reported metric is the 95/95 confidence interval, which is essentially a set of bounds that contain 95% of the population with 95% certainty. UQ calculations rely on output data alone, and thus do not elucidate the relations between input and output. Since it is not reasonable to perturb all inputs for most codes, UQ studies use a Phenomena Identification and Ranking Table (PIRT) comprised of all relevant inputs with their corresponding range.

1.1.4 Sensitivity Analysis

Sensitivity Analysis (SA) determines the sensitivity of an output to each of the relevant input uncertainties. SA studies can act as a sifting process to narrow a PIRT to include only inputs of signification contribution. Furthermore, SA may shed light on the characteristics of the input and output relation (i.e. linearity, coupled interactions between inputs). SA can serve as a method of verification in addition to being a guide for research and development in increasing model accuracy. If increased fidelity of a specific output is desired, then relatively benign inputs and associated phenomenon are of low importance, while impactful inputs and related models are high priority.

1.2 Literature Review

This literature review summarizes two broad topics: uncertainty quantification (UQ) and sensitivity analysis (SA) methods and past work, and multiphysics environments for PWR design.

1.2.1 Uncertainty Quantification and Sensitivity Analysis

No current mathematical models are a perfect representation of the reality they are designed to reflect. Therefore, code outputs should not be treated as absolutes but rather as estimations with quantifiable uncertainties. This is especially true in reactor safety design,

where large uncertainties are often encountered, and ascertaining conservative estimations in order to meet safety criteria is essential. Code uncertainties fall into two categories: input uncertainty and model uncertainty. Input uncertainties result from the inability to perfectly measure or predict values such as initial conditions, boundary conditions, and code parameters. Model uncertainties stem from the exclusion or simplification of physical phenomena (i.e. the Coriolis effect resulting from the earths rotation is justifiably ignored in thermal hydraulics), as well as numerical errors from round off errors and truncation error. This work addresses input uncertainty by perturbing the inputs across their known ranges, and model uncertainty by biasing specific calculations. It should be noted that perturbation of all inputs and calculations is not feasible for most codes, thus Phenomena Identification and Ranking Tables (PIRT) are formed which include the relevant inputs with their nominal values and corresponding uncertainties.

An uncertainty quantification (UQ) study analyzes the outputs of interest alone to determine the output confidence intervals. Sensitivity analysis (SA) elucidates the relation between inputs and output uncertainties, with a particular interest in determining the largest contributors to an uncertainty. Higher order SA measures may also aid in determining properties of said relations, such as additivity and linearity.

Past Uncertainty Quantification and Sensitivity Analysis Studies of Interest

Uncertainty quantification (UQ) studies within the nuclear community were initially performed on thermal hydraulic codes. Recent thermal hydraulic UQ of interest to this work include an inverse UQ study of the thermal hydraulic code TRACE by Wu *et al.* [2] and a sensitivity analysis by Marcum et at. [3] of RELAP5-3D [4] and the thermal hydraulic code VIPRE-01. Recently, UQ and SA studies have been expanded to fuel performance. Work by Bratton *et al.* [5] and particularly Ikonen *et al.* [6, 7] serve as a point of reference for the UQ/SA of FRAPCON [8] in this work. The BISON team [9] at Idaho National Labs (INL) has performed multiple UQ/SA studies on the code as a whole [10], as well as specific modules such as fission gas release [11]. Brown *et al.* performed UQ and SA studies on neutronics/thermal hydraulic code VERA-CS [12] for a two by two assembly [13], as well

as a Wilks based UQ study of a full core large break LB-LOCA [14]. Though less common, UQ/SA studies of multiphysics environments have been performed, such as LOCA analysis using the transient fuel performance code FRAPTRAN with the thermal hydraulic code GENFLO by Arkoma *et al.* [15, 16].

Uncertainty Quantification

The nuclear community uses two forms of Uncertainty Quantification: Wilks Non-Parametric Method and Monte Carlo 95/95 Confidence Intervals.

Wilks Non-Parametric Method

The ground work for the Wilks method was first presented by Wilks himself in 1941 [17]. The method finds the minimum sample size required in order to determine tolerance limits. In order to find estimate the 95th percentile of a single output, it helpful to first express the probability β that at least one instance of sample size N is above an upper limit below which portion γ of the population resides. This statement is expressed mathematically in 1.1,

$$\beta = 1 - \gamma^N \tag{1.1}$$

In order to obtain a 95/95 confidence interval, γ is set 0.95 after which the smallest integer of N is selected which yields $\beta \geq 0.95$. Setting N to 59 results in a 95.15% probability of that at least one instance of the sample resides above the 95th percentile of the population. Thus after running 59 cases, the largest instance of an output qualifies, albeit conservatively, as a one sided 95/95 confidence value.

The relatively low number of required runs makes the Wilks method of great utility when dealing with hardware constraints. Furthermore, the only assumption made when performing Wilks is a continuous output probability density function (PDF), which although not technically true due to floating point precision, is a very fair approximation.

Wilks can also be performed for two sided confidence intervals. Furthermore, the upper limits can be set with different ranks of the outputs. For instance by setting the

upper limit of the confidence interval as the fourth highest of a sample, a sample size of 153 is required [18]. It should be noted that Wilks is not limited to small sample sizes. As the sample size approaches infinity, the reported rank approaches $0.95 \cdot N$ [18], which mirrors the MC 95/95 confidence interval outlined in the following section.

Recently the Wilks method has been expanded to account for multiple output variables by Guba [19]. This is not to be misinterpreted as the 95th Percentile of an output being dependent on the measuring or analysis of another. Assuming two outputs are analysed for the sake of simplicity, the statement at the start of this section can be altered to expressing the probability β that a specific number of instances of sample fall outside a portion of the population defined by rectangular bounds. Given p outputs of interest, with the upper limit estimates as rank $N + 1 + j$ for each output (where rank N is the largest value, and j is the output index), the probability β is expressed in Eq. 1.2,

$$\beta = \sum_{j=0}^{N-p} \left(\begin{array}{c} N \\ j \end{array} \right) \gamma^j \left(1 - \gamma\right)^{N-j} \tag{1.2}$$

Thus for a sample size of 93, there is greater than 95% probability that the highest value of the first output, and second highest of the second output, bound at least 95% of the population. It is worth noting that in the interest of treating all outputs equal, some works such as that done Frepoli [20], use consistent ranking among the outputs (i.e. for two outputs, the highest outputs of the first and second outputs are treated as bounds). While more conservative, this method still bounds 95% of the population with *at least* than 95% confidence.

Monte Carlo 95/95 Confidence Intervals

Generating Monte Carlo 95/95 confidence intervals involves perturbing all relevant inputs simultaneously for a relatively large number of cases, executing the code, and then analyzing the outputs independent of the inputs. Monte Carlo runs are less conservative then Wilks method but require a larger sample, with most studies using at least 1000 runs. Determining 95/95 confidence intervals using Monte Carlo can be problematic as it assumes

the outputs follow a normal distribution, which is not always the case. However, Monte Carlo based UQ is preferable when sensitivity analysis (SA) is desired, as the data gathered for Monte Carlo UQ can be used for most SA methods, as opposed to Wilks where the typical sample size used is too limited to be used effectively for SA studies. The 95th percentile value is estimated as either a specific value within a sample which is greater than exactly 95% of the sample, or if the specific sample size does not permit, as the smallest value greater than at least 95th percent of the sample. The 95/95 confidence interval is given in Eq. 1.3,

$$Y_{95/95} = \mu_{95\%} \pm 1.96 \cdot SE_{Q95\%} \tag{1.3}$$

where $Y_{95/95}$ is the 95/95 confidence interval, $\mu_{95\%}$ is the 95th percentile value and $SE_{Q95\%}$ is the standard error of $\mu_{95\%}$ given by Eq. 1.4,

$$SE_{Q95\%} = 2.11 \cdot SE_M \tag{1.4}$$

Note that $SE_{Q95\%}$ is slightly more than twice the value of the standard error of the mean (SE_M). A derivation of Eq. 2.4 can be found in [21].

Sensitivity Analysis

Sensitivity Analysis helps to elucidate the relation between input and output uncertainty. SA methods can be used as a filtering process in determining the most impactful contributors from a list of potential candidates. All SA measures can be classified as either a one-at-a-time (OAT) method or global method.

One at a Time Methods

One-at-a-time (OAT) methods perturb each input individually while holding all others constant. This process is ideally repeated for all inputs within a PIRT table. Due to the simplicity of the method, it can be useful during development of codes, particularly for debugging. However, the method is inefficient in comparison to global methods. Furthermore, since the inputs are never concurrently perturbed, the method is unable to detect

interactions between inputs.

Global Methods

Global sensitivity methods perturb all or nearly all (depending on the sampling method) of the inputs simultaneously. This achieves far greater efficiency with high numbers of inputs, particularly for lower order global methods. This property is sometimes controversially referred to as the solution to higher dimensionality (i.e. large numbers of inputs). Although not a panacea for cases of high dimensionality, there is no argument about the increased numerical efficiency over OAT methods. Global SA measures are the preferred method for both the high degree of dimensionality and the often high computational expense of this work. This work utilizes the linear regression methods of Pearson and Spearman, the variance decomposition based Sobol Indices, and the Delta moment independent as well as second and infinity order moment independent measures.

Pearson Measures Coefficients

Pearson measures can be visualized as the degree of agreement of linear fit to a scatter plot. Calculations of Pearson measures are given by Eq. 1.5,

$$R_i^2 = \frac{cov\left(X_i, Y\right)^2}{var\left(X_i\right) var\left(Y\right)} \tag{1.5}$$

where R_i is the Pearson measure for a given input i, X_i and Y are the random variables of the given input and output respectively, and $cov()$ and $var()$ are the covariance and variance operators. If the output is a linear function of the codes inputs, then Pearson is ideal. Pearson is most commonly the preferred measure for SA studies in nuclear application. This is due to the fact that while the relations within codes are complex, the uncertainty within the inputs is typically relativity small, meaning that only a small section of the domain is tested. Fundamental mathematics dictates, that given a small enough domain, all continuous, differentiable functions reduce to linear relations exemplified by Eq. 1.6,

$$Y = a \cdot X_1 + b \cdot X_2 \tag{1.6}$$

where a and b are arbitrary constants. However, if input domains are sufficiently wide over a nonlinear function, Pearson measures will be unable to fully detect complex relations. Fortunately, the linearity of the function can be determined *a posteriori* by summing the squares of Pearson measures. A sum in proximity to unity indicates strong linearity and thus high fidelity in the method. Conversely, sums not near unity indicate nonlinearity and the need for higher order methods.

Spearman Correlation Coefficients

Spearman is an extension of Pearson measures. To calculate Spearman measures, the Pearson measures for the ranks of the inputs and outputs methods are calculated, as shown in Eq. 1.7,

$$\rho_i^2 = \frac{cov\left(X_i^{rnk}, Y^{rnk}\right)^2}{var\left(X_i^{rnk}\right) var\left(Y^{rnk}\right)} \tag{1.7}$$

where ρ_i is the Pearson measure for input , X_i^{rnk} and Y^{rnk} are the ranks of the input i and the output respectively. Spearman coefficients are known to be superior in detecting nonlinear monotonic trends over Pearson. Due to their ability to fit into the same framework as Pearson, reporting of the measures together is common in literature. Similar to Pearson, summation of the squares of Spearman measures indicates the linearity of the ranks.

Sobol Variance Decomposition

Sobol variance decomposition is a higher order method used to determine the fraction of the output variance attributable to a specific input or set of inputs. The total variance of an output can be expressed as a finite sum of output variances conditional upon specific inputs being fixed. The Sobol indices are a ratio of specific elements of said summations to the total variance. First order Sobol indices are a function of variances conditional upon a single input being fixed, as expressed in Eq. 1.8,

$$S_i = \frac{var\left(E\left(Y|X_i\right)\right)}{var\left(Y\right)} \tag{1.8}$$

where S_i is the first order Sobol index of input i, $Y|X_i$ indicates Y conditional upon

a fixed value for X_i, and $E()$ is the expected value operator. Second order Sobol indices involve variances with two inputs fixed. Second order indices are less commonly used and represent the interaction of a pair of inputs on an output. Total effects indices represent the sum of all terms in the infinite summation which include a specific input. Total effects indices are often used but require a specific partitioning structure that currently differs from the sampling methods in this work.

The first order Sobol indices are the preferred measure of this work. All usages of Sobol indices (S_i) hereafter are in reference to first order indices. S_i is essentially the ratio of the variance of Y attributable to X_i alone to the total variance of Y. Ideally, this measure is computed through an expensive double Monte Carlo Loop, however Plischke [22] partitioning (shown in Eq. 1.9) provides an alternative means whereby the S_i can be estimated with traditional Monte Carlo sampling.

$$\hat{S}_i = \frac{\frac{1}{N}\sum_{j=1}^{M} N_j var\left(Y|X_i \in x_{i,j}\right)}{var\left(Y\right)} \tag{1.9}$$

where $\hat{S}_i$ is the numerical approximation of S_i, M is the number of partitions, N_j is the number of instances in partition j, and $Y|X_i \in x_{i,j}$ indicates the instances of Y which have corresponding inputs X_i residing in the group $x_{i,j}$. The group $x_{i,j}$ is formed by ranking all instances of an input X_i, and then partitioning the ranked sample into roughly equal sized groups. The number of groups is selected based on the total sample size according to the procedure documented in the python SA library SALib [23]. It should be noted that the partitioning process results in added noise to the Sobol indices, thus larger sample sizes are required as compared to lower order methods.

Sobol indices are ideal for additive relations such as that shown in Eq. 1.10,

$$Y = f\left(X_1\right) + g\left(X_2\right) \tag{1.10}$$

where f and g are arbitrary functions which may be nonlinear. The ability to detect nonlinear functions is an advantage over low order methods. However, due to S_i being

independent of the higher order terms of the variance decomposition, the measures are unable to detect coupled interactions (i.e. $Y = X_1 X_2$). Fortunately, the additivity of the problem can also be determined *a posteriori* by summing all S_i measures. A sum of unity indicates additivity, and thus fidelity in the measures, while values far from unity indicate the need for methods capable of detecting coupled interactions. Linearity can be further established by testing if $S_i = R_i^2$ for all inputs.

Moment Independent Measures

Moment independent measures were recently introduced by Borgonovo [24]. The measures are independent of both the variance and mean of a probability distribution, also known as the first and second moments. This is advantageous as complex relations have the potential to change the distribution of an output probability density function (PDF) without altering the moments (i.e. a shift in a PDF has no effect on variance). Moment Independent measures are calculated as the expected value of the integration of the difference between a conditional and unconditional density as shown in Eq. 1.11,

$$\delta_i = \frac{1}{2} E\left(s_i\left(X_i\right)\right) \tag{1.11}$$

where $s_i\left(X_i\right)$ represents the shift in output PDF upon fixing an input, given by Eq. 1.12,

$$s_i\left(x_i\right) = \int \left| f_Y\left(y\right) - f_{Y|X_i=x_i}\left(y\right) \right| dy \tag{1.12}$$

where $f_Y\left(y\right)$ and $f_{Y|X_i=x_i}$ are the unconditional output PDF and the output PDF conditional upon X_i being equal to a specific value x_i. Essentially any shift in density from fixing X_i will be detected through the integration in Eq. 1.12. If Y is a function of a single X_i, then $f_{Y|X_i=x_i}$ collapses to a Dirac delta function which will result in $s_i\left(x_i\right) \equiv 2$. Thus, the Delta measures for input i is taken as the average of $s_i\left(x_i\right)$ with respect to the input, divided by 2 for the sake of normalization. Given a sufficient sample size is used to limit numerical noise, the summation of Delta measures will equal unity, provided that the inputs

influences are separable from one another, which in this context means that the average PDF shift caused by fixing an input is independent of the fixing of any other input.

As with Sobol indices, Delta measures also ideally require Monte Carlo double loop sampling; however, this can be resolved in the same way by using Plischke partitioning [25], thereby recasting Eq. 1.11 and 1.12 as Eq. 1.13 and 1.14,

$$\hat{\delta}_i = \frac{1}{2N} \sum_{j=1}^{m} N_j s\left(X_i \in x_j\right) \tag{1.13}$$

where N is the total sample size, M is the number of partitions, N_j is the number of instances within partition j, and $s\left(X_i \in x_j\right)$ is defined as

$$s_i\left(X_i \in x_{i,j}\right) = \int \left| f_Y\left(y\right) - f_{Y|X_i \in x_{i,j}}\left(y\right) \right| dy \tag{1.14}$$

where $f_{Y|X_i \in x_{i,j}}$ is the PDF of Y conditional upon input X_i residing in the group comprised of all values of x_i within group j. Since f_Y or $f_{Y|X_i \in x_{i,j}}$ are not typically known, they must be estimated via kernel density estimation (KDE). f_Y is estimated as the sum of N PDF divided by N for the sake of maintaining unity. Each individual PDF or kernel has a mean corresponding to a specific instance of Y. The formulation of a KDE is shown in Eq. 1.15,

$$\hat{f}_y = \frac{1}{N\lambda} \sum_{i=1}^{N} K\left(\frac{y - y_i}{\lambda}\right) \tag{1.15}$$

where $\hat{f}_y$ is the estimation of f_Y, y_i is a specific instance of Y, K is the kernel density function, and λ is the kernel bandwidth. K can be any PDF with a mean of zero, but is most often a Gaussian profile centered at the origin. The proper selection of λ has been the subject of considerable research as excessively small values create a series of quasi-Dirac delta functions, while overly large values create near uniform distributions. One solution is KDE via diffusion [26], which treats the bandwidth selection problem as a time dependent heat diffusion equation. KDE via diffusion contains multiple methodologies, one of which is available in the python library PyQt-Fit [27] which is used within the computational

framework of this work. A variety of other moment independent measures are based off the Minkowski distances [28]. In terms of Minkowski distances, the PDF integration of Eq. 1.12 measures the first order or rectilinear distance. Moment independent measures can be extended to include second order or Euclid distance, as shown in Eq. 1.16, and infinity order or Chebyshev distance, as shown in Eq. 1.17,

$$s_i^2\left(X_i\right) = \sqrt{\int_{-\infty}^{\infty}\left(f_Y\left(y\right) - f_{Y|X_i}\left(y\right)\right)^2 dy} \tag{1.16}$$

$$s_i^{\infty}\left(X_i\right) = max\left(\left|f_Y\left(y\right) - f_{Y|X_i}\left(y\right)\right|\right) \tag{1.17}$$

where superscripts 2 and ∞ indicate the order of the measure. These extensions are easily implemented into the framework for Delta measure calculation. The order dictates the weighting of larger differences in PDF as compared to their smaller counterparts. For first order, all differences receive equal weight; for second order, the larger differences receive more weight; infinity order distances are a function of the largest difference only. While moment independent measures are superior to lower order measures in detecting nonlinearities, they are often subject to noise due to KDE, as well as Plischke partitioning if single loop Monte Carlo sampling is used. As a result, a relatively high number of runs is required for accurate results.

1.2.2 Multiphysics Environment

A Multiphysics environment permits coupling of multiple codes with differing specialties. Two types of coupling exist: loose couplings and tight couplings. In general, loose couplings solve the equations of different models separately, while tight couplings solve all equations simultaneously. The precise definitions of these coupling may vary depending on the source. Some consider one directional transfer of data from one code to another a data transfer or integration rather than a coupling, while other consider it a loose coupling. Nuances aside, the one directional flow of data of this work is referred to as an integration.

Integrations are preferable from an ease of implementation standpoint. They are appropriate as long there is limited feedback between the separate models, such as with quasi-steady state cases. Tight couplings are preferable from an accuracy and rate of convergence standpoint and are essential for multiphysics modeling of transient phenomena such as LOCA [29]. All of the data transfer in this work is classified as an integration, with future plans to add a loose coupling between RELAP5-3D and BISON.

Relevant Multiphysics Studies

A vast number of Multiphysics studies have been performed and continue to be performed. A sampling of past work which is of particular interest to this work includes a coupling by Wu *et al.* [30] between the neutronics code Serpent and BISON [9] for analysis of FeCrAl cladding during depletion, as well as a comparison of tight and loose coupling of the neutronics code DeCART with BISON [29]. Porter *et al.* [31] examined a union of the thermal hydraulic code TRACE with FRAPCON [8]. Holt *et al.* [32] performed a coupling between fuel performance code TRANSURANUS with reactor dynamics code DYN3D.

Sjenitzer *et al.* [33] coupled an in-house Monte Carlo-based neutronics code (as opposed to a more traditional deterministic code) with an in-house thermal hydraulics code. Work by Nadejda *et al.* [34] explored the difficulties and results of coupling the thermal hydraulic code TRACE with a Nodal Expansion method (NEM) used for neutronics. Lastly, work by Magedanz *et al.* [35] coupled the neutron kinetics code TORT-TD, the thermal hydraulic code CTF, and the transient fuel performance code FRAPTRAN [8].

Multiphysics typically refers to the combining of multiple separately developed codes. However, most codes used for nuclear application can be thought of as multiphysics structures themselves. Work by Williamsen *et al.* [36] describes the tightly coupled, thermomechanical multiphysics structure within BISON. A recent milestone of the neutroncis/thermal hydraulic code VERA-CS by the Consortium of Advanced Simulation of Light Water Reactors CASL [37] assesses the codes progress in fully incorporating codes for neutronics (MPACT), thermal hydraulics (CTF), isotopic depletion (ORIGEN), and fuel performance (BISON).

Plug and Play Concept of LOTUS

LOTUS allows for a plug-and-play environment between codes through the aid of a shared HDF5 database [38]. HDF5 databases allow for efficient and reliable storage and retrieval of data by python scripts. This is a vast improvement over the writing and reading of output files which greatly vary in format between codes. The stored data can be retrieved any time after execution, which allows the database to function similar to a restart file. Because of this feature, multiple codes can have access to the same data. Furthermore, additional codes can be added to the structure in an ad hoc manner, provide that the needed inputs for the new code were previously stored.

These plug-and-play features allow for an effective transfer of data as compared to traditional manual input file manipulation, especially when Monte Carlo sampling is performed. A schematic of the data storage within LOTUS is shown in Fig. 1.3. Note that many features such as risk assessment are currently unavailable, but will be implemented in the near future.

1.3 Summary

A large variety of multiphysics environments have been created and continue to be developed for modeling the interrelated physical phenomena within pressurized light water reactors (PWR). Uncertainty quantification (UQ) and sensitivity analysis (SA) of individual codes have been performed extensively. However, UQ and particularly higher order SA of interdisciplinary multiphysics environments (those including system analysis, fuel performance, and neutronics) are still in their infancy, and warrant further investigation.

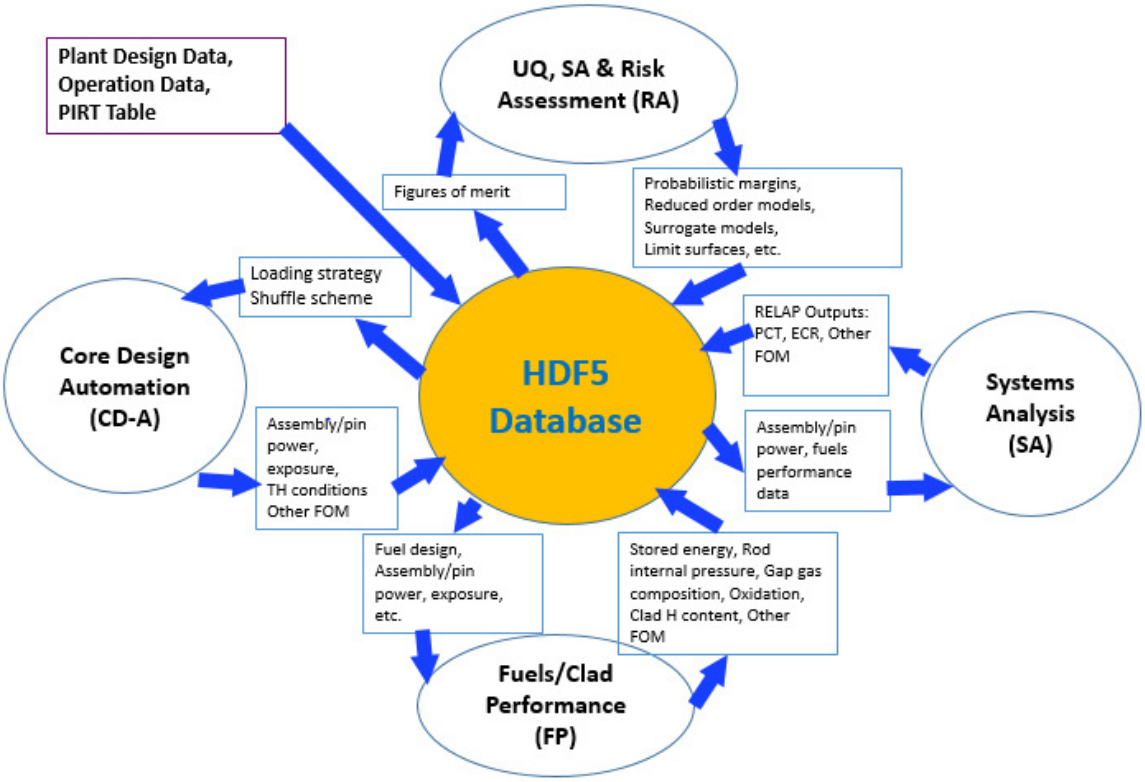

Fig. 1.3: LOTUS Data Flow Structure.

REFERENCES

[1] Glaeser, H., "GRS Method for Uncertainty and Sensitivity Evaluation of Code Results and Applications," *Science and Technology of Nuclear Installations*, Vol. 2008, 2008.

[2] Wu, X., Mui, T., Hu, G., Meidani, H., and Kozlowski, T., "Inverse uncertainty quantification of TRACE physical model parameters using sparse gird stochastic collocation surrogate model," *Nuclear Engineering and Design*, Vol. 319, 2017, pp. 185 – 200.

[3] Marcum, W. and Brigantic, A., "Applying uncertainty and sensitivity on thermal hydraulic subchannel analysis for the multi-application small light water reactor," *Nuclear Engineering and Design*, Vol. 293, 2015, pp. 272 – 291.

[4] The RELAP5-3D Code Development Team, "The RELAP5-3D Code Manual Volume I: Code Structure, System Models, and Solution Methods," 2012, Rev. 4, Idaho National Laboratory, INEEL-EXT-98-00834.

[5] Bratton, R. N., Jessee, M. A., and Wieselquist, W. A., "Rod internal pressure quantification and distribution analysis using Frapcon," *Proc. 2016 Conference on Physics of Reactors*, May 2016, pp. 2588–2602, ORNL/TM-2015/557.

[6] Ikonen, T., "Comparison of global sensitivity analysis methods Application to fuel behavior modeling," *Nuclear Engineering and Design*, Vol. 297, 2016, pp. 72 – 80.

[7] Ikonen, T. and Tulkki, V., "The importance of input interactions in the uncertainty and sensitivity analysis of nuclear fuel behavior," *Nuclear Engineering and Design*, Vol. 275, 2014, pp. 229 – 241.

[8] http://frapcon.labworks.org, Accessed: 2018.

[9] https://bison.inl.gov/, Accessed: 2018.

[10] Swiler, L. P., Gamble, K. A., Schmidt, R. C., , and Williamson, R. L., "Sensitivity Analysis of OECD Benchmark Tests in BISON," 2015, Sandia National Laboratories, SAND2015-8808.

[11] Pastore, G., Swiler, L., Hales, J., Novascone, S., Perez, D., Spencer, B., Luzzi, L., Uffelen, P. V., and Williamson, R., "Uncertainty and sensitivity analysis of fission gas behavior in engineering-scale fuel modeling," *Journal of Nuclear Materials*, Vol. 456, 2015, pp. 398 – 408.

[12] https://www.casl.gov/, Accessed: 2018.

[13] Brown, C. and Zhang, H., "Uncertainty quantification and sensitivity analysis with CASL Core Simulator VERA-CS," *Annals of Nuclear Energy*, Vol. 95, 2016, pp. 188 – 201.

[14] Brown, C., Zhang, H., Kucukboyaci, V., and Sung, Y., "Best estimate plus uncertainty analysis of departure from nucleate boiling limiting case with CASL core simulator VERA-CS in response to PWR main steam line break event," *Nuclear Engineering and Design*, Vol. 309, 2016, pp. 8 – 22.

[15] Arkoma, A., Hnninen, M., Rantamäki, K., Kurki, J., and Hämäläinen, A., "Statistical analysis of fuel failures in large break loss-of-coolant accident (LBLOCA) in EPR type nuclear power plant," *Nuclear Engineering and Design*, Vol. 285, 2015, pp. 1 – 14.

[16] Arkoma, A. and Ikonen, T., "Sensitivity analysis of local uncertainties in large break loss-of-coolant accident (LB-LOCA) thermo-mechanical simulations," *Nuclear Engineering and Design*, Vol. 305, 2016, pp. 293 – 302.

[17] Wilks, S. S., "Determination of Sample Sizes for Setting Tolerance Limits," *The Annals of Mathematical Statistics*, Vol. 12, No. 1, 1941, pp. 91–96.

[18] Frepoli, C. and Iyengar, S., "A comparison of non-parametric tolerance limits with linear combinations of order statistics in safety analysis," *Proc. ICAPP 2011*, 2011, p. 2851.

[19] Guba, A., Makai, M., and Pál, L., "Statistical aspects of best estimate method−I," *Reliability Engineering and System Safety*, Vol. 80, No. 3, 2003, pp. 217 – 232.

[20] Frepoli, C., "An Overview of Westinghouse Realistic Large Break LOCA Evaluation Model," *Science and Technology of Nuclear Installations*, Vol. 2008, 2008.

[21] Harding, B., Tremblay, C., and Cousineau, D., "Standard errors: A review and evaluation of standard error estimators using Monte Carlo simulations," *Tutorials in Quantitative Methods for Psychology*, Vol. 10, No. 2, 2014, pp. 107 – 123.

[22] Plischke, E., "An adaptive correlation ratio method using the cumulative sum of the reordered output," *Reliability Engineering and System Safety*, Vol. 107, 2012, pp. 149 – 156, SAMO 2010.

[23] Herman, J. and Usher, W., "SALib: An open-source Python library for Sensitivity Analysis," *The Journal of Open Source Software*, Vol. 2, No. 9, jan 2017.

[24] Borgonovo, E., "A new uncertainty importance measure," *Reliability Engineering and System Safety*, Vol. 92, No. 6, 2007, pp. 771 – 784.

[25] Plischke, E., Borgonovo, E., and Smith, C. L., "Global sensitivity measures from given data," *European Journal of Operational Research*, Vol. 226, No. 3, 2013, pp. 536 – 550.

[26] Botev, Z. I., Grotowski, J. F., and Kroese, D. P., "Kernel density estimation via diffusion," *Ann. Statist.*, Vol. 38, No. 5, 10 2010, pp. 2916–2957.

[27] http://pyqt-fit.readthedocs.io/en/latest/, Accessed: 2018.

[28] Zhai, Q., Yang, J., Xie, M., and Zhao, Y., "Generalized moment-independent importance measures based on Minkowski distance," *European Journal of Operational Research*, Vol. 239, No. 2, 2014, pp. 449 – 455.

[29] Hales, J., Tonks, M., Gleicher, F., Spencer, B., Novascone, S., Williamson, R., Pastore, G., and Perez, D., "Advanced multiphysics coupling for LWR fuel performance analysis," *Annals of Nuclear Energy*, Vol. 84, 2015, pp. 98 – 110.

[30] Wu, X., Kozlowski, T., and Hales, J. D., "Neutronics and fuel performance evaluation of accident tolerant FeCrAl cladding under normal operation conditions," *Annals of Nuclear Energy*, Vol. 85, 2015, pp. 763 – 775.

[31] Porter, I., Knight, T. W., and Raynaud, P., "Potential Impacts of Modeling Full Reactor Cores Using Combined Fuel Performance and Thermal Hydraulics Codes," *Nuclear Technology*, Vol. 190, No. 2, 2015, pp. 174–182.

[32] Holt, L., Rohde, U., Seidl, M., Schubert, A., Uffelen, P. V., and Macián-Juan, R., "Development of a general coupling interface for the fuel performance code TRANSURANUS Tested with the reactor dynamics code DYN3D," *Annals of Nuclear Energy*, Vol. 84, 2015, pp. 73 – 85.

[33] Sjenitzer, B. L., Hoogenboom, J. E., Escalante, J. J., and Espinoza, V. S., "Coupling of dynamic Monte Carlo with thermal-hydraulic feedback," *Annals of Nuclear Energy*, Vol. 76, 2015, pp. 27 – 39.

[34] Todorova, N. K. and Ivanov, K. N., "Investigation of spatial coupling aspects for coupled code application in PWR safety analysis," *Annals of Nuclear Energy*, Vol. 30, No. 2, 2003, pp. 189 – 209.

[35] Magedanz, J., Avramova, M., Perin, Y., and Velkov, A., "High-fidelity multi-physics system TORT-TD/CTF/FRAPTRAN for light water reactor analysis," *Annals of Nuclear Energy*, Vol. 84, 2015, pp. 234 – 243.

[36] Williamson, R., Hales, J., Novascone, S., Tonks, M., Gaston, D., Permann, C., Andrs, D., and Martineau, R., "Multidimensional multiphysics simulation of nuclear fuel behavior," *Journal of Nuclear Materials*, Vol. 423, No. 1, 2012, pp. 149 – 163.

[37] Stimpson, S. G., Powers, J. J., Clarno, K. T., Pawlowski, R., and Bratton, R., "Assessment of Pellet-Clad Interaction Indicators in Watts Bar Unit 1 using the VERA Framework," *Proc. PHYSOR 2016 - Unifying Theory and Experiments in the 21st Century*, May 2016.

[38] The HDF Group, "Hierarchical data format version 5," http://www.hdfgroup.org/HDF5, Accessed: 2018.

aiaa

CHAPTER 2

Goals and Objectives

2.1 Objectives

The primary objective of this work is to perform uncertainty quantification (UQ) and sensitivity analysis (SA) on a variety of integrated simulations. As noted in the literature review of section 1.2, many UQ and SA studies have been performed and a large variety of multihpysics environments have been created and continue to be developed. However, UQ and SA of interdisciplinary multiphysics environments are still in their infancy.

The aim of this work is to conduct new UQ and SA studies which incorporate multiple design disciplines. These studies will allow for more complete UQ and SA for a variety of figures of merit (FOM). For instance, fuel performance FOM will be subject to the input perturbations of advanced thermal hydraulics (which affect cladding heat transfer) and neutronics (which affect power distributions). SA will also use recently developed higher order measures in the interests of gaining new insights otherwise unattainable with more traditional measures. The problems of interest and corresponding UQ and SA studies are as follows.

1. Determine uncertainty of thermal hydraulic and fuel performance FOM of quasi-steady state depletion cases using UQ and a variety of SA measures. UQ and SA are to be more comprehensive, taking into account uncertainties from thermal hydraulics, neutronics, and fuel performance.

2. Quantify uncertainty of safety metrics for transient loss of coolant accident (LOCA) cases. The UQ study will include perturbations to initial conditions supplied by fuel performance and neutronics calculations, as well as for transient system analysis calculations.

2.2 Scope of Work

The specific integrations and corresponding forms of UQ and SA are contained in this section. For all of the integrations, inconsistencies must be limited to the extent possible, and carefully documented if significant and unresolved.

1. Perform quasi-steady state, fuel depletion case for three full fuel cycle (4.5 years) of a single fuel assembly using VERA-CS and FRAPCON.
   (a) Perform Monte Carlo UQ of the thermal hydraulic Figure of Merit (FOM) minimum departure from nucleate boiling ratio (MDNBR), and the fuel performance metrics maximum fuel centerline temperature (MFCT) and gap conductance at peak power (GCPP).
   (b) SA of the aforementioned FOM using Pearson Correlation Coefficients, Sobol Indices, and Delta Moment Independent Measures.
2. Perform quasi-steady state, fuel depletion case for three full fuel cycle (4.5 years) of a single fuel assembly using VERA-CS and BISON.
   (a) Perform Monte Carlo based UQ of the FOM mentioned in objective 1.a.
   (b) SA of FOM in objective 1.a using Pearson Correlation Coefficients, Spearman Correlation Coefficients, Sobol Indices, and Delta Moment Independent Measures, and second and infinity order Moment Independent Measures.
   (c) Compare results with objective 1
3. Perform LB-LOCA of full reactor system. Determine initial conditions for fuel performance parameters using FRAPCON and power shapes from PHISICS. All transient LB-LOCA simulation will be handled by RELAP5-3D.
   (a) Perform Wilks UQ of peak cladding temperature ratio (PCTR) and equivalent cladding reacted ratio (ECRR).

Each of the primary objectives is presented in the form of a reformatted journal article. Select results of objectives 1 and 2 have been published in the *Annals of Nuclear Energy* [1]

and *Nuclear Engineering and Design* [2] respectively. A summary of the results from the third objective has been submitted to *Annals of Nuclear Energy* as of April 2018, and is awaiting revision and/or approval.

REFERENCES

[1] Blakely, C., Zhang, H., and Ban, H., "Sensitivity analysis of VERA-CS and FRAPCON coupling in a multiphysics environment," *Annals of Nuclear Energy*, Vol. 111, 2018, pp. 683 – 701.

[2] Blakely, C., Zhang, H., Folsom, C., Ban, H., and Szilard, R., "Application of regression, variance, and density based global sensitivity methods to integrated VERA-CS and BISON simulations," *Nuclear Engineering and Design*, Vol. 332, 2018, pp. 186 – 201.

aiaa

CHAPTER 3

Transition to Integration of VERA-CS and FRAPCON

The first integration is between the Virtual Environment for Reactor Applications - Core Simulator (VERA-CS) currently under the the development of the U.S. Department of Energys Consortium for Advanced Simulation of Light Water Reactors, and the well established fuel performance code FRAPCON created by Pacific Northwest National Laboratory. The problem of interest is a steady state depletion case. This work serves as a starting point for LOTUS.

The Monte Carlo sampling of this work requires thousands of perturbed cases to be executed. Ideally, all cases should successfully converge with the same solver parameters (i.e. recommended time step). This need for robustness was one of the primary motivations in selecting both VERA-CS and FRAPCON as well as the quasi-steady problem itself.

The incorporation of well behaved codes allowed for more focus to be placed on the development of higher order sensitivity analysis methods. The incorporation and integration of software for variance and density based sensitivity measures is of great utility in works presented herein as well as in continued future works.

As a point of correction, the word coupling is use improperly at times in the subsequent chapter. Later revelations gained after the time of publication shown light on the subjective, even controversial nature of the word. While some sources would consider the data transfer between VERA-CS and FRAPCON as a one-way or even loose coupling, it is more common for coupling to indicate feedback between codes. Since none of the data transfer presented herein contain feedback, all later works use the word integration.

CHAPTER 4

SENSITIVITY ANALYSIS OF VERA-CS AND FRAPCON COUPLING IN A MULTIPHYSICS ENVIRONMENT [1]

This chapter contains a reformatted version of an article appearing in volume 111 (2018) of the journal *Annals of Nuclear Energy* [1].

4.1 Abstract

A demonstration and description of the LOCA Toolkit for US light water reactors (LOTUS) is presented. Through LOTUS, the core simulator VERA-CS developed by CASL is coupled with the fuel performance code FRAPCON. The coupling is performed with consistent uncertainty propagation with all model inconsistencies being well-documented. Monte Carlo sampling is performed on a single 17 x 17 fuel assembly with a three cycle depletion case. Both uncertainty quantification (UQ) and sensitivity analysis (SA) are used at multiple states within the simulation to elucidate the behavior of minimum departure from nucleate boiling ratio (MDNBR), maximum fuel centerline temperature (MFCT), and gap conductance at peak power (GCPP). The SA metrics used are the Pearson correlation coefficient, Sobol sensitivity indices, and the density-based, delta moment independent measures. Results for MDNBR show consistency among all SA measures, as well for all states throughout the fuel lifecycle. MFCT results contain consistent rankings between SA measures, but show differences throughout the lifecycle. GCPP exhibits predominantly linear relations at low and high burnup, but highly nonlinear relations at intermediate burnup due to abrupt shifts between models. Such behavior is largely undetectable to traditional regression or variance-based methods and demonstrates the utility of density-based methods.

4.2 Introduction

[1] Coauthors: Hongbin Zhang, Heng Ban

Nuclear plant modeling contains a plethora of physical phenomena in the fields of neutronics, fluid dynamics, heat transfer, solid mechanics, material sciences, and chemistry. The approach in past years has been to develop codes which emphasize a particular field and include simplified models for all other essential phenomena. For instance, FRAPCON-4.0 [2] has extensive fuel performance modules with idealized thermal hydraulics in the form of a single channel enthalpy rise mode. This partitioning among disciplines has allowed the nuclear research community to maintain a structured approach for furthering modeling capabilities in a variety of fields. However, when phenomena are interrelated, as is the case in many nuclear application, this siloed approach prevents proper mathematical coupling of the models involved.

Multiphysics environments allow for the combining of programs with differing specialties by treating each code as modules in a larger structure. Past research which is of particular interest within the scope of this work includes a coupling between the fuel performance code FRAPCON-3.5 [2] and the fluid dynamics code TRACE-V5P3 [3] by PORTER *et al.* [4], FRAPCON-3.5 with lattice physics code SCALE-Polaris [5] by Bratton *et al.* [6], and the fuel performance code BISON [7] with the reactor physics code Serpent [8] by Wu *et al.* [9].

At present, a LOCA Toolkit for U.S. light water reactors (LOTUS) is being developed at Idaho National Laboratory (INL). LOTUS will employ a multiphysics environment that utilizes VERA-CS [10] for neutronics and thermal hydraulics, FRAPCON-4.0 [2] for steady state fuel performance, FRAPTRAN-2.0 [2] for transient fuel performance, BISON [7] as a more extensive and computationally expensive second option for fuel performance, and RELAP5-3D [11] for transient thermal hydraulics. The scope of the work presented herein is based on a coupling between the well-established fuel performance code FRAPCON-4.0 [2] and VERA-CS [10], which is currently under development by the U.S. Department of Energys Consortium for Advanced Simulation of Light Water Reactors (CASL).

LOTUS will aid in the development of uncertainty quantification (UQ) and sensitivity analysis (SA) methodologies in a versatile multiphysics environment. UQ establishes con-

fidence intervals for outputs of interest while SA quantifies the amount of output variance attributable to specific inputs. Both UQ and SA play critical roles in the safety analyses of nuclear power plants. In the past, UQ and SA have typically focused on the plants thermal hydraulics [12]. Fairly recently, UQ and SA have been extended into fuel performance [13, 14] with assumed representative power history, power shapes, and thermal hydraulic conditions as inputs. Initial analysis has also been performed on coupled neutronics/thermal hydraulics models with VERA-CS [15, 16]. While work is currently being done at CASL to implement the fuel performance code BISON into VERA-CS [17], to our knowledge no UQ/SA work has been done for coupled neutronics/thermal hydraulics and fuel performance calculations.

Uncertainty propagation is achieved via a direct data flow between the codes. Such a connection has often not been possible in the past when dealing with computationally expensive codes. In such cases, a smaller sample size is used for the expensive program, from which probability density functions (PDF) for outputs are estimated. These PDF are then used to create larger samples for faster codes not subject to hardware constraints. Fortunately, the high performance computer (HPC) resources at INL allow for a large sampling of VERA-CS with a direct data connection to FRAPCON. While more expensive, this method negates the need for the aforementioned PDF generation and multiple samplings. The direct connection framework will also be imperative for future work involving strong coupling (see section 4.3.3).

UQ and SA are performed on a quasi-steady state, three cycle depletion case for a single PWR fuel assembly. The SA metrics used are Pearson correlation coefficients, Sobol sensitivity indices, and delta moment independent measures [18]. The figures of merit are the minimum departure from nucleate boiling ratio (MDNBR), maximum fuel centerline temperature (MFCT), and gap conductance at peak power (GCPP).

Results for MDNBR indicate consistent rankings among all SA measures for inputs with significant impact. The measures of greatest impact are core power, inlet temperature, outlet pressure, and rated flow. The SA measures show relatively low variation among all

states. The measures also indicate a high degree of linearity for input relations to MDNBR.

MFCT also maintains consistent rankings among all SA measures; however, significant changes occur for SA measures between states. Initial states show a strong impact from fuel thermal conductivity with substantial contributions from fuel and cladding radii. With the onset of fuel and cladding contact, the significance of geometric factors vanishes, leaving nearly all uncertainty resulting from fuel thermal conductivity. In later phases of burnup, core power and fuel density begin to play minor roles in MFCT due to their effect on burnup, which in turn affects fuel thermal conductivity.

GCPP studies reveal large nonlinearities, large difference in rankings between SA measures, and radical changes from state to state. This behavior is in accordance with past work performed by Ikonen *et al.* [13, 14]. Uncertainty in lower burnup states mainly originates from fuel and cladding radii, causing relatively large GCPP uncertainties with linear relations to inputs.

In states near the initial state of contact, some data remains within the open-gap group, while other data contains closed-gaps with low interfacial pressures. This latter group contains roughly a twentieth of the variance of the open-gap models. In the low interfacial pressure closed-gap states, the little uncertainty that exists is largely due to variation in water side corrosion. While counterintuitive, the insulating effect of the outer layer of zirconium dioxide causes a roughly 10 temperature jump in the cladding, gap, and fuel. This corresponds to a 1.3% rise in gas conductivity, thereby increasing gap conductance.

Later states show a secondary shift to high pressure/high burnup models. Initially, fuel swelling and cladding creep contribute the most to GCPP uncertainty due to their effect on interfacial pressure, which in turn increases the solid gap conductance. With higher burnup states, core power, cladding radius, fuel density, and fuel radius affect burnup which in turn alters the interfacial pressure due to fuel swelling and densification.

The change between open-gap, low pressure closed-gap, and high pressure closed-gap cases causes abrupt switching between three models. Each of these models is linear, however the abrupt shift between the models can create bimodal or trimodal PDF. The modes

within these PDF can differ in variance by an order of magnitude. Such behavior is largely undetectable by more traditional regression or variance methods, thus demonstrating the utility of the density-based delta moment independent measures.

4.3 LOTUS Toolkit

LOTUS seeks to create a multiphysics environment for modeling various phenomena under loss of coolant accident (LOCA) as well as other transient scenarios. LOUTS incorporates well-established computer codes as well as those currently under development. In such environment, codes are treated as modules that are under the hood, which can be called upon similar to a traditional subroutine. This methodology is superior to the time intensive, error prone method of manually creating and modifying input files.

The problems of interest for LOTUS span five areas of research: core design automation (CD-A); fuel/clad performance (FP); systems analysis (SA); uncertainty quantification, sensitivity analysis and risk assessment (RA); and core design optimization (CD-O). LOTUS contains UQ tools designed to satisfy the industry standard best estimate plus uncertainty (BEPU) methodology as well as the framework for SA to identify which inputs are most relevant (see sections 4.6.1 and 4.6.2 for details). A conceptual schematic of the LOTUS framework is shown in Fig. 4.1.

The scope of this work only involves a subset of the LOTUS framework, focusing on core design automation using VERA-CS [10] which is currently under development, and the well-established FRAPCON-4.0 [2] code for fuels performance. Both UQ and SA are performed on the three FOM described in section 4.2. The case selected for study is a quasi-steady state depletion case. Future studies involving transient calculations, such as LOCA cases for which LOTUS is designed, will use the steady state case to supply initial conditions.

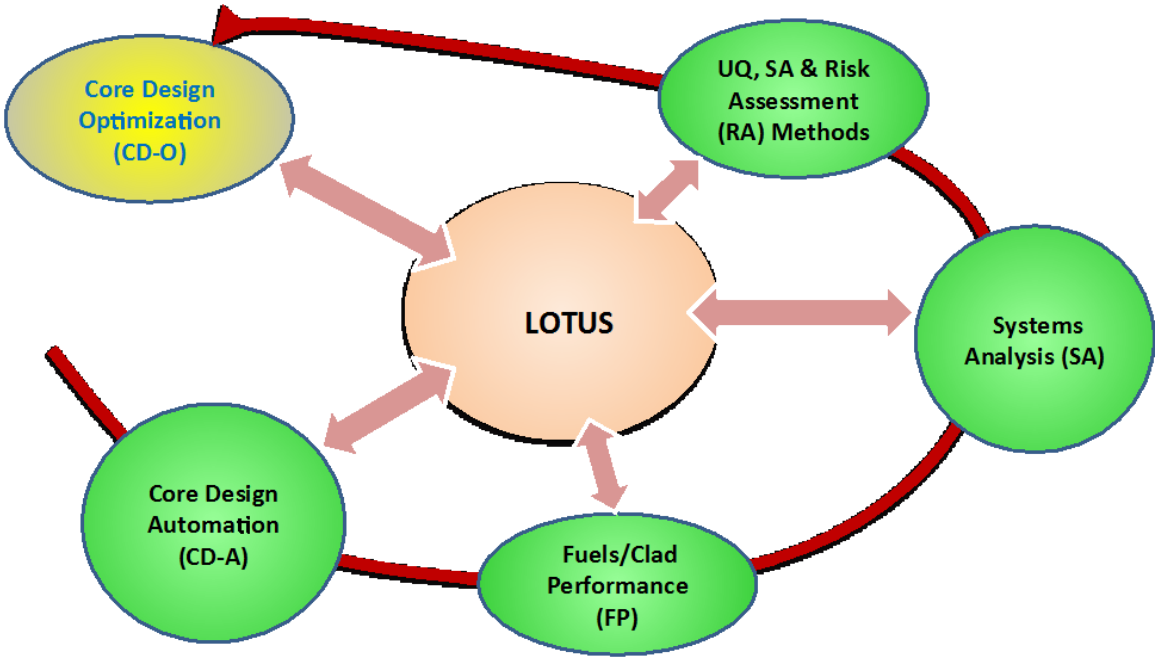

Fig. 4.1: Schematic illustration of LOTUS.

4.3.1 Virtual Environment for Reactor Applications - Core Simulator (VERA-CS)

VERA-CS includes three main components: MPACT [19] for reactor physics and neutron transport, Coolant-Boiling in Rod Arrays-Two Fluids (COBRA-TF) [20] for thermal-hydraulics, and ORIGEN [21] for isotopic depletion. Ongoing work at CASL is incorporating the fuel performance code BISON [17]. VERA-CS is expected to contain burnup dependent fuel thermal conductivity as well as dynamics gap conductance capability in the near future.

VERA-CS includes built-in cross sections generation, neutron transport, depletion, and sub-channel thermal hydraulics. The code is capable of 3-D whole core simulations resolved at the sub-pin level, as opposed to using smeared average properties. While this resolution is beneficial in supplying more accurate power histories for each pin, it does come at relatively high computational cost. In this work, due to the thousands of cases required by UQ and SA, a single assembly is modeled for demonstration purposes instead of modeling a full core.

Past UQ/SA work on VERA-CS includes a 2 x 2 assembly model with extensive sampling [15] based on the Monte-Carlo method and full core analyses under main steam line

break conditions with a relatively small number of runs based on the Wilks nonparametric statistical method [16].

4.3.2 FRAPCON

FRAPCON is a fuels performance code developed by Pacific Northwest National Labs. FRAPCON-3v1.0 was released in 1997, followed by eight updated versions, and then the current FRAPCON-4.0 used by this work [2]. The code has been extensively validated over the years, and is thus more established than VERA-CS. The code is used for analysis of a single fuel rod, as opposed to the full core environments of VERA-CS. FRAPCON models include heat transfer from fuel to cladding to coolant, thermal expansion, solid mechanics, creep, corrosion, single channel thermal hydraulics, and fission gas release.

FRAPCON is a 1 $\frac{1}{2}$ D code, meaning that the equations are simplified to radial form at multiple axial locations. The equations are fully solved radially, while axially effects are only partially modeled. The user inputs power profiles, and thermal hydraulic profiles are obtained either by a single channel enthalpy rise model, which utilizes axial calculations, or by user supplied profiles.

While the 1 $\frac{1}{2}$ D model is less accurate due to the neglecting of all azimuthal gradients and many axial effects, it is advantageous in its computational performance. This work uses one fuel assembly which contains 264 fuel rods. Since 2500 cases are run for each fuel rod, this corresponds to 660000 FRAPCON cases. This task is rendered substantially less cumbersome by case runtimes of approximately two seconds.

Past work on UQ and SA has been performed on stand-alone FRAPCON runs with assumed power history, power shapes and thermal hydraulic conditions [13, 14]. Past research showed the effectiveness of lower order methods in analyzing MFCT, but the need for higher order methods to capture the complexities involved in GCPP.

4.3.3 Data Flow Structure

Great care must be taken to assure consistent uncertainty propagation. The precise methodology is greatly dependent upon runtime and available resources. If the workload

of programs is above or near the limit of available computational resources, then large samples are not attainable. In such cases, probability density functions (PDF) of outputs of interest are estimated from a limited sample size. Codes not hindered by hardware constraints may then use large sample sizes which are generated from the aforementioned PDFs. However, the high performance computer (HPC) resources at INL far exceed the required power for a single assembly VERA-CS case. Furthermore, FRAPCON runtimes are miniscule. Thus a large number of runs in VERA-CS followed by FRAPCON runs for each pin is feasible. This method negates the need for intermediate PDF generation and resampling. In addition, the direct connection structure will be of great use in future work involving feedback between the codes. A schematic of the data flow is shown in Fig. 4.2 with rectangular boxes representing files and elliptical shapes indicating programs.

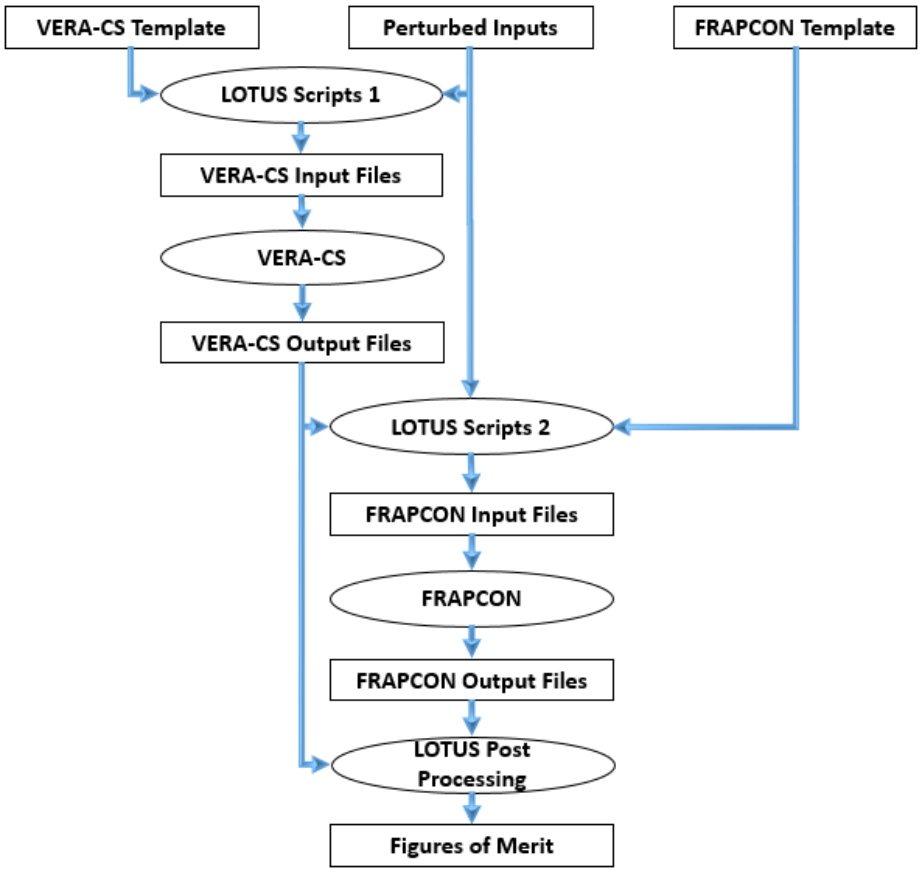

Fig. 4.2: LOTUS Data Flow Structure for VERA-CS and FRAPCON.

The process begins by creating a list of perturbed inputs. The first set of LOTUS scripts combines perturbed inputs specific to VERA-CS with a VERA-CS input template to create an input file for each set of perturbed inputs. After a VERA-CS run for each input file, the second set of LOTUS scripts creates FRAPCON input files from VERA-CS output files, perturbed inputs specific to FRAPCON, and a FRAPCON template file.

The data transferred from VERA-CS to FRAPCON includes power histories, thermal hydraulic profiles, mass flow rates, and the neutron fast flux per specific power (NFFSP). The transfer was facilitated by maintaining a consistent axial mesh spacing between codes. While VERA-CS stores data as elemental averages, FRAPCON only accepts nodal values. This difference was remedied by treating each element as having linear shape functions, thereby allowing for each nodal value to be estimated via extrapolation.

The power histories transferred included both the axial averaged linear heat rate and axial peaking power shapes for each state. The thermal hydraulics profiles contained radially averaged temperature and pressure values for the coolant channel at the same axial locations specified in the power profiles.

The mass flow rates from VERA-CS were axial averaged, and inputted to FRAPCON as an inlet condition (see section 4.3.4). The NFSSP was estimated by first obtaining the neutron fast flux through summation and interpolation of pertinent VERA-CS energy groups, and then dividing by core power (see section 4.3.4). It is important to note that VERA-CS output files contain all VERA-CS input data as well. Hence any shared data is supplied to VERA-CS first, and then later retrieved from the VERA-CS output files before being supplied to FRAPCON.

After all FRAPCON cases are executed, LOTUS post processing scripts retrieve all figures of merit (FOM) data from both FRAPCON and VERA-CS output files. Lastly all UQ and SA metrics are calculated for each fuel pin.

The data flow structure between VERA-CS and FRAPCON is a loose coupling, meaning that there is no feedback between the two codes. The alternative strong coupling, such as the MPACT and COBRA-TF coupling within VERA-CS, entails an iterative process be-

tween codes to enhance model consistencies. For the quasi-steady state analyses carried out in this work, the loose coupling approach is adequate. However, for transient calculations, such as under LOCA conditions, strongly coupled calculations will be required. This is left for future work.

4.3.4 Model Inconsistencies

Due to differences in the assumptions of VERA-CS and FRAPCON, model inconsistencies are inherent. The most critical difference is the fundamentally different models of fuel thermal conductivity, a property with which past SA on FRAPCON [13,14] established as the most critical input in FRAPCON with regards to MFCT. The fuel thermal conductivity for FRAPCON and COBRA-TF (which is used by VERA-CS) are shown in Eq. 4.1 and 4.1,

$$k_{FRAP} = \frac{1}{A + B \cdot T + f\left(Bu\right) + \left(1 - 0.9e^{-0.04Bu}\right) g\left(Bu\right) h\left(T\right)} + \frac{C}{T^2} e^{-\frac{D}{T}} \tag{4.1}$$

$$k_{VERA} = E\left(\frac{1 - \left(F - G \cdot T_C\right)\left(1 - \rho\right)}{1 - H\left(F - G \cdot T_C\right)}\right)\left\{max\left(\frac{I}{J + T_C}, K\right) + L \cdot e^{M \cdot T_C}\right\} \tag{4.2}$$

where letters $A - M$ are constants which can be found in FRAPCON-4.0 and COBRA-TF theory manuals [2, 22]. These functions differ in that FRAPCON is a function of temperature and burnup while VERA-CS is dependent on temperature and fuel density. These inconsistencies cause discrepancies as large as 50 °C in hot rods with a temperature on the order of 1000 °C. These are the largest differences caused by the current weak couplings between the codes.

The solution to this problem will be solved in the future by having VERA-CS utilize the same conduction model as FRPACON, which is currently available within COBRA-TF. At present, the option to switch between conduction models is not possible in VERA-CS due to its inability to transfer burnup data for conductivity calculations. Current developmental

plans slate alternate conductance models to be available in the near future.

The codes differ in gap conductance methodology. VERA-CS uses COBRA-TF for both fluid and solid structure analysis. While COBRA-TF does contain a gap conductance model, VERA-CS does not yet have the capability to run coupled simulations with dynamic gap conductance values. At present, VERA-CS is limited to a user defined, constant gap conductance. FRAPCON contains an extensive gap conductance model which takes into account variable material properties, corrosion, swelling, and radiative effects among others. This shortcoming will be remedied in the future with either a strong coupling between VERA-CS and FRAPCON which includes gap conductance feedback, or more likely a later version of VERA-CS which allows for dynamics gap conductance.

The codes use different models for isotropic depletion and burn up profiles models. VERA-CS uses ORIGEN [21] to perform depletion calculations, while FRAPCON uses a simpler subroutine based off of the TRANSURANUS code system [23]. As discussed in section 4.3.3, the power profiles for each pin are transferred from VERA-CS to FRAPCON for each time step. There are slight differences due to VERA-CS outputs being element based while FRAPCONS are nodal, nevertheless, the radially averaged burnup for each pin are within 2% of each other. Past sensitivity studies have determined the enrichment factor to have negligible impact on all FOM [13], hence differing radial burnup profiles and fission products, will have no ramifications within the scope of this work.

The codes also differ in their treatment of mass flux. VERA-CS uses COBRA-TF to model flow for the entire core, including crossflow between sub-channels. FRAPCON uses a single channel, resulting in an axially constant mass flux. LOTUS handles this difference by calculating the axially averaged mass flux for each fuel pin, and treating this value as the inlet mass flux along a single channel. Previous work [13] established the mass flux to have very low impact on both MFCT and GCPP (recall MDNBR is not calculated in FRAPCON). Furthermore, since the thermal hydraulic profiles are directly imported from VERA-CS, as opposed to being calculated from the single channel enthalpy rise model, the impact of mass flux is further negated from the thermal hydraulic perspective of this work.

Lastly, the codes use different methods for fast neutron flux. VERA-CS uses the neutronics code MPACT [19], which solves the neutron transport equation with 54 energy groups. FRAPCON uses a far more rudimentary method requiring a user defined neutron fast flux per specific power (NFFSP). The NFFSP allows the code to estimate neutron fluxes with energies in in excess of 1 MeV based solely on the local power.

The method for converting from energy groups fluxes to NFFSP was based off of the methodology presented in [6]. The NFFSP is derived from the average neutron fluxes of the high energy groups in the VERA-CS outputs. An approximate integration shown in Eq. 4.3 is used to estimate the fast neutron flux with energy exceeding 1 MeV.

$$\Phi_{E>1MeV,i} = \sum_{j=L+1}^{L+N} \Phi_{j,i} + \frac{E_L - 1MeV}{E_L - E_{L+1}} \Phi_{L,i} \tag{4.3}$$

where Φ is neutron flux, E is the lower energy bound for a given flux, subscript i and j denote state and energy group respectively, L is the index number corresponding to the energy group which straddles 1 MeV, and N is the number of energy groups with lower bounds in excess of 1 MeV. Thus the flux of neutrons with energy in excess of 1 MeV ($\Phi_{E>1,i}$), is a summation of the N groups whose lower bound exceeds 1 MeV, and the portion of the transitionary group above 1 MeV determined via interpolation. The NFFSP is calculated by Eq. 4.4,

$$\overline{F_{E>1MeV}} = \frac{1}{\Delta T} \sum_{i=1}^{M} \frac{\Delta t_i \Phi_{E>1MeV,i}}{\dot{q}_i} \tag{4.4}$$

where $\overline{F_{E>1MeV}}$ is the temporally averaged NFFSP, $\dot{q}_i$ is the core average specific power, ΔT is the total time of the core simulation, Δt_i is the time step, and M is the number of time steps. The vast neutronics simplifications necessary to transition VERA-CS calculation into FRAPCON framework loose much of the detail available in VERA-CS data, but maintain the average magnitude of fast neutron flux.

While all these discrepancies present issues which cannot be resolved or dismissed within this work, it is essential to stress that the most critical data exchanged by the

LOTUS scripts are the power and thermal hydraulic profiles. VERA-CS is at the cutting edge of coupled neutronics and thermal hydraulics reactor core simulations, and is capable of producing sub pin level power profiles of high fidelity, yet currently lacks various fuel performance analysis models. FRAPCON has well established fuel performance models, but is dependent upon idealizations or user supplied data for power history and thermal hydraulics data. The scope of this work is to create a more complete, but not yet all encompassing, framework reflective of true reactor physics. All discrepancies are minimized to the extent possible, documented, and highlight industry needs that may be resolved through future codes and/or new couplings.

4.4 Problem Description and Methodology

This section contains a description of the case of interest, a list of the perturbed inputs, and the figures of merit (FOM).

4.4.1 Model Description

The case under study is a depletion case lasting four and half years or three cycles for typical light water pressurized reactors. The resulting SA measures are valuable for the larger LOCA based vision of LOTUS. Since LOCA may occur at any point in the fuel lifecycle, it is therefore crucial to obtain an understanding of the most impactful inputs at a sufficient number states.

A single 17 17 assembly containing 264 fuel rods is modeled for demonstration purposes, with full core simulations being left to future work. The problem parameters are shown in Table 4.1 with X indicating the parameters are used by VERA-CS and/or FRAPCON.

4.4.2 Perturbed Inputs

The inputs of primary importance were selected from past work on FRAPCON [13] and VERA-CS [15]. From these works, 22 previously perturbed inputs were selected in addition to the plenum fill gas pressure. The plenum fill gas pressure was added due to its known impact on modeling contact, which past work by Ikonen [13, 14] has identified as a

Table 4.1: Design and simulation parameters for the model problem.

Parameter Name	Parameter Value	VERA-CS	FRAPCON
Fuel Height	3.657 m	X	X
Pin Pitch	1.26 cm	X	X
Plenum Height	16 cm	X	X
Fuel Material	Uranium Dioxide	X	X
Fill Gas Type	Helium	X	X
Cladding Material	Zircaloy 4	X	X
Boron	1640 ppm	X	
Plate Material	Stainless Steel	X	
Plate Thickness (Lower/Upper)	5.0 / 7.6	X	
Plate Volume Fraction	0.5	X	
Spacer Material (Middle/End)	Inconel/Zircaloy 4	X	
Spacer Height (Middle/End)	3.810 cm / 3.866 cm	X	
Spacer Mass (Middle/End)	875 g / 1017 g	X	
Nozzle Material	Stainless Steel	X	
Nozzle Height (Lower/Upper)	6.053 cm / 8.827 cm	X	
Nozzle Mass	6250 g	X	
Pellet Height	0.983 cm		X
Height of Pellet Dish	0.0335 cm		X
Pellet End-Dish Shoulder Width	0.0665 cm		X
Fuel Surface Roughness	6.45e-4 cm		X
Cladding Surface Roughness	6.45e-4 cm		X

phenomenon effecting both MFCT and GCPP. The full list of common perturbed inputs used by both codes is shown in Table 4.2 with X indicating the perturbed input parameters used by VERA-CS and/or FRAPCON. All distributions are a truncated normal distribution extending out two standard deviations.

As indicated at the base of Table 4.2, the star (*) denotes an input that very strongly affects a FRAPCON input, though it is not a direct input. The core power for instance, directly impacts the linear heat generation rate input of FRAPCON. Likewise, the mass inlet flux of FRAPCON is a result of the rated flow inputted to VERA-CS (see section 4.3.4 for more details). The table positions with - entries, indicate that a nominal value does not exist in the FRAPCON code. Values such as fuel thermal conductivity vary greatly and are routinely updated. FRAPCON allows for manipulations of these values by biasing all calculation of the variable by a specified amount.

4.4.3 Figures of Merit

Three figures of merit (FOM) are presented in this study: minimum departure from nucleate boiling ratio (MDNBR), maximum fuel centerline temperature (MFCT), and gap conductance at peak power (GCPP). All FOM are calculated and reported at a specified state. Hence the words maximum and minimum should be understood as purely spatial and not temporal.

The MDNDR, given by Eq. 4.5 is a measure of the proximity of a heat flux to the critical heat flux at which a transition from nucleate to film boiling occurs, which is highly undesirable from a cooling and safety standpoint.

$$MDNBR = min\left(\frac{q^{DNB}}{q}\right) \tag{4.5}$$

where q is the heat flux and q^{DNB} is the heat flux at which a departure from nucleate boiling occurs, and the $min()$ operator denotes the minimum. The MDNBR is calculated in VERA-CS alone, and is thus passed directly to post processing from the VERA-CS output file.

Table 4.2: Design and simulation parameters for the model problem.

Input Name	Nominal Value	Range(+/-)	VERA-CS	FRAPCON
Inlet Temperature	554.9 (290.5)	3 (1.667)	X	X
Outlet Pressure	15.513 MPa	2%	X	X
Fuel Radius	0.4096 cm	0.001 cm	X	X
Clad Inner Radius	0.418 cm	0.002 cm	X	X
Clad Outer Radius	0.475 cm	0.002 cm	X	X
Fuel Density (% Theoretical)	94.50%	1.60%	X	X
Fuel Enrichment (% Weight)	4.80%	0.00%	X	X
Direct Mod. Heating Fraction	0.02	10%	X	X
Assembly Power				
Cycle 1	17.674 MW	2%	X	*
Cycle 2	13.256 MW			
Cycle 3	8.837 MW			
Rated Flow	3.410 Mlbs/hr (1.5467 Mkg/hr)	2.00%	X	*
Mid Spacer Grid Form Loss	0.907	20%	X	
End Spacer Grid Form Loss	0.9065	20%	X	
Void Drift Coefficient	1.4	10%	X	
Turbulent Mixing Coefficient	0.005	10%	X	
Plenum Fill Gas Pressure	1.207 MPa	2.00%		X
Fuel Thermal Conductivity	-	10%		X
Fuel Thermal Expansion	-	15%		X
Fission Gas Release	-	+200% -67%		X
Fuel Swelling	-	20%		X
Cladding Creep	-	30%		X
Cladding Axial Growth	-	50%		X
Cladding Corrosion	-	40%		X
Cladding Hydrogen	-	80 ppm		X

Note: * indicates an input which strongly effects a FRAPCON input, but is not directly inputted.

Analysis of the MFCT is essential in avoiding fuel melting or excessive fuel fracturing. The MFCT is calculated in both VERA-CS and FRAPCON. Since FRAPCON specializes in fuel performance and is the more established of the two codes, the MFCT from FRAPCON is reported in this work.

The GCPP in particular highlights the unique ability of LOTUS to acquire fuel performance properties from a core simulation. The GCPP refers to the thermal conductance of the gas filled gap between the fuel and cladding, and is of particular importance from a heat transfer standpoint. GCPP is of particular interest for proper initialization of LOCA simulations. The GCPP in FRAPCON is defined as

$$h = h_r + h_g + h_s \tag{4.6}$$

where h_r, h_g, and h_s are the conductance due to radiation, gas, and fuel cladding contact. These terms are define as

$$h_r = \sigma F \left(T_{fs}^2 + T_{ci}^2\right)\left(T_{fs} + T_{ci}\right) \tag{4.7}$$

$$h_g = \frac{k_{gas}}{d_{eff} + 1.8\left(g_f + g_c\right) - b + d} \tag{4.8}$$

$$h_s = \frac{C \cdot k_{mean} f\left(P_{rel}\right)}{\sqrt{R_f^2 + R_c^2 \cdot g\left(R_f\right)}} \tag{4.9}$$

In the radiation conductance F represents the effects of geometry and emissivity, T_{fs} and T_{ci} are fuel surface and inner cladding temperature respectively. In the gas conductance, k_{gas} is the gas thermal conductance, d_{eff} is the effective gap conductance which is a function of surface roughness and interfacial pressure, g_f and g_c are the temperature jump distances of the fuel and cladding respectively, b is a constant corrective term, and d is the open fuel cladding gap size. Lastly, in the solid conductance k_{mean} is the geometric mean of fuel and cladding thermal conductivity, P_{rel} is the ratio of interfacial pressure to Meyer hardness, R_f

and R_c are the surface roughness of fuel and cladding respectively, C is a constant which depends upon the range in which P_{rel} resides, f and g are arbitrary functions which also change based upon P_{rel}.

Results discussed in section 4.7.2 show little variation due to radiation, but high amounts due to gap dimensions and interfacial pressure. The shifting between models that occurs at the onset of fuel and cladding contact, as well as the switching between the functions within the gas and interfacial models themselves, result in atypical GCPP probability distributions which necessitate higher order methods to properly analyze.

4.5 Uncertainty Quantification

Uncertainty quantification determines the level of fidelity in a given output based upon input confidence intervals. UQ does not reflect inaccuracies or simplifications in the model calculations themselves. UQ requires sampling of all pertinent inputs over their range of uncertainty. UQ can be performed either by Wilks nonparametric statistical analysis method or Monte Carlo sampling method.

Wilks method requires a small number of samples and has been the method of choice in the traditional safety analyses. The Monte Carlo method, which is used in this work, provides more accurate estimates of FOM with reduced confidence intervals, but requires a large number of simulations. Both methods result in a sample of outputs, from which a 95/95 confidence interval is calculated. A 95/95 confidence interval as expressed in Eq. 4.10 and 4.11 contains 95% of the population with 95% certainty [24].

$$Y_{95/95} = \mu_{95\%} \pm 1.96 \cdot SE_{Q95\%} \tag{4.10}$$

$$SE_{Q95\%} = 2.11 \cdot SE_M \tag{4.11}$$

where $Y_{95/95}$ is the 95/95 confidence interval, $\mu_{95\%}$ is the 95th percentile value, and $SE_{Q95\%}$ and SE_M are standard error of $\mu_{95\%}$ and the mean respectively. Note that these

methods are based upon a Gaussian distributions, which while appropriate for MDNBR and MFCT, are currently lacking for GCPP results, and will be the focus of future research.

4.6 Global Sensitivity Measures for Sensitivity Analysis

With ever increasing computational power, sensitivity analyses have become more viable for expensive models such as VERA-CS. As opposed to the more primitive one-at-a-time methods (OAT), which entail varying one input while maintaining all others constant, global sensitivity analysis methods allow for concurrent perturbations of all inputs of interest. Here we focus on the regression based method of Pearson, variance based method of Sobol, and density-based delta moment independent measures [18].

4.6.1 Pearson Correlation Coefficients

Pearson correlation coefficients are found by Eq. 4.12,

$$R_i^2 = \frac{cov\left(X_i, Y\right)^2}{var\left(X_i\right) var\left(Y\right)} \tag{4.12}$$

where X_i and Y are the input and output random variables, $var()$ and $cov()$ are the variance and covariance operators, and R_i^2 is the Pearson measure squared (the squared values represent the contribution of an input to output variance for linear problems). The sampling is simple and requires no isolation of variables or partitioning of data as is recommended for higher order measures. However, for nonlinear relations, Pearson measures may indicate no correlation between strongly related variables. For instance the simple model $Y = X^2$, with a random sampling in $X \in (-1, 1)$, has a Pearson correlation coefficient value that nears zero as the sample size approaches infinity.

The Pearson measures do allow for an assessment of the linearity of the system. For a purely linear system, the sum of all Pearson values $\left(\sum_{i=1}^{N} R_i^2\right)$ is unity, with increases in nonlinearity resulting in a sum closer to zero.

4.6.2 Sobol Indices

The Sobol variance decomposition method compares the contribution of one input to the variance of an output. Sobol indices differ from Pearson correlation coefficients in that Pearson measures are based upon linear regression, while Sobol indices capture more complex interactions. Here only the first order terms are presented. Sobol indices are expressed mathematically in Eq. 4.13,

$$S_i = \frac{var\left(E\left(Y|X_i\right)\right)}{var\left(Y\right)} \tag{4.13}$$

where S_i is the Sobol indices, $Y|X_i$ represents Y conditional upon a fixed X_i, and $E()$ is the expected value operator. The sum of Sobol indices lies between zero (non-additive) and unity (additive). A sum of unity does not indicate homogeneity, thus if a proof of linearity is desired, it must be proven by other means (see section 4.6.1).

If Eq. 4.13 is strictly adhered to, an expensive double loop Monte Carlo method is required, as opposed to the more random sampling typically used for Pearson measures. Plischke's method allows for the partitioning of a typical random distribution into approximately equally spaced partitions based upon the rankings of a given input [25]. Estimators for the Sobol indices can be recast as Eq. 4.14,

$$\hat{S}_i = \frac{\frac{1}{N}\sum_{j=1}^{M} N_j var\left(Y|X_i \in x_{i,j}\right)}{var\left(Y\right)} \tag{4.14}$$

where $x_{i,j}$ represents partition j of input i, N_j is the population of partition j, M is the number of partitions, $Y|X_i \in x_{i,j}$ represents Y conditional upon X_i residing in $x_{i,j}$, and N is the total sample size. In order to reduce bias, the boot strapping method is used with 10 resamples with replacement. Sobol indices were calculated using the SA library in Python [26].

4.6.3 Delta Moment Independent Measures

The delta moment independent measures are a recent metric established by Borogonovo [18]. The delta measure is based upon the expected L^1 norm differences between conditional

and unconditional PDF for a given input. This is expressed mathematically in Eq. 4.15 and 4.16,

$$s_i\left(x_i\right) = \int \left| f_Y\left(y\right) - f_{Y|X_i=x_i}\left(y\right) \right| dy \tag{4.15}$$

$$\delta_i = \frac{1}{2} E\left(s_i\left(X_i\right)\right) = \frac{1}{2} \int f_{X_i}\left(x_i\right) s\left(x_i\right) dx_i \tag{4.16}$$

where y and x_i are the realizations of X_i and Y, $s_i\left(x_i\right)$ is the L^1 norm between the marginal density function $f_Y\left(y\right)$ and the conditional marginal density function $f_{Y|X_i=x_i}\left(y\right)$ (which requires that $X_i = x_i$), and δ_i is the delta moment independent measure. The delta measure is advantageous in that it is density based, meaning it captures complex relations which effect distribution but not necessarily mean or variance [18]. The summation of all delta indices is between zero and unity. Sums close to unity indicate that the contributions from a group of inputs on an output are separable from each other, while lower sums indicate the shifts in distribution are inseparable.

As with the Sobol method, delta measures ideally use a costly double loop Monte Carlo method. Delta measures are obtained from the truncated normal input distributions of this work through the methodology presented in [27], which contains similar partitioning strategies found in [25]. Using said methods, Eq. 4.15 and 4.16 are recast as Eq. 4.17 and 4.18,

$$s_i\left(X_i \in x_{i,j}\right) = \int \left| f_Y\left(y\right) - f_{Y|X_i \in x_{i,j}}\left(y\right) \right| dy \tag{4.17}$$

$$\hat{\delta}_i = \frac{1}{2N} \sum_{j=1}^{m} N_j s\left(X_i \in x_j\right) \tag{4.18}$$

where $x_{i,j}$ represents partition j of the input i, N_j is the population of partition j, M is the number of partitions, $f_{Y|X_i \in x_{i,j}}$ represents the PDF of Y conditional upon X_i residing in $x_{i,j}$, and N the total sample size. The integral used in Eq. 4.17 is estimated via kernel

density estimators. This work uses Gaussian kernels with reflection boundary condition and bandwidth selection using the diffusion methods established in [28]. Delta measures were calculated using Python library SALib [26], which was modified to use PyQt-fit [29] to perform the aforementioned kernel density estimate.

Plischke *et al.* explored KS testing and bootstrapping methods as bias reducing methods [27]. Bootstrapping methods remove bias but never entirely, thus even completely negligible inputs will always yield some small finite values. KS testing has the advantage of zeroing out negligible inputs completely, but at the cost of removing legitimate small effects. For the purposes of this work, the KS testing is preferable, as the summation of all delta measures obtained through extensive bootstrapping would at time yields summations in excess of 4.0 due to noise stemming from partitioning and the kernel density estimates.

4.7 Results

Results are split into the UQ section which reports 95th percentile and their standard error, and the SA section which reports the SA metrics with corresponding ranks between all inputs and outputs. The SA section also includes select PDF for GCPP in the interests of explaining the behavior of specific inputs.

4.7.1 Uncertainty Quantification

The 95th percentile values and corresponding standard errors of MDNBR for the end of cycle (EOC) 1, 2 and 3 are shown in Fig. 4.3, 4.4, and 4.5 respectively.

The increases in MDNBR are reflective of the decreases in core power for each fuel cycle (see Table 4.2). The MDNBR 95th percentile value is relatively consistent across the assembly and the standard error remains proportional to the 95th percentile value for all states. The 95th percentile values and corresponding standard errors of MFCT for the end of each power cycle are shown in Fig. 4.6, 4.7, and 4.8.

The decreases in MFCT correspond to the core power of each cycle (see Table 4.2). Fig. 4.6 and 4.7 essentially only differ in scale, with the highest power pins corresponding to both the highest 95th percentile and standard error. Fig. 4.8 shows maximum uncertainty occurs

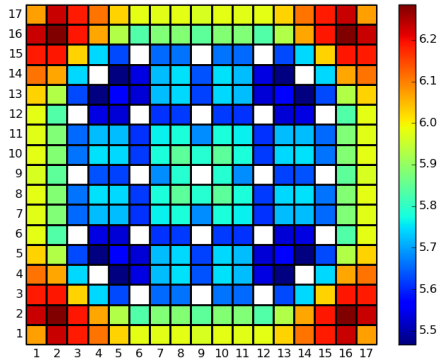

(a) 95th Percentile Value.

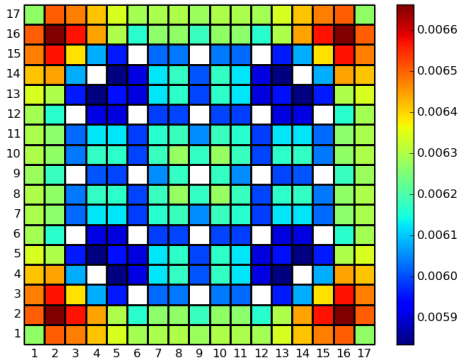

(b) +/- 95% Confidence Interval.

Fig. 4.3: Assembly View of 95/95 Confidence Interval for MDNBR at EOC 1.

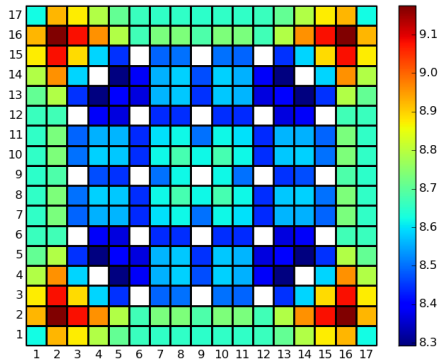

(a) 95th Percentile Value.

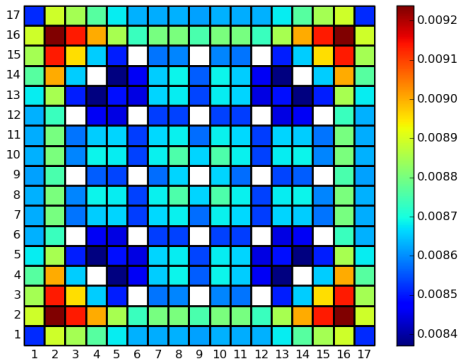

(b) +/- 95% Confidence Interval.

Fig. 4.4: Assembly View of 95/95 Confidence Interval for MDNBR at EOC 2.

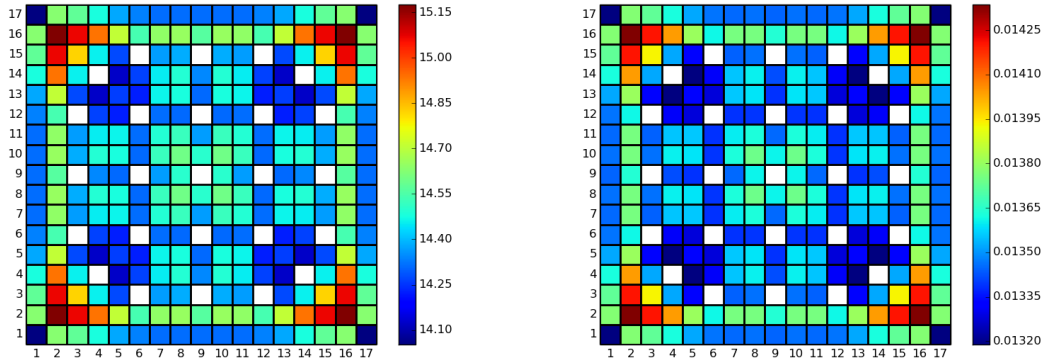

(a) 95th Percentile Value.

(b) +/- 95% Confidence Interval.

Fig. 4.5: Assembly View of 95/95 Confidence Interval for MDNBR at EOC 3.

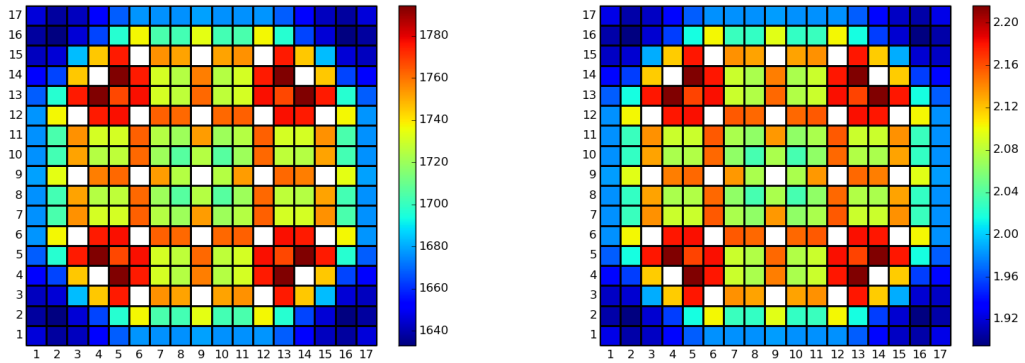

(a) 95th Percentile Value.

(b) +/- 95% Confidence Interval.

Fig. 4.6: Assembly View of 95/95 Confidence Interval for °MFCT at EOC 1.

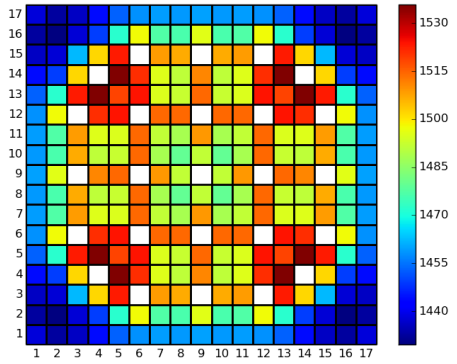

(a) 95th Percentile Value.

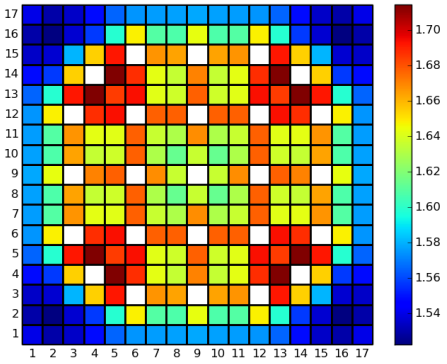

(b) +/- 95% Confidence Interval.

Fig. 4.7: Assembly View of 95/95 Confidence Interval for °MFCT at EOC 2.

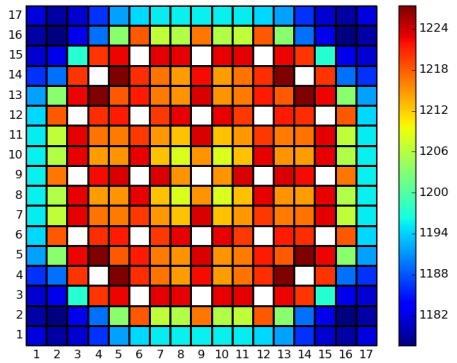

(a) 95th Percentile Value.

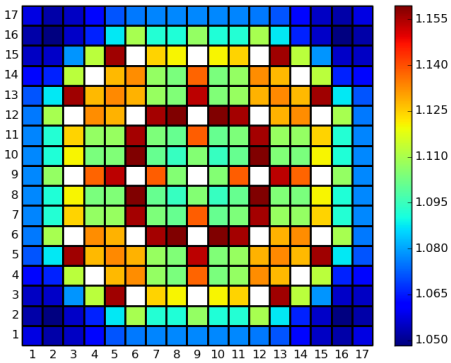

(b) +/- 95% Confidence Interval.

Fig. 4.8: Assembly View of 95/95 Confidence Interval for MFCT (°F) at EOC 3.

at pins with a specific intermediate power level. This is likely due to complex behaviors in gap conductance which effect the MFCT, as evidenced by similar characteristics between Fig. 4.8(b) and 4.11(b). The GCPP for the end of each power cycle are shown in Fig. 4.9, 4.10, and 4.11.

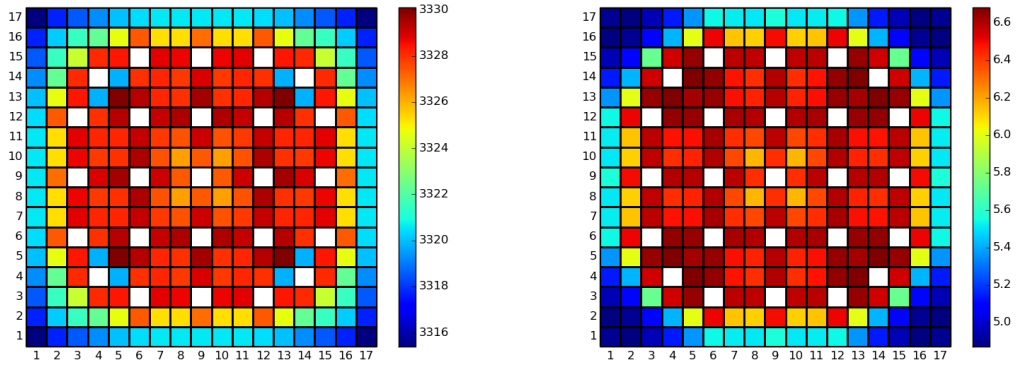

(a) 95th Percentile Value.

(b) +/- 95% Confidence Interval.

Fig. 4.9: Assembly View of 95/95 Confidence Interval for GCPP ($\frac{BTU}{hr \cdot ft^2 \cdot ^\circ F}$) at EOC 1.

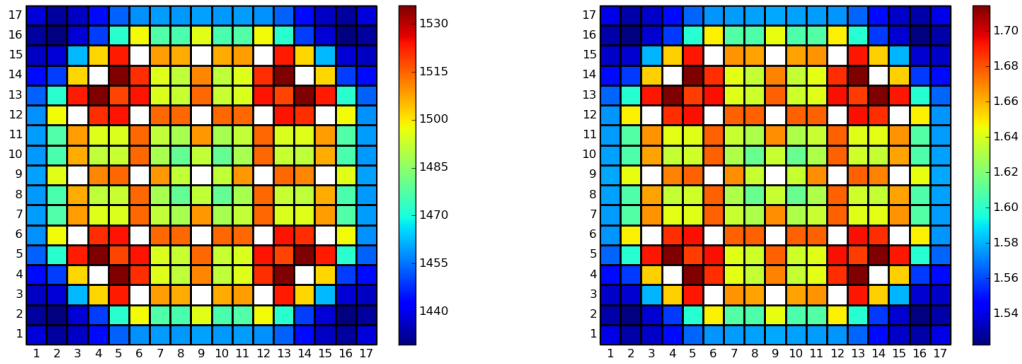

(a) 95th Percentile Value.

(b) +/- 95% Confidence Interval.

Fig. 4.10: Assembly View of 95/95 Confidence Interval for GCPP ($\frac{BTU}{hr \cdot ft^2 \cdot ^\circ F}$) at EOC 2.

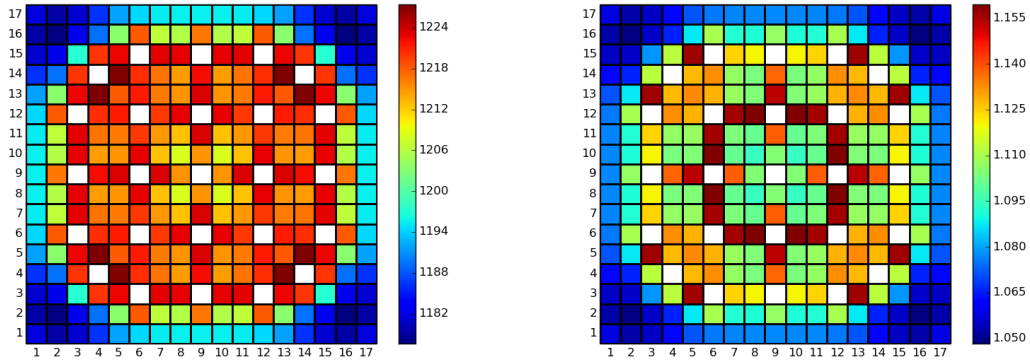

(a) 95th Percentile Value.

(b) +/- 95% Confidence Interval.

Fig. 4.11: Assembly View of 95/95 Confidence Interval for GCPP ($\frac{BTU}{hr \cdot ft^2 \cdot ^\circ F}$) at EOC 3.

The UQ of Fig. 4.9-4.11 hints at the complexity of GCPP which will be further elucidated in section 4.7.2. The abrupt switching between fundamentally different models causes non-monotonic distributions of gap conductance with respective to pin power. Note that unlike MDNBR and MFCT, all of the GCPP 95th percentile and standard error distributions have different characteristics.

4.7.2 Sensitivity Analysis

LOTUS treats all FOM for each pin as outputs, which results in 792 outputs. Delta measures (for each pin) between the MDNBR with outlet pressure and inlet temperature are shown in Fig. 4.12.

Clearly the variation between the pins is different for outlet pressure than for inlet temperature. MDNBR is related to outlet pressure through a complex relation based upon pin power as well as a pin proximity to the assembly edge. Conversely, MDNBR dependence on inlet temperature is a simple relation, with higher power pins being more sensitive to inlet temperature. Although these insights are of value, to report all relations for 23 inputs, at 32 states, with 3 SA measures, is impractical. Since the pin by pin variation is relatively small for MDNBR and MFCT, an assembly averaged ranking is a reasonable metric for representing all pin values.

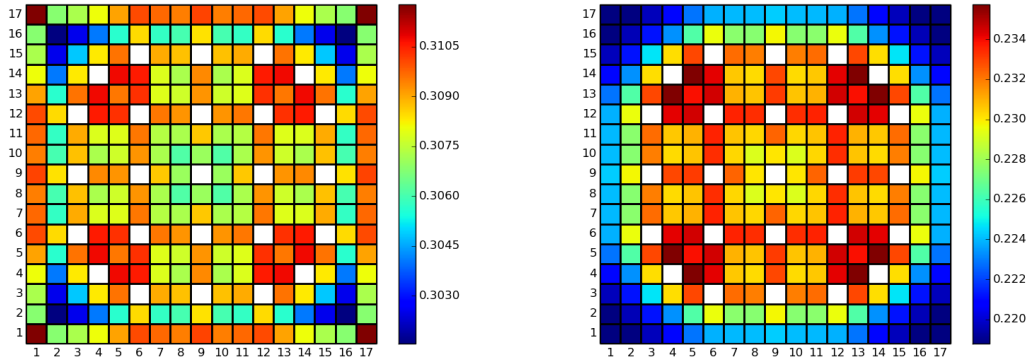

(a) Outlet Pressure

(b) Inlet Temperature

Fig. 4.12: Assembly View of Select Pearson Squared Coefficients of MDNBR.

Sensitivity Analysis of Minimum Departure from Nucleate Boiling Ratio Point

Results for MDNBR at the end of each power cycle are found in Tables 4.3 through 4.5.

The vast majority of variance in MDNBR comes from the core power percentage, inlet temperature, and outlet pressure. Additional influence stems from the rated flow and cladding outer radius, due to their effects on heat transfer and the heat flux surface area respectively. While the rankings do change between each power cycle, the actual changes in the SA measures are relatively small. A change in ranking only occurs due to the proximity of the top three SA measures to each other.

The top five rankings are consistent between the three SA measures for each of the power cycles, indicating good fidelity. All other factors have less than a 1.4% effect on MDNBR, and hence have inconsistent rankings due to SA methodology and noise from the partitioning strategy and kernel density estimations.

Summation of Pearson correlation coefficients indicates approximately 97% of the variance stems from linear terms. Linearity is further established by the fact that $R_i^2 \approx S_i$ for all relevant inputs.

The delta measures do not sum to unity due to the KS testing, which while effective in removing noise, often removes legitimate minor contributions. Thus while the summation

Table 4.3: Assembly averaged Pearson squared (R_i^2), Sobol (S_i), and Delta Moment Independent Measures (δ_i) and corresponding ranks for MDNBR at End of Fuel Cycle 1 (24 MWd/kgU Burnup).

Input Name	r_R	R_i^2	r_S	S_i	r_δ	δ_i
Core Power	1	0.268593	1	0.267411	1	0.173433
Inlet Temperature	3	0.234082	3	0.234029	3	0.159895
Outlet Pressure	2	0.265176	2	0.266936	2	0.167211
Rated Flow	4	0.11744	4	0.11753	4	0.098321
Void Drift Coefficient	14	0.000365	9	0.007612	19	8.24E-05
Turbulent Mixing Coefficient	9	0.000827	6	0.009638	22	0
Direct Mod. Heating Fraction	6	0.001618	7	0.008146	7	0.013405
Fuel Radius	11	0.00074	14	0.005109	18	0.000248
Clad Inner Radius	7	0.001611	16	0.004655	14	0.006049
Clad Outer Radius	5	0.072442	5	0.077913	5	0.069227
Fuel Density	10	0.000779	20	0.003351	22	0
Fuel Enrichment	20	7.49E-05	15	0.004893	13	0.00606
End Spacer Grid Form Loss	17	0.000238	12	0.005646	8	0.012154
Mid Spacer Grid Form Loss	12	0.000735	11	0.005846	6	0.013803
Plenum Fill Gas Pressure	13	0.000368	13	0.005562	16	0.00291
Fuel Thermal Conductivity	23	5.62E-06	21	0.002842	22	0
Fuel Thermal Expansion	8	0.001525	10	0.006703	17	0.002076
Fission Gas Release	21	5.97E-05	17	0.004449	22	0
Fuel Swelling	22	3.18E-05	22	0.002575	12	0.006298
Cladding Creep	18	0.000217	8	0.007745	11	0.006313
Cladding Axial Growth	15	0.000315	19	0.004043	9	0.011451
Cladding Corrosion	19	0.000211	23	0.001642	15	0.005652
Cladding Hydrogen Concentration	16	0.000253	18	0.00428	10	0.010899
Summation of Measures		0.967708		1.058555		0.765487

Table 4.4: Assembly averaged Pearson squared (R_i^2), Sobol (S_i), and Delta Moment Independent Measures (δ_i) and corresponding ranks for MDNBR at End of Fuel Cycle 2 (43 MWd/kgU Burnup).

Input Name	r_R	R_i^2	r_S	S_i	r_δ	δ_i
Core Power	2	0.259302	2	0.258528	2	0.170445
Inlet Temperature	3	0.22645	3	0.226718	3	0.150957
Outlet Pressure	1	0.279997	1	0.281642	1	0.172764
Rated Flow	4	0.108685	4	0.10892	4	0.083726
Void Drift Coefficient	14	0.000337	9	0.007459	17	0
Turbulent Mixing Coefficient	11	0.000802	6	0.009567	17	0
Direct Mod. Heating Fraction	6	0.001864	7	0.008628	6	0.013564
Fuel Radius	9	0.000965	14	0.005275	17	0
Clad Inner Radius	7	0.001594	16	0.004619	17	0
Clad Outer Radius	5	0.084568	5	0.08994	5	0.073978
Fuel Density	10	0.000864	20	0.003426	17	0
Fuel Enrichment	20	7.96E-05	15	0.004882	17	0
End Spacer Grid Form Loss	17	0.000197	13	0.005515	8	0.006452
Mid Spacer Grid Form Loss	12	0.000574	11	0.005735	7	0.006527
Plenum Fill Gas Pressure	13	0.000389	12	0.005629	17	0
Fuel Thermal Conductivity	23	2.32E-06	21	0.002882	17	0
Fuel Thermal Expansion	8	0.001553	10	0.006732	17	0
Fission Gas Release	21	5.30E-05	17	0.004429	17	0
Fuel Swelling	22	3.39E-05	22	0.002597	17	0
Cladding Creep	19	0.000158	8	0.007617	9	0.006415
Cladding Axial Growth	15	0.000283	19	0.004099	17	0
Cladding Corrosion	18	0.000172	23	0.00168	17	0
Cladding Hydrogen Concentration	16	0.000242	18	0.004215	17	0
Summation of Measures		0.969164		1.060734		0.684828

Table 4.5: Assembly averaged Pearson squared (R_i^2), Sobol (S_i), and Delta Moment Independent Measures (δ_i) and corresponding ranks for MDNBR at End of Fuel Cycle 3 (52 MWd/kgU Burnup).

Core Power	3	0.22589	3	0.225694	2	0.157725
Inlet Temperature	2	0.228224	2	0.228527	3	0.152285
Outlet Pressure	1	0.307992	1	0.309263	1	0.183499
Rated Flow	4	0.100849	5	0.101441	4	0.086879
Void Drift Coefficient	14	0.000295	8	0.007417	18	0
Turbulent Mixing Coefficient	10	0.000741	6	0.00942	18	0
Direct Mod. Heating Fraction	6	0.002201	7	0.009194	6	0.013568
Fuel Radius	11	0.000705	14	0.00507	18	0
Clad Inner Radius	7	0.001627	16	0.004602	12	0.000646
Clad Outer Radius	5	0.097772	4	0.102957	5	0.078806
Fuel Density	9	0.000783	20	0.003398	18	0
Fuel Enrichment	20	6.54E-05	15	0.004882	11	0.002313
End Spacer Grid Form Loss	17	0.000157	13	0.00545	9	0.006242
Mid Spacer Grid Form Loss	12	0.000598	11	0.005851	7	0.006691
Plenum Fill Gas Pressure	13	0.000399	12	0.005469	18	0
Fuel Thermal Conductivity	23	3.00E-07	21	0.002947	18	0
Fuel Thermal Expansion	8	0.001515	10	0.006782	18	0
Fission Gas Release	21	6.14E-05	17	0.004483	18	0
Fuel Swelling	22	3.99E-05	22	0.002626	10	0.003687
Cladding Creep	18	0.000104	9	0.007373	8	0.006555
Cladding Axial Growth	15	0.00026	18	0.004297	18	0
Cladding Corrosion	19	0.0001	23	0.001772	18	0
Cladding Hydrogen Concentration	16	0.000236	19	0.004151	18	0
Summation of Measures		0.970613		1.063067		0.698895

Table 4.6: Assembly averaged Pearson squared (R_i^2), Sobol (S_i), and Delta Moment Independent Measures (δ_i) and corresponding ranks for MFCT at End of Fuel Cycle 1 (24 MWd/kgU Burnup).

Core Power	5	0.024648	5	0.029556	4	0.033055
Inlet Temperature	13	0.000558	11	0.005898	17	0
Outlet Pressure	16	7.89E-05	20	0.004294	10	0.005831
Rated Flow	22	8.21E-06	19	0.004844	17	0
Void Drift Coefficient	8	0.001777	8	0.010552	17	0
Turbulent Mixing Coefficient	14	0.000134	21	0.004144	17	0
Direct Mod. Heating Fraction	11	0.001225	22	0.003996	17	0
Fuel Radius	3	0.087284	3	0.08915	3	0.065213
Clad Inner Radius	2	0.347893	2	0.348355	2	0.19298
Clad Outer Radius	17	7.74E-05	10	0.006245	7	0.014194
Fuel Density	6	0.019287	6	0.024938	6	0.015643
Fuel Enrichment	12	0.000619	17	0.005273	17	0
End Spacer Grid Form Loss	21	1.40E-05	14	0.00568	8	0.008638
Mid Spacer Grid Form Loss	15	8.87E-05	16	0.005309	17	0
Plenum Fill Gas Pressure	20	1.64E-05	15	0.005565	17	0
Fuel Thermal Conductivity	1	0.490859	1	0.491358	1	0.280868
Fuel Thermal Expansion	4	0.040786	4	0.043415	5	0.031547
Fission Gas Release	23	4.08E-06	13	0.005758	17	0
Fuel Swelling	9	0.001371	12	0.005841	9	0.006021
Cladding Creep	10	0.001299	9	0.007618	17	0
Cladding Axial Growth	18	5.17E-05	23	0.001693	17	0
Cladding Corrosion	7	0.006767	7	0.012188	17	0
Cladding Hydrogen Concentration	19	2.60E-05	18	0.005096	17	0
Summation of Measures		1.024873		1.126767		0.65399

of delta measures is low, the influence of the inputs is still likely separable from each other as defined by Borogonov [18]. To summarize, MDNBR depends almost entirely on linear relations with thermal hydraulic factors and core power. The relations show very little variation throughout fuel lifecycle in the core.

Sensitivity Analysis of Maximum Fuel Centerline Temperature

SA measures for MFCT at low burnup, onset of contact, and high burnup are shown in tables 4.6 through 4.8.

The MFCT is highly linear with a summation of roughly one, thus the Pearson measures have high fidelity. However, unlike MDNBR, certain measures do change over the

Table 4.7: Assembly averaged Pearson squared (R_i^2), Sobol (S_i), and Delta Moment Independent Measures (δ_i) and corresponding ranks for MFCT at End of Fuel Cycle 2 (43 MWd/kgU Burnup).

Core Power	2	0.061934	2	0.066016	2	0.058285
Inlet Temperature	6	0.002822	11	0.005094	8	0.00673
Outlet Pressure	7	0.000832	8	0.00629	21	0
Rated Flow	22	5.89E-06	23	0.002028	14	0.001474
Void Drift Coefficient	9	0.000694	6	0.007236	12	0.003418
Turbulent Mixing Coefficient	19	0.000137	22	0.002172	21	0
Direct Mod. Heating Fraction	18	0.000144	19	0.003295	6	0.007264
Fuel Radius	10	0.000654	7	0.006751	16	0.000209
Clad Inner Radius	5	0.00417	5	0.010068	13	0.002434
Clad Outer Radius	8	0.00078	10	0.005743	11	0.005442
Fuel Density	3	0.061605	3	0.065916	3	0.04815
Fuel Enrichment	13	0.000272	20	0.003046	10	0.006307
End Spacer Grid Form Loss	15	0.000188	16	0.004015	5	0.007963
Mid Spacer Grid Form Loss	20	6.53E-05	21	0.002462	21	0
Plenum Fill Gas Pressure	21	7.31E-06	17	0.003815	15	0.000279
Fuel Thermal Conductivity	1	0.845456	1	0.8369	1	0.538135
Fuel Thermal Expansion	14	0.000209	9	0.006212	9	0.006346
Fission Gas Release	23	4.34E-06	15	0.004221	21	0
Fuel Swelling	17	0.000152	18	0.003389	17	0.000183
Cladding Creep	12	0.000378	14	0.004269	21	0
Cladding Axial Growth	11	0.000418	12	0.004691	7	0.007069
Cladding Corrosion	4	0.013984	4	0.023164	4	0.026669
Cladding Hydrogen Concentration	16	0.000164	13	0.004481	21	0
Summation of Measures		0.995072		1.081274		0.726357

Table 4.8: Assembly averaged Pearson squared (R_i^2), Sobol (S_i), and Delta Moment Independent Measures (δ_i) and corresponding ranks for MFCT at End of Fuel Cycle 3 (52 MWd/kgU Burnup).

Core Power	2	0.080247	2	0.083861	2	0.074936
Inlet Temperature	5	0.010396	5	0.013041	7	0.011376
Outlet Pressure	8	0.001043	10	0.006102	23	0
Rated Flow	22	1.25E-05	22	0.00247	16	0.004377
Void Drift Coefficient	11	0.000604	9	0.006874	9	0.007167
Turbulent Mixing Coefficient	21	3.13E-05	21	0.002476	18	0.000731
Direct Mod. Heating Fraction	14	0.000143	18	0.003276	10	0.006682
Fuel Radius	9	0.000923	6	0.007331	11	0.006576
Clad Inner Radius	13	0.000186	12	0.004825	19	0.000453
Clad Outer Radius	6	0.002582	7	0.007256	17	0.003697
Fuel Density	3	0.069351	3	0.073641	3	0.057501
Fuel Enrichment	17	0.000113	20	0.002785	12	0.006543
End Spacer Grid Form Loss	12	0.000248	13	0.004632	8	0.011356
Mid Spacer Grid Form Loss	20	4.24E-05	23	0.002261	21	0.000182
Plenum Fill Gas Pressure	19	4.64E-05	15	0.003926	13	0.006503
Fuel Thermal Conductivity	1	0.808941	1	0.799918	1	0.50573
Fuel Thermal Expansion	7	0.001053	8	0.007117	6	0.011636
Fission Gas Release	23	3.11E-06	17	0.003554	20	0.000371
Fuel Swelling	15	0.000141	19	0.003265	15	0.004805
Cladding Creep	18	4.70E-05	16	0.003594	23	0
Cladding Axial Growth	10	0.000613	11	0.005196	5	0.011835
Cladding Corrosion	4	0.020194	4	0.025512	4	0.023923
Cladding Hydrogen Concentration	16	0.000137	14	0.00445	14	0.0061
Summation of Measures		0.997098		1.077365		0.762483

fuel lifecycle. The Pearson squared value of fuel thermal conductivity begins at 0.5, with substantial forms of uncertainty also stemming from the effects of cladding inner radius and fuel radius on gap thickness. As the gap closes, influence of geometric inputs is reduced near zero, resulting in nearly all remaining variance (85%) being attributable to fuel thermal conductivity.

As burnup continues after contact, core power and fuel density begin to play larger roles in MFCT due to their impact on burnup which in turn affects fuel thermal conductivity. Note also the very small role of cladding corrosion on MFCT, caused by the insulating effect of zirconium dioxide, a phenomenon which will play a key role on GCPP as discussed in the following section.

Sensitivity Analysis of Gap Conductance at Peak Power

Due to the nonlinear nature of GCPP, the assembly averaging involved in the presentation of MDNBR and MFCT is inadequate as evidenced by Fig. 4.13.

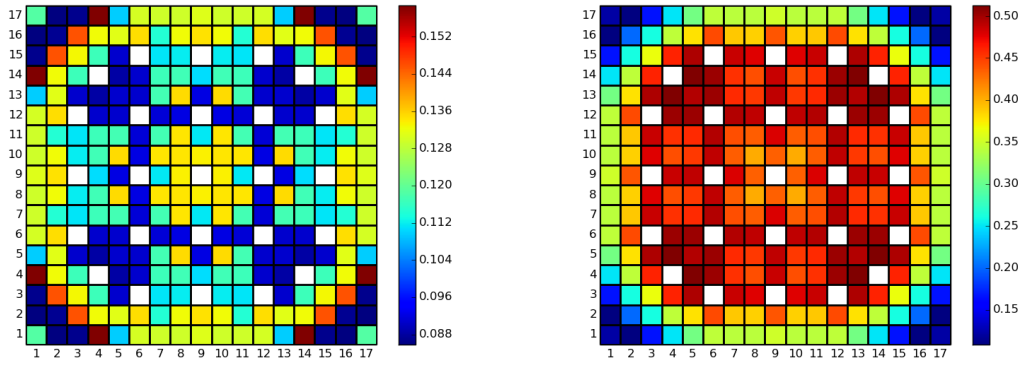

(a) Fuel Radius

(b) Corrosion Biasing

Fig. 4.13: Assembly View of Select Delta Momenta Independent Measures of GCPP.

The dependence of GCPP on fuel radius and corrosion bias varies on a pin basis by a factor of 2 and 3 respectively. Since assembly averaging is inappropriate, all SA data for GCPP is from the highest power pin. As the fuel cycle progresses, the GCPP probability

distribution shifts and blends three distinct profiles: a normal distribution with a range of approximately 1000 $\frac{BTU}{hr \cdot ft^{2} \cdot ^{\circ}F}$ (5678.26 $\frac{W}{m^{2} \cdot K}$), bimodal distribution with a range of roughly 45 $\frac{BTU}{hr \cdot ft^{2} \cdot ^{\circ}F}$ (255.52 $\frac{W}{m^{2} \cdot K}$), and a normal distribution with a range of roughly 300 $\frac{BTU}{hr \cdot ft^{2} \cdot ^{\circ}F}$ (1703.48 $\frac{W}{m^{2} \cdot K}$). These three distributions represent the open-gap model, low pressure closed-gap, and high pressure contact/high burnup closed-gap models respectively.

Five states are reported which correspond to open-gap modeling, a mixture of open-gap and low pressure closed-gap, predominantly closed-gap at low interfacial pressure, a combination of low and high pressure closed-gap, and finally a high pressure/high burnup closed-gap modeling. All five states have significantly different rankings and degrees of nonlinearity. PDF are plotted in order to help visualize the model shifts. These PDFs are overlaid with PDF conditional upon select inputs lying within a given range. While the Sobol and delta measures reported use 14 partitions, the plotting in this report use quartiles so as to make the figures more readable. The plotted conditional PDF have a heuristic value in elucidating differences between moment and density based SA measures.

As evidenced by high Pearson and Sobol summations, this pre-contact state is relatively linear, thus moment based methods are reliable. Both Pearson and Sobol measures indicate roughly 80% of uncertainty coming from the fuel radius and inner cladding radius, with another 10% stemming from fuel thermal expansion. This is to be expected as the gap distance ranges between 5.5 and 11.4 mm (see Table 4.2), which with all else held constant, may cause the gap conductance to change by as much as 107%.

Fig. 4.14 shows the GCPP maximum to be more than double the minimum, with a range of 1000 $\frac{BTU}{hr \cdot ft^{2} \cdot ^{\circ}F}$ (5678.26 $\frac{W}{m^{2} \cdot K}$). Partitioning with respect to fuel radius confirms intuition that with larger radii the GCPP increases. Conversely, with increases in cladding radius gap conductance decreases. The narrowing and translation of the conditional PDF as compared to the unconditional PDF in Fig. 4.14(a) explain both the high delta measure and variance based measures for clad inner radius.

The summation of Pearson and Sobol measures in Table 4.10 indicates that GCPP relations still contains linear terms, but nonlinear effects are present. Note that for cladding

Table 4.9: High Power Pin Pearson squared (R_i^2), Sobol (S_i), and Delta Moment Independent Measures (δ_i) and corresponding ranks for GCPP at 2 MWd/kgU Burnup.

Core Power	7	0.002951	16	0.005046	4	0.013646
Inlet Temperature	19	0.000041	8	0.007326	8	0.007639
Outlet Pressure	6	0.00325	15	0.005379	15	0.005917
Rated Flow	15	0.000228	5	0.008618	7	0.008609
Void Drift Coefficient	11	0.000836	20	0.004214	18	0
Turbulent Mixing Coefficient	20	0.000038	12	0.00584	11	0.006926
Direct Mod. Heating Fraction	10	0.000943	21	0.004143	18	0
Fuel Radius	2	0.155273	2	0.159726	3	0.103298
Clad Inner Radius	1	0.653846	1	0.660381	1	0.389924
Clad Outer Radius	23	0.000014	11	0.006342	18	0
Fuel Density	5	0.003834	7	0.00849	6	0.012572
Fuel Enrichment	16	0.000214	4	0.010155	5	0.012832
End Spacer Grid Form Loss	14	0.00025	18	0.004705	9	0.007551
Mid Spacer Grid Form Loss	22	0.000032	14	0.005434	17	0.005873
Plenum Fill Gas Pressure	17	0.000135	17	0.004818	18	0
Fuel Thermal Conductivity	4	0.005883	6	0.008507	10	0.007494
Fuel Thermal Expansion	3	0.113405	3	0.115846	2	0.107546
Fission Gas Release	21	0.000034	19	0.004524	18	0
Fuel Swelling	8	0.002842	10	0.007012	14	0.005956
Cladding Creep	9	0.001044	9	0.007154	13	0.0062
Cladding Axial Growth	12	0.000824	22	0.004133	16	0.005887
Cladding Corrosion	13	0.000554	23	0.003618	18	0
Cladding Hydrogen Concentration	18	0.00012	13	0.005504	12	0.006248
Summation of Measures		0.946589		1.056921		0.71412

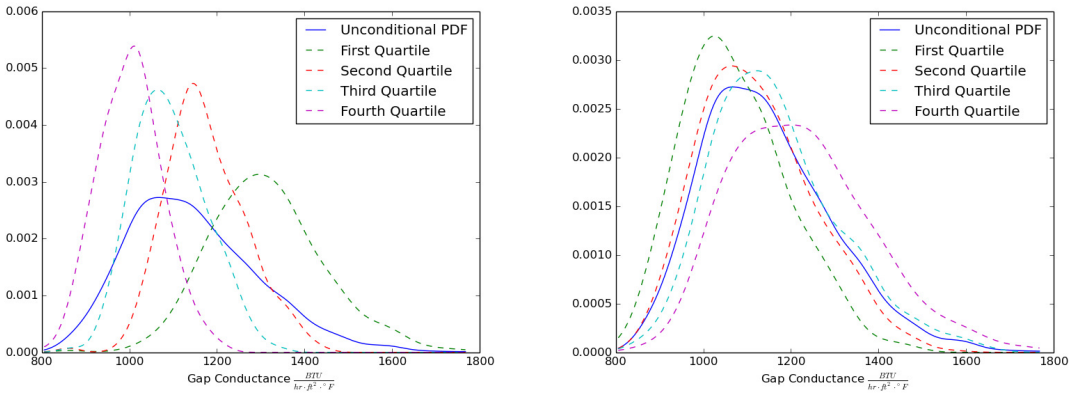

(a) Cladding Inner Radius

(b) Fuel Radius

Fig. 4.14: Unconditional PDF with PDF Conditional upon Select Inputs Lying within a Specified Quartile of Respective Sample at Burnup of 2 MWD/kgU.

Table 4.10: High Power Pin Pearson squared (R_i^2), Sobol (S_i), and Delta Moment Independent Measures (δ_i) and corresponding ranks for GCPP at 9 MWd/kgU Burnup.

Core Power	7	0.004551	6	0.009557	5	0.097208
Inlet Temperature	8	0.002578	14	0.00558	8	0.034953
Outlet Pressure	10	0.002205	9	0.006943	11	0.018445
Rated Flow	15	0.000733	13	0.00567	10	0.018507
Void Drift Coefficient	18	0.000271	18	0.004445	12	0.01797
Turbulent Mixing Coefficient	13	0.001291	16	0.005019	17	0
Direct Mod. Heating Fraction	17	0.000358	22	0.002713	9	0.019256
Fuel Radius	3	0.077755	3	0.08226	6	0.088087
Clad Inner Radius	1	0.279101	1	0.319894	2	0.278173
Clad Outer Radius	12	0.001567	8	0.00823	17	0
Fuel Density	9	0.002381	11	0.006022	7	0.035711
Fuel Enrichment	14	0.001029	12	0.005675	16	0.017395
End Spacer Grid Form Loss	19	0.000207	23	0.002339	17	0
Mid Spacer Grid Form Loss	22	0.00009	17	0.004614	17	0
Plenum Fill Gas Pressure	21	0.000108	20	0.00349	13	0.017894
Fuel Thermal Conductivity	11	0.001825	15	0.005377	17	0
Fuel Thermal Expansion	4	0.053019	4	0.06268	4	0.098393
Fission Gas Release	20	0.000114	21	0.00334	15	0.017807
Fuel Swelling	6	0.005367	7	0.008299	17	0
Cladding Creep	2	0.133758	2	0.139824	3	0.193599
Cladding Axial Growth	23	0.000067	19	0.00428	14	0.017848
Cladding Corrosion	5	0.035894	5	0.05554	1	0.512664
Cladding Hydrogen Concentration	16	0.000561	10	0.006086	17	0
Summation of Measures		0.604828		0.757878		1.48391

corrosion biasing, Pearson and Sobol values of 0.036 and 0.056 are dwarfed by a delta measure of 0.513. This discrepancy is explained in the PDF in Fig. 4.15(a).

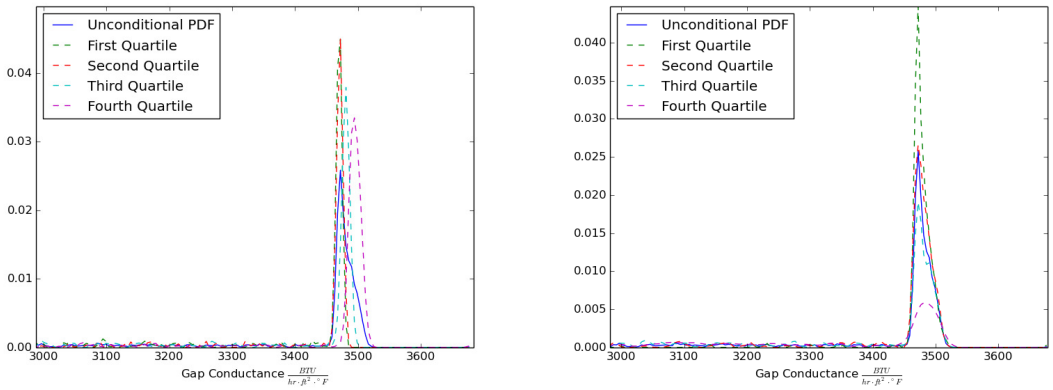

(a) Corrosion Biasing

(b) Cladding Inner Radius

Fig. 4.15: Unconditional PDF with PDF Conditional upon Select Inputs Lying within a Specified Quartile of Respective Sample at Burnup of 9 MWD/kgU.

The PDF in Fig. 4.15 are cropped to gain a clearer view of the narrow clustering of data, however the entire data set begins at roughly 1500 $\frac{BTU}{hr \cdot ft^{2} \cdot ^{\circ}F}$ (8517.39 $\frac{W}{m^{2} \cdot K}$). The data outside of the narrow cluster is relatively noisy. This is caused by the bandwidth selection being influenced by the tight grouping, resulting in an overly small bandwidth for data less than 3450 $\frac{BTU}{hr \cdot ft^{2} \cdot ^{\circ}F}$ (19590.00 $\frac{W}{m^{2} \cdot K}$).

The influence of cladding inner radius is fundamentally different than that of corrosion biasing. Cladding inner radius largely dictates whether a fuel rod experiences contact. From Fig. 4.15(b), the fourth quartile of radii contains far fewer data in the narrow range associated with contact, while the first quartile contains a large amount of points in said range.

Since PDFs by definition contain the same net amount of area, by deduction the fourth quartile contains more data in the wider finite gap thickness range than the first quartile. Thus the variance of the expected values of the partitions is high, meaning such shifts are detectable by variance based techniques. Cladding corrosion however causes a lateral shift

in the closed-gap data (as indicated by the displacement of the narrow distribution), but does not influence shifting from open to closed-gap models. Hence the expected values between partitions have low variance, resulting in low variance based measures. Therefore, only density based methods are able to fully detect this sensitivity.

The influence of cladding corrosion on GCPP is counter intuitive as it effects only water side zirconium dioxide build up. This layer acts as an insulator which raises the cladding, gap, and fuel temperature by as much as 10 . This rise causes a 1.3% increase in gas thermal conductivity [30], which in turn may increase a base gap conductivity of 3350 $\frac{BTU}{hr \cdot ft^{2} \cdot ^{\circ}F}$ (19022.18 $\frac{W}{m^{2} \cdot K}$) by 45 $\frac{BTU}{hr \cdot ft^{2} \cdot ^{\circ}F}$ (255.52 $\frac{W}{m^{2} \cdot K}$).

Note also that the first two quartiles in Fig. 4.15(a) are nearly identical, with some change occurring in the third, and large change occurring in the fourth. This is due to the fact that with negative to near zero biasing no zirconium dioxide build up occurs, hence no change in GCPP is observed. Corrosion biasing begins to affect GCPP only once a threshold is passed.

In the finite gap conductance or later high pressure/high burnup phase, a 45 $\frac{BTU}{hr \cdot ft^{2} \cdot ^{\circ}F}$ (255.52 $\frac{W}{m^{2} \cdot K}$) change would be insubstantial. However, in the initial contact phase where little variance occurs, the changes resulting from corrosion biasing are the largest present.

Note that the primary purpose of achieving high gap conductance is to facilitate heat transfer from the fuel rods to the coolant. Therefore, while a layer of oxidation does increase GCPP, it is far from desirable from a design perspective, as it comes at the cost of increasing the total thermal resistance between fuel and coolant. It is important to reemphasize the purpose of analyzing GCPP. Although insights into the behavior of GCPP are of value, the primary purpose of this exercise is to demonstrate the abilities of the SA measures available in the LOTUS toolkit to elucidate complex nonlinear behavior.

At a burnup of 14 MWd/kgU the highest amount of nonlinearity among states recorded is reached with a Pearson summation of 0.21, meaning nonlinear effects account for nearly 80% of the variance. Hence Pearson and Sobol methods prove unreliable, and emphasis is placed on the delta measures. The two largest contributing factors are the cladding

Table 4.11: High Power Pin Pearson squared (R_i^2), Sobol (S_i), and Delta Moment Independent Measures (δ_i) and corresponding ranks for GCPP at 14 MWd/kgU Burnup.

Core Power	14	0.00053	17	0.004572	4	0.044601
Inlet Temperature	6	0.004276	6	0.009828	2	0.112996
Outlet Pressure	9	0.002395	12	0.005535	11	0
Rated Flow	18	0.000055	19	0.003347	11	0
Void Drift Coefficient	17	0.000062	9	0.006458	11	0
Turbulent Mixing Coefficient	11	0.002203	16	0.004672	11	0
Direct Mod. Heating Fraction	13	0.000728	18	0.003839	8	0.012677
Fuel Radius	5	0.016811	5	0.021763	11	0
Clad Inner Radius	1	0.063653	1	0.088364	3	0.061565
Clad Outer Radius	20	0.000003	8	0.006768	11	0
Fuel Density	8	0.00261	10	0.006114	9	0.012417
Fuel Enrichment	12	0.000985	20	0.003019	11	0
End Spacer Grid Form Loss	22	0.000002	21	0.002834	11	0
Mid Spacer Grid Form Loss	19	0.000024	11	0.005751	11	0
Plenum Fill Gas Pressure	20	0.000003	13	0.00538	11	0
Fuel Thermal Conductivity	10	0.002184	15	0.004784	11	0
Fuel Thermal Expansion	4	0.022454	4	0.029222	6	0.014682
Fission Gas Release	16	0.000064	23	0.001347	10	0.012015
Fuel Swelling	7	0.004191	7	0.008932	11	0
Cladding Creep	2	0.046335	3	0.049137	5	0.028373
Cladding Axial Growth	23	0.000001	14	0.005299	11	0
Cladding Corrosion	3	0.037596	2	0.053205	1	0.504459
Cladding Hydrogen Concentration	15	0.000077	22	0.002464	7	0.012898
Summation of Measures		0.207072		0.332635		0.81668

corrosion and inlet temperature. As noted in the last state, the cladding corrosion causes the rise in temperature, which increases gas conductance in the gap. The inlet temperature causes the same effect, but to a lesser degree since the inlet temperature has an uncertainty range of 3.33, compared to potential 10 rise occurring from corrosion.

The changes caused by cladding corrosion and inlet temperature cause a lateral shift in the narrow grouping of closed-gap cases. Such a shift is poorly detected by both regression methods which measure increased linear dependence, or variance based methods which quantify changes in the variance of conditional expected values. Hence only the delta measure is capable of communicating their true impact. The fact that the inlet temperature is the second largest factor speaks to the lack of variance in the low pressure closed gap model. A 3.33 in gas temperature with all else held constant results in a mere 13 $\frac{BTU}{hr \cdot ft^{2} \cdot ^{\circ}F}$(73.82 $\frac{W}{m^{2} \cdot K}$) increase in GCPP.

Table 4.11 shows the clad inner radius to be ranked third among delta measures. Pearson and Sobol show clad inner radius to be the highest rank despite being of low value, which is to say it is the highest rank because all other inputs register low values. As shown in Fig. 4.15(b), this clad inner radius is a strong indicator in determining if the gap closes, which greatly the affects variance of the conditional expected values. Note that creep and thermal expansion biasing rank high in the variance based methods as they also facilitate in the open to closed gap shift.

The PDFs for this state are the most concentrated of all states. This concentration is evidenced by the peak height of PDF being nearly double that of the peak at 9.5 MWD/kgU and close to 20 times larger than that at 2.5 MWD/kgU. Note that the shifts caused by coolant temperature are small but relatively consistent between quartiles, whereas corrosion biasing shifts are larger but show almost no change between the first and second quartiles. This is due to any shift in temperature causing roughly the same change in GCPP, as opposed to corrosion biasing where changes only occur once biasing exceeds a specific threshold. This delay in response to corrosion biasing causes a bimodal distribution in the closed gap group.

Fig. 4.16 is cropped so as to provide a better view of the narrow grouping, however the data set lies between 1750 $\frac{BTU}{hr \cdot ft^{2} \cdot ^{\circ}F}$ and 3800 $\frac{BTU}{hr \cdot ft^{2} \cdot ^{\circ}F}$ (9936.96 $\frac{W}{m^{2} \cdot K}$ and 21577.40 $\frac{W}{m^{2} \cdot K}$). The grouping to the left is smaller than at 9.5 GWD/kgU, while the grouping to right is significantly larger. This indicates that fewer data have finite gap thickness (grouping to the left), and more data lies within higher interfacial pressure group.

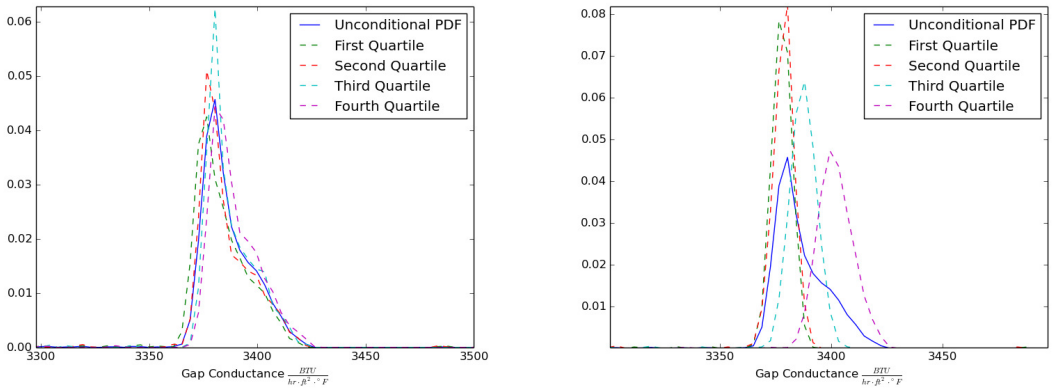

(a) Inlet Temperature

(b) Corrosion Biasing

Fig. 4.16: Unconditional PDF with PDF Conditional upon Select Inputs Lying within a Specified Quartile of Respective Sample at Burnup of 14 MWD/kgU.

At 37 MWd/kgU the majority of the data has shifted to groups which include effects from high pressure contact models. Some data still resided in the low interfacial pressure group, but all data now contain contact. The transition between the low pressure and high pressure models is far less abrupt than the switch between open and close gap. The high pressure closed-gap model is influenced by fuel swelling, creep, and fuel thermal conductivity. Swelling and creep largely influence the amount of expansion and hence interfacial pressure, which in turn affects the solid gap conductance. Fuel thermal conductivity also has an effect on the mean thermal conductivity which effects the interfacial thermal conductivity, and thus solid gap conductance.

At the highest burnup phase all cases share the same models resulting in linear relations. All three rankings show strong consistency for inputs of significant contribution. The four

Table 4.12: High Power Pin Pearson squared (R_i^2), Sobol (S_i), and Delta Moment Independent Measures (δ_i) and corresponding ranks for GCPP at 37 MWd/kgU Burnup.

Core Power	20	0.000123	20	0.003816	11	0.014445
Inlet Temperature	8	0.010107	8	0.013731	18	0.007995
Outlet Pressure	9	0.003132	10	0.008653	16	0.008442
Rated Flow	17	0.000398	16	0.004128	20	0
Void Drift Coefficient	22	0.000037	18	0.003998	17	0.0083
Turbulent Mixing Coefficient	14	0.001236	14	0.004365	14	0.008863
Direct Mod. Heating Fraction	10	0.002993	12	0.005487	20	0
Fuel Radius	6	0.015132	7	0.018578	12	0.011559
Clad Inner Radius	4	0.070674	3	0.104673	5	0.098595
Clad Outer Radius	15	0.001071	9	0.011918	19	0.00792
Fuel Density	12	0.001752	19	0.003945	6	0.024639
Fuel Enrichment	13	0.001542	22	0.002855	10	0.014565
End Spacer Grid Form Loss	23	0.000006	23	0.00219	15	0.008849
Mid Spacer Grid Form Loss	18	0.000283	13	0.004438	13	0.009256
Plenum Fill Gas Pressure	11	0.002206	11	0.005534	9	0.017859
Fuel Thermal Conductivity	5	0.042167	5	0.045642	3	0.136988
Fuel Thermal Expansion	7	0.013023	6	0.019669	7	0.023878
Fission Gas Release	21	0.000044	17	0.004063	20	0
Fuel Swelling	1	0.169465	1	0.174904	1	0.201447
Cladding Creep	2	0.15569	2	0.16365	2	0.141419
Cladding Axial Growth	19	0.000198	15	0.004182	8	0.021845
Cladding Corrosion	3	0.073517	4	0.088959	4	0.105286
Cladding Hydrogen Concentration	16	0.000638	21	0.002862	20	0
Summation of Measures		0.565431		0.702239		0.872148

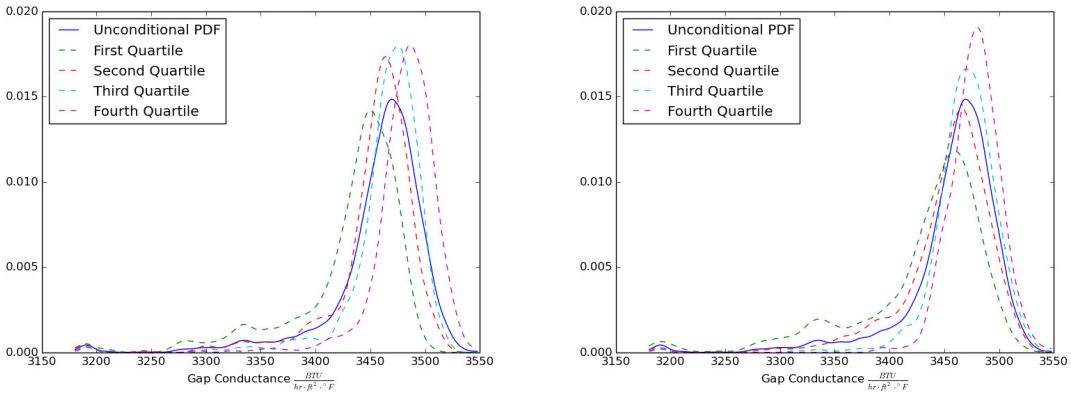

(a) Fuel Swelling Biasing

(b) Cladding Creep Biasing

Fig. 4.17: Unconditional PDF with PDF Conditional upon Select Inputs Lying within a Specified Quartile of Respective Sample at Burnup of 37 MWD/kgU.

Table 4.13: High Power Pin Pearson squared (R_i^2), Sobol (S_i), and Delta Moment Independent Measures (δ_i) and corresponding ranks for GCPP at 52 MWd/kgU Burnup.

Core Power	1	0.321044	1	0.316374	1	0.19172
Inlet Temperature	9	0.004567	9	0.014746	10	0.007269
Outlet Pressure	18	0.000106	18	0.004492	12	0
Rated Flow	20	0.000012	10	0.00866	12	0
Void Drift Coefficient	16	0.001018	19	0.004316	12	0
Turbulent Mixing Coefficient	17	0.000139	13	0.007315	12	0
Direct Mod. Heating Fraction	12	0.002229	14	0.006389	9	0.014375
Fuel Radius	4	0.051191	4	0.055047	4	0.049509
Clad Inner Radius	2	0.278614	2	0.280699	2	0.1711
Clad Outer Radius	10	0.004076	11	0.008189	12	0
Fuel Density	3	0.167586	3	0.167467	3	0.111822
Fuel Enrichment	22	0.000002	23	0.003175	12	0
End Spacer Grid Form Loss	14	0.001113	16	0.005672	12	0
Mid Spacer Grid Form Loss	23	0	17	0.005388	12	0
Plenum Fill Gas Pressure	7	0.017923	7	0.021698	8	0.020506
Fuel Thermal Conductivity	6	0.043239	6	0.045811	5	0.048262
Fuel Thermal Expansion	15	0.001048	12	0.007585	12	0
Fission Gas Release	21	0.000005	22	0.004134	12	0
Fuel Swelling	5	0.045052	5	0.046689	6	0.03644
Cladding Creep	8	0.017477	8	0.01918	7	0.028961
Cladding Axial Growth	13	0.001511	20	0.004254	12	0
Cladding Corrosion	11	0.003855	15	0.006099	11	0.00662
Cladding Hydrogen Concentration	19	0.000024	21	0.004201	12	0
Summation of Measures		0.961828		1.047578		0.686588

prevalent rankings of core power, cladding inner radius, fuel theoretical density, and fuel radius all affect the specific burnup in the fuel, which in turn effects densification and swelling.

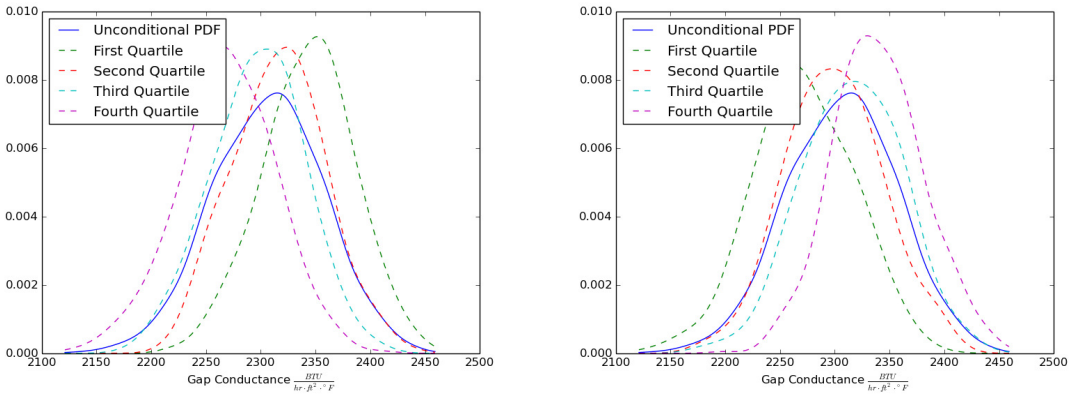

(a) Core Power

(b) Cladding Inner Radius

Fig. 4.18: Unconditional PDF with PDF Conditional upon Select Inputs Lying within a Specified Quartile of Respective Sample at Burnup of 52 MWD/kgU.

The PDF in Fig. 4.18 are similar to those of Fig. 4.14, in that the distribution is roughly Gaussian. The conditional densities narrow and shift compared to their unconditional counterparts, hence variance based methods are reliable at this state. Note that the domain of the sample has a width of $350\ \frac{BTU}{hr \cdot ft^2 \cdot ^\circ F}$ ($1987.39\ \frac{W}{m^2 \cdot K}$) which is roughly ten times greater than that of the low pressure closed-gap state, and slightly less than half the purely open-gap distribution. The mean location is lower than the previous three reported states due to the lowered core power in the third fuel cycle (see Table 4.2).

4.8 Conclusions

LOTUS utilizes a multiphysics environment that couples the core simulator VERA-CS and fuel performance code FRAPCON. Model inconsistencies are accounted for and either deemed negligible or given plans to be remedied with future work. A direct connection between codes ensures consistent uncertainty propagation. UQ and SA were performed on a fuel depletion case with 2500 VERA-CS executions and 660,000 FRAPCON runs.

UQ studies established 95/95 confidence intervals for all FOM, which demonstrates LOTUS capabilities to supply both multiphysics values and their corresponding confidence intervals to decision makers for potential future design problems. SA quantifies the amount of output variance attributable to specific inputs. MDNBR contains consistent linear relations, with thermal hydraulic and core power being the most prevalent. MFCT is also linear, with little variation in SA measure rankings for all relevant inputs. While some shifts in SA measures occur throughout the lifecycle, the vast majority of MFCT uncertainty at all states stems from fuel thermal conductivity.

GCPP begins with linear relations for lower burnup, shifts to highly nonlinear relations, and then returns to linear relations for higher burnup. This behavior is due to FRAPCON abruptly shifting between three models with differing sensitivities. The initial open-gap model is sensitive to geometric inputs, the low interfacial pressure closed-gap model is sensitive to corrosion biasing, and the high interfacial pressure model is sensitive to fuel and cladding material properties, geometry, and core power. These results demonstrate the capability of LOTUS to obtain not only the values of safety and design parameters, but also their corresponding uncertainty and sensitivity to pertinent inputs.

4.9 Acknowledgements

This work is supported by the U.S. Department of Energy, under DOE Idaho Operations Office Contract DE-AC07-05ID14517. Accordingly, the U.S. Government retains a nonexclusive, royalty-free license to publish or reproduce the published form of this contribution, or allow others to do so, for U.S. Government purposes.

REFERENCES

[1] Blakely, C., Zhang, H., and Ban, H., "Sensitivity analysis of VERA-CS and FRAPCON coupling in a multiphysics environment," *Annals of Nuclear Energy*, Vol. 111, 2018, pp. 683 – 701.

[2] http://frapcon.labworks.org, Accessed: 2018.

[3] https://www.nrc.gov/docs/ML1200/ML120060403.html, Accessed: 2018.

[4] Porter, I., Knight, T. W., and Raynaud, P., "Potential Impacts of Modeling Full Reactor Cores Using Combined Fuel Performance and Thermal Hydraulics Codes," *Nuclear Technology*, Vol. 190, No. 2, 2015, pp. 174–182.

[5] Bowman, S. M., "SCALE 6: Comprehensive Nuclear Safety Analysis Code System," *Nuclear Technology*, Vol. 174, No. 2, 2011, pp. 126–148.

[6] Bratton, R. N., Jessee, M. A., and Wieselquist, W. A., "Rod internal pressure quantification and distribution analysis using Frapcon," *Proc. 2016 Conference on Physics of Reactors*, May 2016, pp. 2588–2602, ORNL/TM-2015/557.

[7] https://bison.inl.gov/, Accessed: 2018.

[8] Leppänen, J., Pusa, M., Viitanen, T., Valtavirta, V., and Kaltiaisenaho, T., "The Serpent Monte Carlo code: Status, Development and Applications in 2013," *Annals of Nuclear Energy*, Vol. 82, 2015, pp. 142–150.

[9] Wu, X., Kozlowski, T., and Hales, J. D., "Neutronics and fuel performance evaluation of accident tolerant FeCrAl cladding under normal operation conditions," *Annals of Nuclear Energy*, Vol. 85, 2015, pp. 763 – 775.

[10] https://www.casl.gov/, Accessed: 2018.

[11] The RELAP5-3D Code Development Team, "The RELAP5-3D Code Manual Volume I: Code Structure, System Models, and Solution Methods," 2012, Rev. 4, Idaho National Laboratory, INEEL-EXT-98-00834.

[12] Boyack, B., Catton, I., Duffey, R., Griffith, P., Katsma, K., Lellouche, G., Levy, S., Rohatgi, U., Wilson, G., Wulff, W., and Zuber, N., "Quantifying reactor safety margins part 1: An overview of the code scaling, applicability, and uncertainty evaluation methodology," *Nuclear Engineering and Design*, Vol. 119, No. 1, 1990, pp. 1 – 15.

[13] Ikonen, T., "Comparison of global sensitivity analysis methods Application to fuel behavior modeling," *Nuclear Engineering and Design*, Vol. 297, 2016, pp. 72 – 80.

[14] Ikonen, T. and Tulkki, V., "The importance of input interactions in the uncertainty and sensitivity analysis of nuclear fuel behavior," *Nuclear Engineering and Design*, Vol. 275, 2014, pp. 229 – 241.

[15] Brown, C. and Zhang, H., "Uncertainty quantification and sensitivity analysis with CASL Core Simulator VERA-CS," *Annals of Nuclear Energy*, Vol. 95, 2016, pp. 188 – 201.

[16] Brown, C., Zhang, H., Kucukboyaci, V., and Sung, Y., "Best estimate plus uncertainty analysis of departure from nucleate boiling limiting case with CASL core simulator VERA-CS in response to PWR main steam line break event," *Nuclear Engineering and Design*, Vol. 309, 2016, pp. 8 – 22.

[17] Stimpson, S. G., Powers, J. J., Clarno, K. T., Pawlowski, R., and Bratton, R., "Assessment of Pellet-Clad Interaction Indicators in Watts Bar Unit 1 using the VERA Framework," *Proc. PHYSOR 2016 - Unifying Theory and Experiments in the 21st Century*, May 2016.

[18] Borgonovo, E., "A new uncertainty importance measure," *Reliability Engineering and System Safety*, Vol. 92, No. 6, 2007, pp. 771 – 784.

[19] Collins, B., Stimpson, S., Kelley, B. W., Young, M. T., Kochunas, B., Graham, A., Larsen, E. W., Downar, T., and Godfrey, A., "Stability and accuracy of 3D neutron transport simulations using the 2D/1D method in MPACT," *Journal of Computational Physics*, Vol. 326, 2016, pp. 612 – 628.

[20] Glück, M., "Sub-channel analysis with F-COBRA-TFCode validation and approaches to CHF prediction," *Nuclear Engineering and Design*, Vol. 237, No. 6, 2007, pp. 655 – 667.

[21] Croff, A. G., "ORIGEN2: A Versatile Computer Code for Calculating the Nuclide Compositions and Characteristics of Nuclear Materials," *Nuclear Technology*, Vol. 62, No. 3, 1983, pp. 335–352.

[22] https://www.ne.ncsu.edu/rdfmg/cobra-tf/, Accessed: 2018.

[23] Lassmann, K., "TRANSURANUS: a fuel rod analysis code ready for use," *Journal of Nuclear Materials*, Vol. 188, 1992, pp. 295 – 302.

[24] Harding, B., Tremblay, C., and Cousineau, D., "Standard errors: A review and evaluation of standard error estimators using Monte Carlo simulations," *Tutorials in Quantitative Methods for Psychology*, Vol. 10, No. 2, 2014, pp. 107 – 123.

[25] Plischke, E., "An adaptive correlation ratio method using the cumulative sum of the reordered output," *Reliability Engineering and System Safety*, Vol. 107, 2012, pp. 149 – 156, SAMO 2010.

[26] Herman, J. and Usher, W., "SALib: An open-source Python library for Sensitivity Analysis," *The Journal of Open Source Software*, Vol. 2, No. 9, jan 2017.

[27] Plischke, E., Borgonovo, E., and Smith, C. L., "Global sensitivity measures from given data," *European Journal of Operational Research*, Vol. 226, No. 3, 2013, pp. 536 – 550.

[28] Botev, Z. I., Grotowski, J. F., and Kroese, D. P., "Kernel density estimation via diffusion," *Ann. Statist.*, Vol. 38, No. 5, 10 2010, pp. 2916–2957.

[29] http://pyqt-fit.readthedocs.io/en/latest/, Accessed: 2018.

[30] Gandhi, J. M. and Saxena, S. C., "Correlated thermal conductivity data of rare gases and their binary mixts. at ordinary pressures," *Journal of Chemical and Engineering Data*, Vol. 13, No. 3, 1968, pp. 357–361.

aiaa

CHAPTER 5

Transition to Integration of VERA-CS and BISON

As previously stated, one of the primary goals of LOTUS is to aid in the simulation of new fuel technologies, namely accident tolerant fuel and higher burnup fuel. However, FRAPCON does not contain the material modules required by the newly proposed designs. It was therefore a logical progression to bring fuel performance code BISON into the LOTUS framework.

The fuel performance code BISON currently under development at Idaho National Laboratory using the Mulitphisics Object Oriented Simulation Environment (MOOSE). By building BISON within MOOSE, the code is able to incorporate an ever expanding libraries of modules. This library contains the necessary material modules for modeling new fuel concepts.

In order to avoid redundancy, LOTUS scripts were created to allow BISON access to the 2500 VERA-CS cases generated for the Monte Carlo sampling of the VERA-CS and FRAPCON integration. This sharing of data was also beneficial in that it allowed for a comparison between the two fuel performance codes. However, due to BISON requiring considerable more computational resources than FRAPCON, only the highest power pin of the fuel assembly was supplied to BISON.

CHAPTER 6

APPLICATION OF REGRESSION, VARIANCE, AND DENSITY BASED GLOBAL SENSITIVITY METHODS TO INTEGRATED VERA-CS AND BISON SIMULATIONS[1]

This chapter contains a reformatted version of an article appearing in volume 332 (2018) of the journal *Nuclear Engineering and Design* [1].

6.1 Abstract

Uncertainty quantification (UQ) and sensitivity analyses (SA) are performed for coupled simulations between VERA-CS, a coupled pin resolved neutron transport and subchannel thermal hydraulics code, and the fuel performance code BISON. The interface between VERA-CS and BISON is performed in a multiphysics environment known as the LOCA Toolkit for U.S. light water reactors (LOTUS) currently under development at Idaho National Laboratory (INL). A focus is placed on using a variety of SA measures, including two regression based (Pearson and Spearman), one variance based (Sobol indices), and three moment independent measures (Delta moment independent measures with L1, L2, and L norms). The problem under inspection is a single assembly depletion case for three fuel cycles. The figures of merit are the minimum departure from nucleate boiling ratio (MDNBR), maximum fuel centerline temperature (MFCT), and gap conductance at peak power (GCPP). SA results show MDNBR to be linear with consistent rankings throughout the fuel cycles. MFCT is linear, but with a change in rankings at the switch from open gap to closed gap models. GCPP is nonlinear at intermediate states that coincide with the onset of contact between fuel and cladding. These nonlinear states allow for the showcasing of higher order SA measures over first order methods.

[1]Coauthors: Hongbin Zhang, Charlie Folsom, Heng Ban, Ronaldo Szilard

6.2 Introduction

The current fleet of the U.S. nuclear power plants is expected to undergo a variety of technological developments including the use of accident tolerant fuel and higher burnup fuel to improve its economic performance. In order to help facilitate this shift, improved predictive methods are currently under development, in particular multiphysics environments.

The word multiphysics indicates a set of calculations involving multiple physical models. It is worth noting that it is rather arbitrary when a simulation enters the realm of multiphysics, as most engineering codes model multiple physical phenomena. For instance, legacy codes such as FRAPCON solve mechanical and thermal equilibrium equations as well as irradiative effects, oxidation, thermal hydraulics, and fission gas release. However, code documentation for FRAPCON [2] never refers to itself as a multiphysics code. This is partly due to the term being less common during the development of FRAPCON, but also due to the fact that all the phenomena receiving particular focus reside within the fuel performance discipline. The usage of multiphysics within this work implies the combining of interdisciplinary calculations which have commonly been treated separately in the past.

The definition of an environment in the computational context is amorphous as well noted by Sloan *et al.* [3]. In this work, the word environment indicates a computational space in which users may utilize a variety of tools to generate, exchange, and process large amounts of data. Within this work, an environment is created that treats codes as modules which can readily and reliably be called upon in order to perform large Monte Carlo samplings. This environment allows for the collaboration of multiple large scale projects for a more thorough modeling of designs to be employed in the nuclear industry.

Multiphysics studies have been implemented and studied extensively. In nuclear applications, work on multiphysics tends to focus on combining fuel performance, thermal hydraulics, neutronics, and/or isotopic depletion codes. Two multiphysics environments utilized by this work are the Virtual Environment for Reactor Analysis - Core Simulator (VERA- CS) [4] developed by the Consortium for Advanced Simulation of Light Water Re-

actors (CASL) and the Multiphysics Object-Oriented Simulation Environment (MOOSE) developed at Idaho National Labs (INL). The version of VERA-CS used in this work performs tightly coupled calculations between the neutronics code MPACT, the thermal hydraulic code CTF, and the isotopic depletion code ORIGEN (see section 6.3.1). MOOSE uses a modularized approach to allow for increased flexibility in code development. MOOSE employs fully-coupled, fully-implicit numerical methods to solve nonlinear equations within an adaptable, finite element framework [5] (see section 6.3.2). This work uses the fuel performance code BISON, which is developed within MOOSE.

Notable instances of thermal hydraulics and neutronics coupling include the thermal hydraulics code Trace-PFI with a neutronics code based on the nodal expansion method (NEM) [6] and a coupling of Monte Carlo based neutronics with subchannel thermal hydraulics [7]. Examples of fuel performance and neutronics coupling include the fuel performance code TRANSURANUS and neutronics code DYN3D [8], and BISON with DeCART [9].

Couplings between fuel performance and thermal hydraulics include FRAPCON with TRACE-V5P3 [10] and BISON [11] with RELAP5-3D [12]. Furthermore a coupling between the transient fuel performance code FRAPTRAN, subchannel thermal hydraulics code COBRA-TF, and the neutronics code TORT-TD has been performed [13]. A notable instance of a coupling between isotopic depletion and neutronics is the MCWO script [14] developed at INL which couples the isotopic depletion code ORIGEN2 with the Monte Carlo N-Particle transport code MCNP.

The Serpent Monte Carlo code [15] developed at the VTT technical center is also noteworthy for its widespread use in multiphysics studies, which include couplings of thermal hydraulics, computational fluid dynamics, isotopic depletion, fuel performance, and neutron and photon transport. Considerable work is also underway in the U.S. Department of Energys program known as Nuclear Energy Advanced Modeling Simulation (NEAMS) to develop a workbench [16] to handle the integration of neutronics, fuel performance, thermal hydraulics, and isotopic depletion codes. Finally the reactor and lattice physics code SCALE

[17] developed by Oak Ridge National Laboratory (ORNL) has been coupled with thermal hydraulic, computational fluid dynamics, and fuel performance codes. It is worth noting that the specified problem (i.e. reactivity insertion accident (RIA), loss of coolant accident (LOCA), quasi-steady state depletion) often varies among the aforementioned works.

An essential aspect in the development of multiphysics environments is the incorporation of uncertainty quantification (UQ) and sensitivity analysis (SA) methodologies. UQ and SA studies of multiphysics environments ensure that the results are not treated as absolutes, but rather as estimates with inherent uncertainty. In essence, UQ and SA studies assure that decision makers are privy to the best estimate plus uncertainty (BEPU) methodology which has become the de-facto industry standard.

UQ and SA in reactor design and analysis had predominantly been used in the field of thermal hydraulics [18,19], but recently have been extended to fuel performance [20,21]. UQ and SA have been performed on the fuel performance code BISON [22,23] using DAKOTA software, as well as with the RAVEN software developed at INL [24]. UQ and SA have also been extended to VERA-CS [25, 26]. UQ has also been performed on VERA-CS via the Crud Induced Power Shift studies (CIPS) [27]. Notable UQ and SA have also been performed on SCALE [28]. UQ and SA on large multiphysics environments are still at their infancy and warrant further systematic studies.

In this work, a Monte Carlo based UQ and SA have been performed on an integration of CASLs VERA-CS code [4] and INLs advanced fuel performance code BISON [11]. The integration of VERA-CS and BISON and the subsequent UQ/SA studies are performed within the context of a multiphysics environment known as LOTUS which stands for LOCA Toolkit for the U.S. light water reactors.

For each instance in the Monte Carlo sampling, a VERA-CS output file was generated, from which the power histories and thermal hydraulic profiles for a pin of interest were inputted into BISON. The pin of interest in this case was defined as the pin with the highest linear heat rate at the end of the fuel life cycle. This selection criteria was chosen due to the fact that the fuel performance figures of merit (FOM) of this work always coincided with the

highest power pin for all observed cases. While the maximum power pin changes location throughout the fuel cycle, a consistent pin location based solely on the maximum pin power at the end of three fuel cycles was used so as to maintain consistency. The outputs from VERA-CS and BISON were then used to obtain the FOM, from which all UQ and SA were performed.

The problem of interest presented in this work is a three cycle, single assembly, fuel depletion case. This case was selected based on its similarities with typical operational behavior of an assembly in a LWR. While ideally a full core would be simulated, a single assembly is more feasible for a Monte Carlo sampling given current computational limits. The quasi-steady depletion case will also eventually serve as a means of supplying initial conditions (particularly gap conductance) to LOCA cases which are to be the primary focus of future LOTUS studies as the name suggests.

The FOM for this case are the minimum departure from nucleate boiling ratio (MDNBR), maximum fuel centerline temperature (MFCT), and the gap conductance at peak power (GCPP). The GCPP results from BISON are of particular interest as past work with FRAPCON [29], showed GCPP uncertainty to be highly nonlinear. This nonlinear behavior is likely attributable to abrupt shifts in certain empirical functions used within FRAPCON, as opposed to the more mechanistic models used within BISON (see section 6.3.2).

All SA studies must decide upon which SA measure to employ and report among an ever expanding list of possible candidates. Each SA measure has advantages and disadvantages typically in the realms of required sample size and the ability to detect nonlinearities. The LOTUS environment provides a post processing toolkit for the calculation of a variety of SA measures for any set of recorded inputs and corresponding outputs. This work employs two regression based SA measures (Pearson and Spearman), one variance based (Sobol indices), and three moment independent measures (Delta Moment Independent [30] with, L^2 and L^∞ norm variations [31]).

Results show MDNBR to behave linearly and consistently among all SA measures and states throughout the fuel cycle. The most impactful inputs for MDNBR are the assembly

power, inlet temperature, and outlet pressure. Lesser contributions also come from rated flow and clad outer diameter.

MFCT also behaves linearly with consistency among SA measures, but with significant shifts in SA measures from state to state. Initially, MFCT depends primarily on fuel thermal conductivity in addition to cladding inner radius and fuel radius due to their direct effect on gap conductance. Uncertainties of later states stem almost exclusively from fuel thermal conductivity, with lesser contributions from fuel density and assembly power due to their effect on burnup which in turn effects fuel thermal conductivity.

GCPP contains a variety of nonlinearities allowing for differences among SA measures which highlight their unique benefits. At the start of the fuel cycle, GCPP is relatively linear with a strong dependence on fuel radius and clad inner radius due to their direct role in gap width. Near the end of the first fuel cycle, many cases are a mixture of open and closed gap models, causing nonlinear relations. Impactful inputs at this state are the fuel and inner cladding radii, fuel and cladding roughness (as a result of the gap width used in closed gap modeling), and gap gas thermal conductivity. Later states show a return to linearity as all cases become closed gap, with no interaction from initial gap width, and larger dependencies on surface roughness and fission gas release diffusion coefficients.

The purpose of this work is to demonstrate the LOTUS environment and better understand the uncertainty of the aforementioned FOM. The LOTUS demonstration will serve as a starting point from which later work on code integrations can be performed, specifically for accident tolerant fuel and higher burnup fuel simulations. The FOM subject to UQ and SA were selected in the interests of eventually narrowing reactor safety margins (see section 6.5.1). In particular, insights gained from the study of MFCT and GCPP will be of value in later LOCA studies. Performing BEPU methodology with a Monte Carlo based UQ within the multiphysics framework of LOTUS creates a less conservative estimate as compared to the more commonly used Wilks method. This improved estimate has the potential to allow higher operational power and/or greater flexibility when performing power maneuvers.

6.3 LOTUS Multiphysics Environment

The larger vision for LOTUS is to have a single multiphysics environment with the ability to perform Core Design-Automation (CD-A), Fuel Performance, Systems Analysis, Risk Assessment (RA), and Core Design-Optimization (CD-O). A conceptual layout for LOTUS is shown in Fig. 6.1.

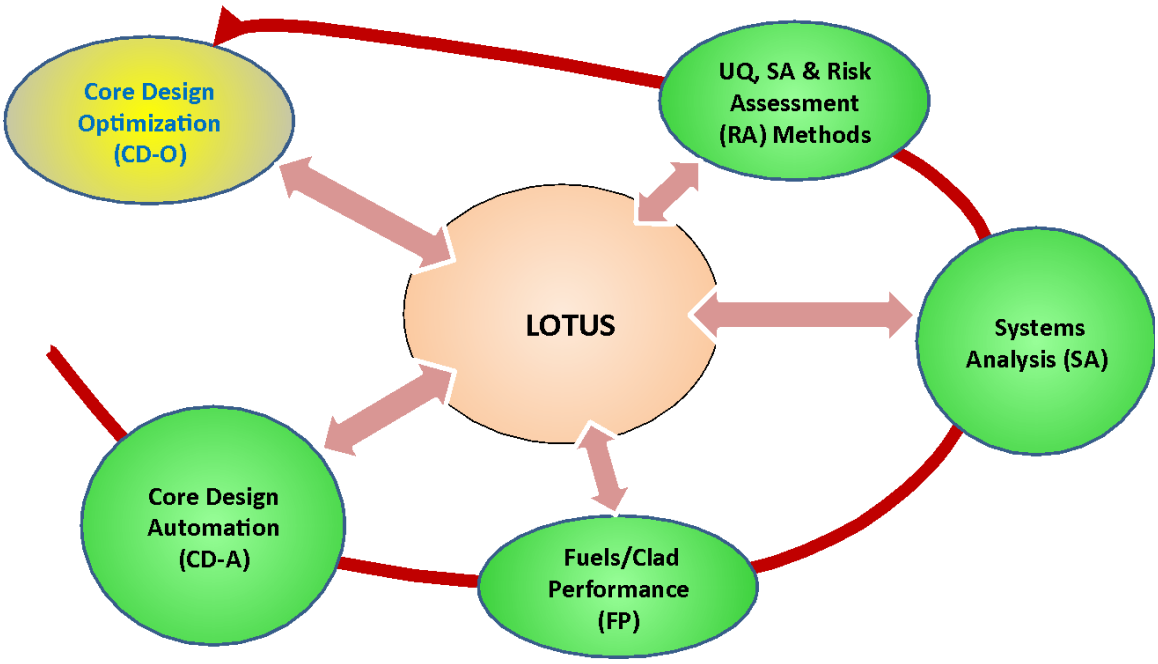

Fig. 6.1: Schematic illustration of LOTUS.

The focus of this work is a subset of the LOTUS framework development which involves the coupling of the core design automation code VERA-CS with the fuel performance code BISON. While the modeling of LOCA is the eventual goal of LOTUS, this is not possible without supplied initial conditions from steady state simulations. Thus, while future work will center on LOCA, present work focuses on the preliminary step of ascertaining data from quasi steady state depletion cases (see section 6.5).

6.3.1 VERA-CS

VERA-CS employs MPACT for neutron transport, COBRA-TF for subchannel thermal

hydraulics, and ORIGEN for isotopic depletions [4]. Due to the coupling of these codes, VERA-CS is a multiphysics environment for reactor core simulations [32].

VERA-CS generates sub pin level power profiles. While computationally expensive, this level of detail automatically creates a power history specific to each pin which can then be used for fuel performance analysis. This is superior to the less computational demanding approach of using few-group coarse-mesh nodal diffusion methods with pin powers reconstructed from the intra-nodal flux distributions [33].

The version 3.6 of VERA-CS used by this work utilizes table lookups of BISON generated tables for fuel performance data (specifically temperature profiles) in place of coupled fuel performance calculations. While this table lookup reduces computational workload, from an accuracy standpoint it is less than ideal as the optimal configuration is to tightly couple fuel performance calculations with neutronics, thermal hydraulic, and isotopic depletion calculations [34]. Also, the exclusion of concurrent fuel performance calculations prevents the reporting of outputs exclusive to fuel performance codes such as GCPP. Furthermore within COBRA-TF, the gap conductance is treated as a constant both temporally and spatially and the fuel thermal conductivity is burnup independent.

Current development at CASL is incorporating a 1 D version BISON in order to improve fuel performance modeling [34], in the interests of improving neutron cross section estimations as well as including dynamic gap conductance and burnup dependent fuel thermal conductivity. Various strategies for partitioning and streamlining of the workload are being investigated in order to maintain reasonable computational expense [34].

6.3.2 BISON

BISON is a finite element based multidimensional and multiphysics fuel performance code [11, 35]. BISON allows for steady state and transient simulation of single fuel rod. Thermodynamic, mechanical, and species diffusion equations are fully-coupled and solved in a fully implicit manner. BISON is being developed with INLs Multiphysics Object-Oriented Simulation Environment (MOOSE).

MOOSE is built to handle the systems of nonlinear partial differential equations often

encountered in nuclear design. MOOSE allows for the equations of interest to be solved in a fully coupled manner using the Jacobian-free Newton-Krylov method [5]. The physical models involved are all modularized so as to allow for a flexible framework wherein new physics models can be added and combined in novel ways. This modularized approach allows for any reasonable combination of modules to be constructed in a less cumbersome manner than traditional code development. MOOSE coupling has been particularly successful in coupling material science calculations involving the atomistic, mesoscale, and engineering scale of fuel performance [36, 37].

BISON may be thought of as a set of MOOSE modules specific to fuel performance. Modules available to the fuel include temperature, burnup, and porosity dependent material properties, fission product swelling and densification strains, thermal and irradiation creep, fracture, and fission gas production and release. Models for cladding materials include plasticity, thermal expansion, irradiation growth, hydrogen uptake and creep. BISON also has models for coolant channels, cladding oxidation, plenum gas behavior, gap heat transfer, and contact between fuel and cladding.

BISON supports a variety of meshes including, 2-D smeared mesh, 3-D meshes, and 3-D discrete pellet meshes. BISON utilizes more complex, mechanistic methods to model phenomena such as fission gas release and contact, contrary to less mechanistic approaches used in other fuels performance codes such as FRAPCON (interested readers are referred to the user manual for FRAPCON [2] and BISON [11], specifically for fission gas release and the fuel and cladding mechanical response). While this comes at higher computational costs, the resulting output distributions for UQ and SA are less nonlinear compared to the abrupt shifts common in the piecewise functions of FRAPCON, as evidenced by past SA results [29]. BISONs 2D axisymmetric mesh allows for relatively fast running simulations and is used in this work.

6.3.3 Code Inconsistencies

Due to differences in domain, methodologies, and specific material property calculations, model inconsistencies between BISON and VERA-CS are inevitable. The aim of this

work is either to minimize differences to an acceptable level and/or establish them as negligible. When neither of these is possible, the difference is carefully documented and given plans for future work.

In regards to the domain, VERA-CS can model entire assemblies and/or full cores. The thermal hydraulic models used account for cross flow between the sub-channels. BISON models single fuel rods. Typical BISON models use a single coolant channel module to calculate heat transfer from the rod to coolant. However, this work transfers outer cladding data from VERA-CS in order to supply BISON with spatially and temporally varying temperature and pressure boundary conditions at the outer cladding surface. Therefore, the inconsistency is avoided by having the outer radial boundary condition of the cladding supplied by the thermal hydraulic models of VERA-CS alone without any thermal hydraulic modeling from BISON.

The discrepancy of greatest concern between the two codes is the fuel thermal conductivity. Past work [20, 29] has established it as the most dominant input in terms of impact on MFCT. The differences arise from VERA-CS currently not allowing burnup dependent fuel thermal conductivity. The exact empirical formulas used by BISON are available in COBRA-TF, however burnup data is currently not passed to the thermal conductivity routines. Fortunately this discrepancy will be remedied in the near future as CASL is currently developing burnup dependent thermal conductivity capabilities to be employed in later builds.

VERA-CS currently uses a constant gap conductance for all spatial and temporal locations. In reality, the gap conductance can vary greatly due to the differences in gap widths, gap gas temperature and composition, and interfacial pressures after contact. BISON currently models gap conductance with an extensive, mechanistic model. Past work established that when pins have open gaps, MFCT is sensitive to gap conductance parameters [29], hence the inconsistency may be of concern. This issue will also be addressed with later builds of VERA-CS which will include a dynamic gap conductance model.

VERA-CS has a highly advanced capability to model neutron transport while BISON

is more rudimentary. Typically BISON uses a constant fast neutron flux to power density ratio, but also allows for a user defined average fast neutron flux power history. VERA-CS has the average fluxes available for 51 energy groups, however BISON is only interested in energies exceeding 1 MeV. The fast neutron flux for BISON is estimated according to the methodology presented in past work [38] and shown in Eq. 6.1,

$$\Phi_{E>1MeV,i} = \sum_{j=L+1}^{L+N} \Phi_{j,i} + \frac{E_L - 1MeV}{E_L - E_{L+1}} \Phi_{L,i} \tag{6.1}$$

where $\Phi_{i,j}$ is the flux for energy group j at time i, and L is index of the energy group which straddles 1 MeV, N is the number of energy groups entirely above 1 MeV, and E_L is the lower energy bound of group L. Essentially, Eq. 6.1 performs a summation of the higher energy groups in addition to the portion of group L above 1 MeV determined via interpolation.

The average fast flux is then divided by the total core power to supply BISON with a core averaged (or assembly averaged in this case) fast flux to specific energy ratio. This method is still less than ideal as fast flux received by a given cladding is not a function alone of the fuel rod it encases, but also of the fuel rods in the local vicinity, as noted by Stimpson *et al.* [39]. A more ideal exchange of data would transfer the fast neutron flux averaged over each cladding surface. Unfortunately, this data is currently not available within the VERA-CS output files. Hence this level of coupling is only possible within the VERA-CS environment or with a custom version containing more in depth neutron flux output data. However, due to the shared enrichment and relatively low power variation within a single assembly case, the application of the average neutron fluxes to each individual rod is a fair approximation.

VERA-CS calculates isotopic depletion through the use of ORIGEN [40], while BISON uses TUBRNP or TRANSURANUS burnup [41]. The FOM of this work rely upon thermo-mechanics and thermal hydraulics, which are only slightly sensitive to isotopic depletion as a result of secondary effects related to changes in radial power peaking profiles. Therefore, it is safe to assume that this discrepancy is minor.

The aforementioned differences in fast neutron flux and isotopic depletion, as well as differences in calculating neutron cross sections create a difference in radial power profiles. Due to the buildup of plutonium near the outer radius of a fuel pellet, the local heat generation may be as much as three times that of average source term for a given axial location [11]. For this reason, the radial power profile has received particular attention from BISON developers, including a finer secondary grid for higher resolution of burnup and fission rates. As previously mentioned, VERA-CS contains far more in-depth neutronics calculations, however it is less adept at computing the temperature dependent cross sections.

Currently, this discrepancy is not resolvable as VERA-CS output files do not contain radial power profiles. The differences in the profile will be greatest near the outer radius edge, where the source terms are largest, thereby effecting properties such as outer fuel temperature and outer fuel burnup. However it will be far less impactful on properties calculated at locations other than the outer fuel radius (MFCT and MDNBR). The GCPP on the other hand may be effected by these discrepancies, as increased outer radius temperature affects gap gas temperature which in turn alters gas thermal conductivity. Thus the differences in radial profile merit further research to be conducted in later work.

While the fuel thermal conductivity, radial power profiles, and dynamic gap conductance discrepancies need be resolved in the future in the interests of improving LOTUS, it is essential to stress that the most critical data exchanged by the LOTUS scripts are the power and thermal hydraulic profiles. VERA-CS is at the cutting edge of coupled neutronics and subchannel thermal hydraulics reactor core simulations, and is capable of producing sub pin level power profiles of high fidelity, yet currently lacks various fuel performance analysis models. BISON has sophisticated fuel performance models, but is dependent upon idealizations or user supplied data for power history and thermal hydraulics data. The scope of this work is to create a more complete, but not yet all encompassing, framework reflective of true reactor physics. All discrepancies are minimized to the extent possible, documented, and highlight industry needs that may be resolved through future codes and/or new couplings.

6.4 Problem Description

The computational resources required to perform full-core simulations with VERA-CS are not affordable for a Monte Carlo based sensitivity analysis. Therefore, the current work focuses on single assembly depletion cases lasting three fuel cycles for a total of four and a half years. Fuel design is a typical 17x17 fuel assembly with 264 fuel rods, 24 guide tubes, and 1 instrumentation tube. The assembly layout is shown in Fig. 6.2, with the color blue denoting fuel rods, red indicating guide tubes for control rods, and the central yellow tile representing the guide/instrument tube. VERA-CS takes into account core and fuel assembly properties such as the upper and lower core plates, lower and upper assembly nozzles, and guide/instrument tubes. Eight spacer grids are included in the assembly to provide structural support as well as improve coolant mixing. The spacer grid form losses are a user input to the VERA-CS input file (see Table 6.2).

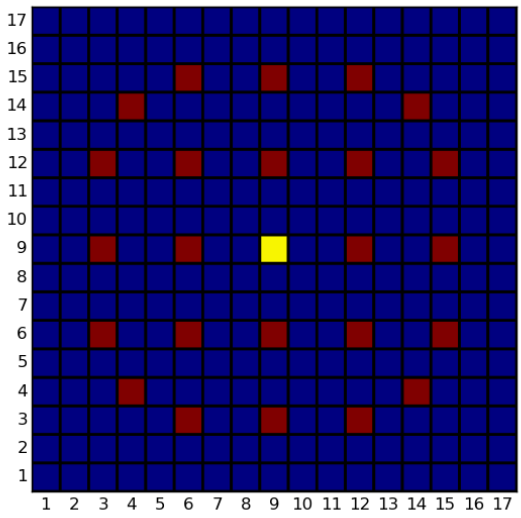

Fig. 6.2: Assembly Layout with Colors Blue, Red, and Yellow Corresponding to Fuel Rods, Control Rods, and Guide/Instrument Tube Respectively.

Each case was modeled without symmetry in order to get a better sense of the required computational load per assembly for a Monte Carlo sample. This gained experience will

Table 6.1: Design and simulation parameters for the model problem.

Parameter Name	Parameter Value	VERA-CS	BISON
Fuel Height	3.657 m	X	X
Pin Pitch	1.26 cm	X	X
Plenum Height	16 cm	X	X
Clad Top and Bottom Thickness	1.67 cm	X	X
Fuel Material	Uranium Dioxide	X	X
Fill Gas Type	Helium	X	X
Cladding Material	Zircaloy 4	X	X
Boron	1640 ppm	X	
Plate Material	Stainless Steel	X	
Plate Thickness (Lower/Upper)	5.0 / 7.6	X	
Plate Volume Fraction	0.5	X	
Spacer Material (Middle/End)	Inconel/Zircaloy 4	X	
Spacer Height (Middle/End)	3.810 cm / 3.866 cm	X	
Spacer Mass (Middle/End)	875 g / 1017 g	X	
Nozzle Material	Stainless Steel	X	
Nozzle Height (Lower/Upper)	6.053 cm / 8.827 cm	X	
Nozzle Mass	6250 g	X	
Pellet Height	0.983 cm		X
Number of Pellets	372		X
Height of Pellet Dish	0.0335 cm		X
Pellet End-Dish Shoulder Width	0.0665 cm		X
Clad Fuel Bottom Gap	0.001 cm		X

be of value when allocating resources for future work involving potentially hundreds of assemblies. Due to the problem having 1/8 symmetry, the maximum power locations are not limited to a single rod. Minor differences occur between theoretically identical pins as dictated by symmetry, due to the serendipitous nature of round off error. It was verified that all hot pin locations at the final state were in a consistent location according to 1/8 symmetry for each instance of the Monte Carlo sampling.

Fuel performance is achieved via a full length rod with a smeared pellet mesh within BISON. The BISON model included solid mechanics, LWR specific heat transfer, burnup, contact, fuel relocation, fuel swelling, fission gas release, fuel and cladding creep, and cladding irradiative effects. The constant parameters supplied to both VERA-CS and BISON are given in Table 6.1. Note that columns 3 and 4 indicate if the parameter of a given row is used by VERA-CS and/or BISON.

6.5 Analysis Methodology

6.5.1 Figures of Merit

The figures of merit (FOM) for this study are the minimum departure from nucleate boiling ratio (MDNBR), maximum fuel centerline temperature (MFCT), and gap conductance at peak power (GCPP).

The MDNBR is a thermal hydraulic variable defined as the ratio of the critical heat flux to a surface heat flux. This is expressed mathematically in Eq. 6.2,

$$MDNBR = min\left(\frac{q_{crit}}{q}\right) \tag{6.2}$$

where q and q_{crit} refer to the heat flux and critical heat flux respectively, and the $min()$ operator refers to the minimum across all spatial locations for a given time. An MDNBR equal to or less than unity indicates an undesirable boiling regime shift from nucleate boiling to transitional boiling, while MDNBR greater than one indicates the critical heat flux has not been reached. MDNBR is valuable from both a core performance and safety perspective.

The MFCT is a fuel performance metric which is simply the highest temperature calculated along the centerline of the fuel at a given time. Its worth noting that the MFCT may be different from the maximum fuel temperature of the entire rod, since radial power profiles can cause the maximum to exist between the center and outer radius. However, this is only encountered in the transient Reactivity Insertion Accidents (RIA), where fission rates are more extreme. In the standard operating conditions of this work, the maximum fuel temperature always resides on the center line, and thus MFCT represents the true maximum as well. Excessive temperatures are undesirable due to fuel cracking, and in extreme cases, fuel melting. MFCT is indirectly related to LOCA as it is closely related to the stored rod internal energy, an important initial condition to LOCA cases. MFCT was selected over stored rod internal energy due to it being more common in UQ/SA fuel performance studies.

The GCPP is a fuel performance metric which reports the thermal conductance of the gas filled gap between fuel and cladding at the location where peak power occurs for a given fuel rod. The gap conductance can be expressed as the summation of three separate terms shown in Eq. 6.3,

$$h_{total} = h_{gas} + h_{solid} + h_{rad} \tag{6.3}$$

where h_{total} is the total gap conductance, h_{gas} accounts for gas thermal conductivity, h_{solid} models the interfacial effects between cladding and fuel, and h_{rad} represents radiative effects. Unlike MDNBR and MFCT which are predominantly linear, GCPP can, depending of the fuel performance model and fuel burnup, exhibit complex nonlinear interaction.

GCPP is of particular interest to LOCA cases since it is impactful on safety criteria such as peak cladding temperature. Unfortunately, data transfer of gap conductance to SA codes specializing in LOCA entails transferring gap conductance data at all axial locations. This set of gap conductance data will differ slightly to the GCPP which is from a single higher power location. However, GCPP is still similar in behavior to the gap conductance at other all other locations. Thus UQ and SA studies are helpful in elucidating the nature

of gap conductance uncertainty at any arbitrary location.

6.5.2 Perturbed Inputs

The perturbed inputs and their respective ranges are included in Table 6.2. Note that an X in columns 4 and 5 indicate if VERA-CS and/or BISON use the input corresponding to a given row. Uncertainty ranges were obtained from [25] for thermal hydraulic parameters, [20, 22] for fuel performance, [23] for properties specific to fission gas release, and [42] for emissivities.

The * indicates that an input is not directly inputted into BISON, but rather directly affects an output from VERA-CS which is then treated as a BISON input. Specifically, the assembly power input directly affects power history supplied to VERA-CS. Similarly, the inlet temperature and outlet pressure have strong influence on the supplied temperature and pressure outer cladding boundary conditions used by BISON. Inputs which do not have a nominal value listed (such as fuel thermal conductivity), vary throughout the fuel cycle, and are thus biased by a consistent, specified amount (i.e. 10%) throughout the simulation.

All input distributions are a truncated normal distribution of two standard deviations with the exceptions of the intra-granular diffusion coefficient, grain boundary diffusion coefficient, and intra-granular diffusion coefficient. As denoted by †, these uncertainties are logarithmic, and vary by a factor of 100 (0.1 to 10) [23]. These scaling factors in the LOTUS scripts are of the form $10^{0.5\sigma}$, where σ is a random variable selected from a truncated random distribution of two standard deviations, with a mean of zero and a standard deviation of unity.

It is worth noting that many of the inputs, such as cladding inner and outer radius are highly correlated. Plans for future work hope to properly sample the inputs with the appropriate correlations. However, this is a large undertaking and is outside the scope of this work. The assumption of independent inputs is not uncommon in UQ/SA literature [20] and serves as a starting point in understanding the uncertainty of a given output.

Lastly it must be acknowledged that many fuel performance inputs, such as fuel radius, should ideally be treated as separate for each pin. However, there are two disadvantages

Table 6.2: List of common uncertain parameters with their uncertainty range.

Input Name	Nominal Value	Range(+/-)	VERA-CS	BISON
Fuel Radius	0.4096 cm	0.001 cm	X	X
Clad Inner Radius	0.418 cm	0.002 cm	X	X
Clad Outer Radius	0.475 cm	0.002 cm	X	X
Fuel Density (% Theoretical)	94.50%	1.60%	X	X
Fuel Enrichment (% Weight)	4.80%	0.00%	X	X
Assembly Power				
Cycle 1	17.674 MW	2%	X	*
Cycle 2	13.256 MW			
Cycle 3	8.837 MW			
Inlet Temperature	554.9(290.5)	3(1.667)	X	*
Outlet Pressure	15.513 MPa	2%	X	*
Direct Mod. Heating Fraction	0.02	10%	X	
Rated Flow	3.410 Mlbs/hr (1.5467 Mkg/hr)	2.00%	X	
Mid Spacer Grid Form Loss	0.907	20%	X	
End Spacer Grid Form Loss	0.9065	20%	X	
Void Drift Coefficient	1.4	10%	X	
Turbulent Mixing Coefficient	0.005	10%	X	
Plenum Fill Gas Pressure	2.0 MPa	0.08 MPa		X
Fuel Surface Roughness	2.0 m	0.0333 m		X
Clad Surface Roughness	1.0 m	0.02 m		X
Fuel Surface Emissivity	0.8	6.80%		X
Clad Surface Emissivity	0.325	0.1		X
Fuel Grain Radius	-	60%		X
Intra-Granular Diffusion Coefficient	-	0.1 to 10†		X
Grain-Boundary Diffusion Coefficient	-	0.1 to 10†		X
Intra-Granular Resolution Coefficient	-	0.1 to 10†		X
FGR Temperature Scaling Factor	-	5%		X
Cladding Creep	-	30%		X
Cladding Oxidation	-	10%		X
Gas Gap Thermal Conductivity	-	5%		X
Fuel Thermal Conductivity	-	10%		X
Clad Thermal Conductivity	-	31.25%		X
Fuel Thermal Expansion	10 *10-6 K-1	15%		X
Clad Thermal Expansion	5 *10-6 K-1	15%		X

* indicates an input which strongly effects a BISON input, but is not directly inputted. † denotes a logarithmic range.

to this treatment. First, a smoothing effect occurs since each fuel assembly becomes a mix of the individually perturbed fuel rods, causing the mean value of any fuel property to remain relatively consistent between Monte Carlo perturbations. Secondly, treating 22 fuel performance inputs as unique to each of the 264 fuel rods results in 5808 separate inputs. While this large set of inputs is acceptable for UQ studies, such a vast number is unreasonable when conducting an effective SA study.

6.5.3 Monte Carlo Sampling and Data Flow

All UQ and SA metrics are obtained from a Monte Carlo sampling among the perturbed inputs listed in Table 6.2. The single assembly case in conjunction with the high performance computing powers available at INL allows for a Monte Carlo sampling of VERA-CS followed by a direct data exchange for power histories and thermal hydraulic profiles to BISON for the hottest pin (the highest power pin at the end of the fuel cycles). The precise methodology is shown in Fig. 6.3.

In instances where the computational expense of a code does not permit a large sample size, a smaller sample must be used, from which PDF of the desired outputs are estimated. The more computationally inexpensive codes then perform a larger resample from the generated PDF. Fortunately at INL, the high performance computer (HPC) resources negate the need for PDF generation and resampling and permit a more ideal direct data connection.

While past work with FRAPCON allowed for a run of every pin in the assembly due to FRAPCON run times of approximately two seconds [29], the current work is hindered by BISON runtimes of approximately two hours. Fortunately, the fuel performance FOM of MFCT and GCPP have maximums which reside on the highest power pin for all cases observed in this work. Since the highest power pin position varies throughout the fuel lifecycle, the pin of interest was selected on the basis of highest power pin at the end of the fuel lifecycle. The data for this pin was passed to VERA-CS for all states, despite it not necessarily being the hottest pin for a given time. While this selection method is less than ideal, it assures that all data analysis is applied to a consistent pin location. The data transfer from VERA-CS includes cladding and fuel dimension, outer cladding temperatures

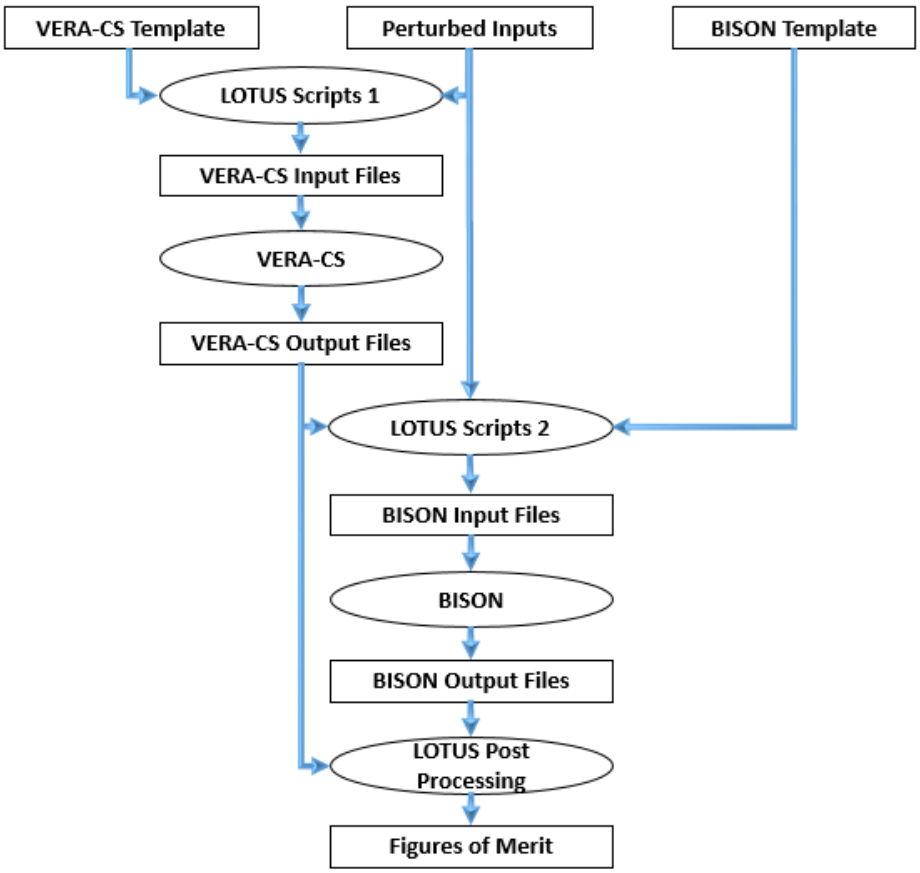

Fig. 6.3: Data Flow for Monte Carlo Sampling.

and pressures, pin power histories including axial power shapes, and assembly averaged fast neutron flux history.

6.5.4 Uncertainty Quantification

LOTUS allows for uncertainty quantification (UQ) and sensitivity analysis (SA) of figures of merit (FOM) resulting from calculations in a multiphysics environment. The uncertainty within LOTUS is quantified via a 95/95 confidence interval given by Eq. 6.4 and 6.5,

$$Y_{95/95} = \mu_{95\%} \pm 1.96 \cdot SE_{Q95\%} \tag{6.4}$$

$$SE_{Q95\%} = 2.11 \cdot SE_M \tag{6.5}$$

where $Y_{95/95}$ is the 95th percentile value for a given output, and $SE_{Q95\%}$ is the standard error associated with said value [43]. Put simply, the 95/95 confidence interval is a bound which contains 95 percent of the total population with 95 percent certainty. It should be noted that estimation of the standard error assumes a normal profile, which is not strictly true in the case of GCPP. Research into Monte Carlo based UQ for arbitrary probability distributions will be a focus of future work.

6.5.5 Sensitivity Analysis

Unlike UQ which contains a relatively linear set of common methodologies, SA methods contain an ever expanding list of measures. The methods vary in computational cost and in their ability to elucidate complex behavior. The SA measures of this work include two regression based measures (Pearson and Spearman), one variance based (Sobol), and three moment independent measures (Borogonov Delta measure and L2 and L variations).

Regression Based Sensitivity Measures

Pearson correlation coefficients are a regression based measure. A useful visualization

of regression methods is the passing of a straight line through a scatterplot of data. If all the data lies perfectly on the fitted line, the Pearson measure is unity. If all straight lines have no bearing on the data (excluding lines with zero slope), then the measure is zero. Pearson correlation coefficients can be found by Eq. 6.6,

$$R_i^2 = \frac{cov\left(X_i, Y\right)^2}{var\left(X_i\right) var\left(Y\right)} \tag{6.6}$$

Among Monte Carlo methods, Pearson measure requires smaller sample sizes. As opposed to more advanced methods, the Pearson measure does not require a computationally expensive Monte Carlo double loop sampling, or data partitioning which generates additional noise in the data.

While the method is capable of detecting linear trends, strong nonlinear trends do not manifest. For instance, the simple relation $Y = |X|$ yields an R^2 which approaches zero as the sample size of approaches infinity. Fortunately the linearity of the system may be tested *a posteriori* via the summation $\sum_{i=1}^{N} R_i^2$, where N is the number of inputs. Summations equal to unity are fully linear systems, while summations far from unity contains large nonlinearities.

This testing is of great utility to decision makers. If a low summation is found then the decision maker knows a higher order method, and thus large sample size, is needed. However, if the sum is nearly unity, a large sample for higher order methods is unnecessary and Pearson measures may become the highest fidelity measure due to their low noise.

A natural extension of the Pearson measure is the Spearman correlation coefficient. Spearman differs in that it evaluates the rankings of inputs and outputs as opposed to the actual values. This can be expressed mathematically in Eq. 6.7,

$$\rho_i^2 = \frac{cov\left(X_i^{rnk}, Y^{rnk}\right)^2}{var\left(X_i^{rnk}\right) var\left(Y^{rnk}\right)} \tag{6.7}$$

where ρ_i^2 is the Spearman correlation coefficient, and X_i^{rnk} and Y^{rnk} are the rankings of an arbitrary input and output. Spearman is advantageous over Pearson in that it is

superior in detecting nonlinearities, as long as the relations are monotonic. However, if the trends are non-monotonic, then Spearman may perform poorly.

Variance Based Sensitivity Measures

Sobol indices are a variance based measure, which is to say they quantify the impact a given input has on the variance of an output. The indices are a function of the variance of the expected value of the output conditional upon the fixing of an input. The indices are normalized by dividing the aforementioned variance by the total variance of the output. This is expressed mathematically in Eq. 6.8,

$$S_i = \frac{var\left(E\left(Y|X_i\right)\right)}{var\left(Y\right)} \tag{6.8}$$

If the output is predominantly a function of said input, then the expected value of the conditional output will vary greatly, yielding a large variance in the numerator of Eq. 6.8. However, if the output is a relatively weak function, then the expected value of the conditional output will be nearly the expected value of the unconditional output, with zero to very low variance.

The main benefit to variance based methods over regression based methods is the ability to detect nonlinear effects that do not include interactions between inputs. Sobol indices are very adept at analyzing an additive systems (i.e. $Y = f\left(X_1\right) + \left(X_2\right)$). This is true even if the individual functions are nonlinear. However, Sobol indices become ineffective in detecting the interactions between inputs (i.e. $Y = X_1X_2$).

Sobol indices ideally require a double loop Monte Carlo sampling. Fortunately Plischke partitioning [44] allows for the partitioning of data from a large single loop Monte Carlo sampling, as shown in Eq. 6.9,

$$\hat{S}_i = \frac{\frac{1}{N}\sum_{j=1}^{M} N_j var\left(Y|X_i \in x_{i,j}\right)}{var\left(Y\right)} \tag{6.9}$$

where $\hat{S}_i$ is the approximation of the Sobol indices, N is the total sample size, M is the number of partitions, N_j is the number instances in partition j and $Y|X_i \in x_{i,j}$ represents

Y given that the corresponding X_i is one of the instances of X_i in partition j. $x_{i,j}$ is formed by first ranking all instances of X_i, placing them in order, and then partitioning M roughly equal spaced groups. The number of partitions is selected based upon an SA library available in Python [45] and shown in Eq. 6.10,

$$M = min\left(\uparrow\left(N^{\left(\frac{2}{7-tanh\left(\frac{1500-N}{500}\right)}\right)}\right), 48\right) \tag{6.10}$$

where $\uparrow$ () operator rounds real numbers up to the next integer. This process allows for estimating Sobol indices with a purely random distribution. A bootstrapping method with 10 resamples is also employed in the interests of reducing noise caused by the Plischke partitioning [46].

Density Based Sensitivity Measures

Density based moments are independent of the moments of the data (i.e. mean and variance) [30]. Delta measures seek to quantify changes between the probability distribution functions (PDF) of the output and the PDF of the output conditional upon the fixing of a given input. The most widely used Delta measure established by Borogonov is the L^1 norm between said densities as shown in Eq. 6.11,

$$\delta_i^1 = \frac{1}{2} E_{X_i}\left(s_i^1\left(X_i\right)\right) \tag{6.11}$$

where δ_i^1 is the L^1 norm Delta measure, $E_{X_i}()$ is the expected value operator when input X_i is varied, and $s_i^1\left(X_i\right)$ is given by Eq. 6.12,

$$s_i^1\left(X_i\right) = \int_{-\infty}^{\infty} \left|f_Y\left(y\right) - f_{Y|X_i}\left(y\right)\right| dy \tag{6.12}$$

where f_Y is the unconditional probability distribution function, and $f_{Y|X_i}$ is the probability density conditional upon fixing input X_i. Thus if the density is affected in any way by the fixing of an input, the Delta measure will register the change. Furthermore the summation of all δ_i^1 is equal to unity if the inputs are separable, which is to say the density

shifts of any given input is independent of the fixing of additional inputs. Recently the Delta measure has been extended to include L^2 and L^∞ [31]. The L^2 norm is given by Eq. 6.13,

$$\delta_i^2 = E_{X_i}\left(s_i^2\left(X_i\right)\right) \tag{6.13}$$

where δ_i^2 is the L^2 norm Delta measure and $s_i^2()$ is given by Eq. 6.14,

$$s_i^2\left(X_i\right) = \sqrt{\int_{-\infty}^{\infty}\left(f_Y\left(y\right) - f_{Y|X_i}\left(y\right)\right)^2 dy} \tag{6.14}$$

Unlike L^1 norms which given equal weight between all differences in densities, L^2 norms give greater weight to larger differences. The summation of all the s_i^2 for each input does not have any significant meaning. The infinity norm is a function of the largest density difference alone. The infinity norm is given by Eq. 6.15,

$$\delta_i^\infty = E_{X_i}\left(s_i^\infty\left(X_i\right)\right) \tag{6.15}$$

where δ_i^∞ is the L^∞ norm Delta measure and δ_i^∞ is given by Eq. 6.16,

$$s_i^\infty\left(X_i\right) = max\left(\left|f_Y\left(y\right) - f_{Y|X_i}\left(y\right)\right|\right) \tag{6.16}$$

Like the L^2 norm Delta measure, the summation of L^∞ norm Delta measures has no significant meaning. To make s_i^2 and s_i^∞ comparable between two different FOM, each FOM is mapped to a domain from zero to unity. Furthermore, s_i^2 and s_i^∞ are also normalized in the interests of being more comparable to the other SA measures of this work. Note that the normalization does not affect rankings when comparing two inputs.

Like variance based methods, density based measures also ideally require a double Monte Carlo loop. This is remedied by using the Plischke partitioning [46] to group the outputs into sets of roughly equal size according to the ranking of a given input. The number of partitions is selected in the same manner as variance based measures (see section

6.5.5, Eq. 6.10). Eq. 6.11, 6.13 and 6.15 can be recast as Eq. 6.17,

$$\hat{\delta_i^p} = \frac{1}{N} C_p \sum_{j=1}^{m} N_j s_i^p \left(X_i \in x_{i,j} \right) \tag{6.17}$$

where N is the total sample size, C_p is a constant based off the order p of the partition ($\frac{1}{2}$ for $p = 1$ and 1 for all others), N_j is the size of partition j, $x_{i,j}$ are the instances of input X_i residing in group j, and $s_i^p \left(X_i \in x_{i,j} \right)$ is the L norm of order p (i.e. 1,2, ∞) between the unconditional density and density conditional upon X_i residing within $x_{i,j}$ group. $s_i^p \left(X_i \in x_{i,j} \right)$ is expressed mathematically as Eq. 6.18,

$$s_i^p \left(X_i \in x_{i,j} \right) = \sqrt[p]{\int_{-\infty}^{\infty} \left| \hat{f}_Y \left(y \right) - \hat{f}_{Y|X_i \in x_{i,j}} \left(y \right) \right|^p dy} \tag{6.18}$$

Note that Eq. 6.18 contain the terms $\hat{f}_Y$ and $\hat{f}_{Y|X_i \in x_{i,j}}$ which are the kernel density estimates of the unconditional and conditional PDF respectively given by Eq. 6.19,

$$\hat{f}_y = \frac{1}{N\lambda} \sum_{i=1}^{N} K \left(\frac{y - y_i}{\lambda} \right) \tag{6.19}$$

where N is the sample size, y_i is an instance of the random variable Y, λ is the kernel bandwidth, and $K()$ is the kernel function. This work employs Gaussian kernels as shown in Eq. 6.20 with bandwidth selection based on Botevs method [47].

$$K \left(z \right) = \frac{1}{\sqrt{2\pi}} e^{-\frac{z^2}{2}} \tag{6.20}$$

A reflective boundary condition is enforced at the upper and lower bound which forces all integrations of the PDF to maintain unity regardless of bandwidth selection [47],

$$\hat{f}_y^R = \frac{1}{N\lambda} \sum_{j=-R}^{R} \sum_{i=1}^{N} K \left(\frac{y - y_i - j \cdot W}{\lambda} \right) \tag{6.21}$$

where $\hat{f}_y^R$ is the kernel density estimate with reflective boundary conditions, W is the width of the domain, and R is the number of reflections ($R = 1$ is sufficient with the exception of cases with bandwidths near or greater than the domain width, i.e. near uniform

distributions). The implementation of these kernel density estimates was achieved via the Python library PyQt-Fit [48].

6.6 Results

6.6.1 Uncertainty Quantification Results

All UQ results follow the format of the 95th percentile value and the +/- range for a 95% confidence interval. This information is shown roughly every 50 days throughout the 3 fuel cycles which corresponds to four and a half years.

UQ results for MDNBR are shown in Fig. 6.4. The abrupt increases in MDNBR correspond to differences in core power among fuel cycles (see Table 6.2). The confidence interval is nearly proportional to the 95th percentile value and relatively small, never exceeding 0.21% of the 95th percentile value. The MDNBR increases as power decreases for each fuel cycle due to the relation stated in Eq. 2. Simply put, as the core power decreases, the heat flux decreases proportionally, and thus the denominator of Eq. 2 decreases, causing an increase in MDNBR. Fig. 6.4 indicates that the case under investigation in this work is not in proximity to a departure from nucleate boiling at any point in time. The aforementioned narrow confidence interval indicates the 95th percentile value is of high fidelity.

UQ results for MFCT are shown in Fig. 6.5. As before, the abrupt drops in MFCT coincide with the lowering of power between fuel cycles. The relative size of the confidence interval values is very similar to MDNBR, with the confidence interval values never greater than 0.26% of the 95th percentile value. However, the relative error is significantly higher for the higher temperature states than proportionality to the 95th percentile alone can account for. This is due to the added uncertainty from open gap conductance models in the earlier states (see section 6.6.2).

The MFCT initially decreases during cycle one due to the closing of the gap (see Fig. 6.6), then slightly increases towards the end of cycle one and all of cycle two. This increase is likely attributable to a gradual decrease in fuel thermal conductivity due to fuel swelling, which increases porosity. The third cycle only slightly decreases for the majority of the

fuel cycle, most likely due to the buildup of plutonium in the outer radius, leading to a decreased radial power peaking factor in the interior of the rod, causing a small decrease in MFCT. The final MFCT increase is likely due to irradiation creep reducing the interfacial pressure between fuel and cladding, thereby decreasing gap conductance and increasing MFCT slightly.

The UQ results for GCPP are shown in Fig. 6.6. Fig. 6.6(a) shows some minor drops for the changes in fuel cycles, but the dominant behavior is attributable to the closing of the gap. The initial increase after closure is likely due to increased interfacial pressure from swelling, after which cladding irradiation creep becomes more dominant causing a decrease in interfacial pressure. The closing of the gap results in a higher gap conductance and a shift in models which changes the associated uncertainty. The largest spike in uncertainty corresponds to a time in which a portion of the Monte Carlo sampled cases are in contact while the remainder retain an open gap. This stratifying of the sample increases the total variance, thus widening the 95/95 confidence interval to as high as 4.2% of the 95th percentile value.

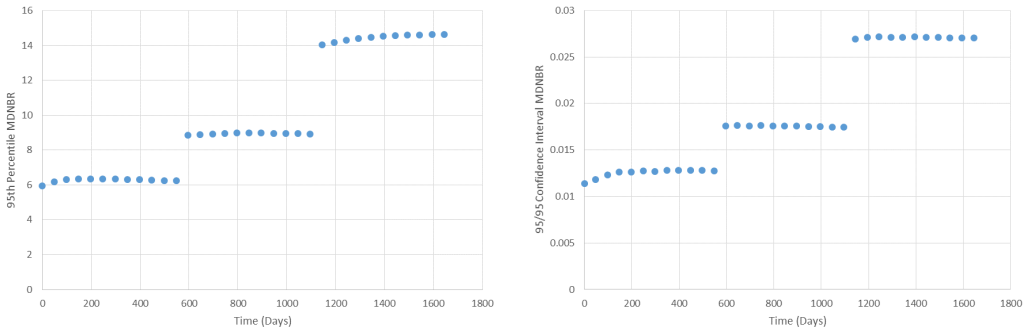

(a) 95th Percentile Value.

(b) +/- 95% Confidence Interval.

Fig. 6.4: MDNBR 95/95 Confidence Interval.

6.6.2 Sensitivity Analysis Results

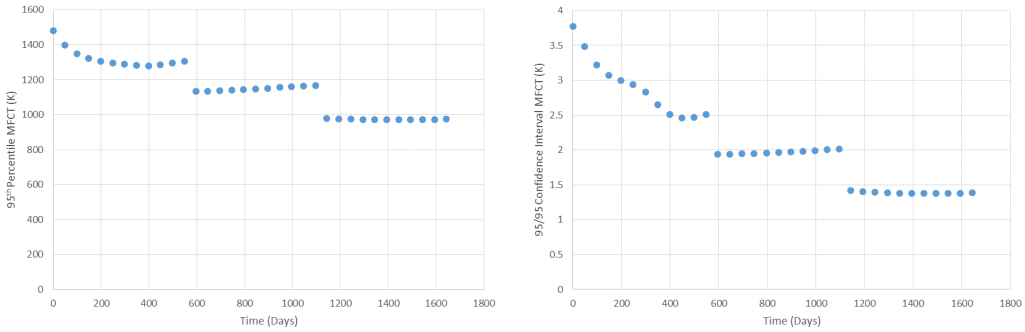

(a) 95th Percentile (b) +/- 95% Confidence Interval

Fig. 6.5: MFCT 95/95 Confidence Interval

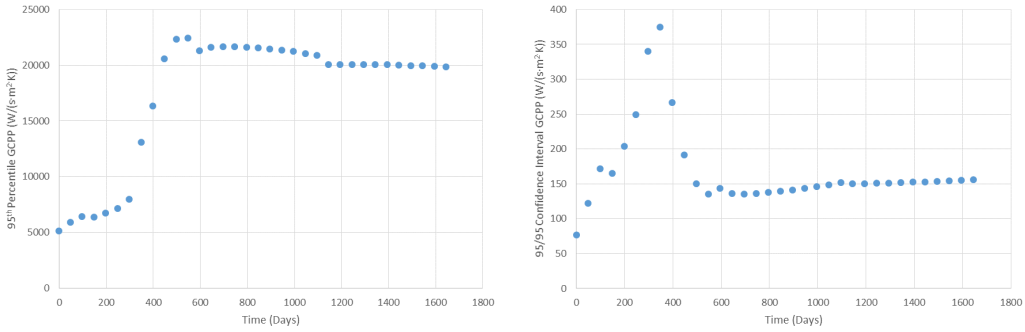

(a) 95th Percentile (b) +/- 95% Confidence Interval

Fig. 6.6: GCPP 95/95 Confidence Interval

Sensitivity Analysis of Minimum Departure from Nucleate Boiling Ratio

Results for MDNBR showed consistent rankings between all SA measures with negligible change in measures from state to state. Thus MDBNR analysis does not gain insight from computing the steady state solution to 34 states across three fuel cycles. However, benefits will be apparent in the UQ and SA results of the fuel performance FOM of MFCT and GCPP, which are far more sensitive to the cumulative effects of depletion. For the sake of brevity, only the final state is reported in Fig. 6.7.

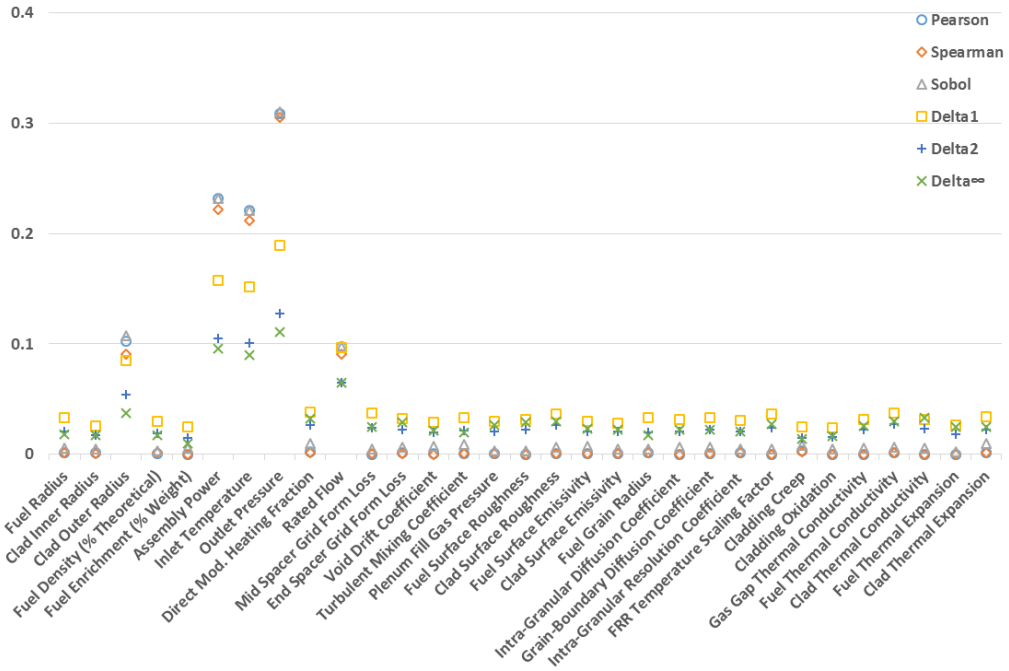

Fig. 6.7: Sensitivity Analysis Measures for MDNBR at 1644 Days.

The summation of Pearson measures is 0.98, indicating highly linear relations, thus all differences in methods will stem from noise in partitioning methods and kernel density estimations. Fig. 6.7 indicates that outlet pressure is the most impactful, with inlet temperature and assembly power also playing significant roles, and notable impact from rated flow and clad outer radius. This indicates that if greater fidelity in MDNBR values is desired, the two primary areas of focus must be thermal hydraulic boundary conditions

(inlet temperature and outlet pressure) and the operating power.

Not surprisingly, all inputs exclusive to fuel performance calculations have no impact on MDNBR. This is due to MDNBR being a thermal hydraulic FOM. In the current framework, the MDNBR reported is obtained directly from VERA-CS, completely independent of all BISON calculations.

Sensitivity Analysis of Maximum Fuel Centerline Temperature

The MFCT behaves predominantly linearly throughout the fuel lifecycle. The rankings among SA measures are consistent for each state. However significant shifts in SA measures do occur throughout the cycle. The shifts coincide with the onset of contact. Fig. 6.8, 6.9, and 6.10 show SA measures for MFCT at the pre-burnup, open gap state, mixed open and closed gap, and predominantly closed gap states respectively.

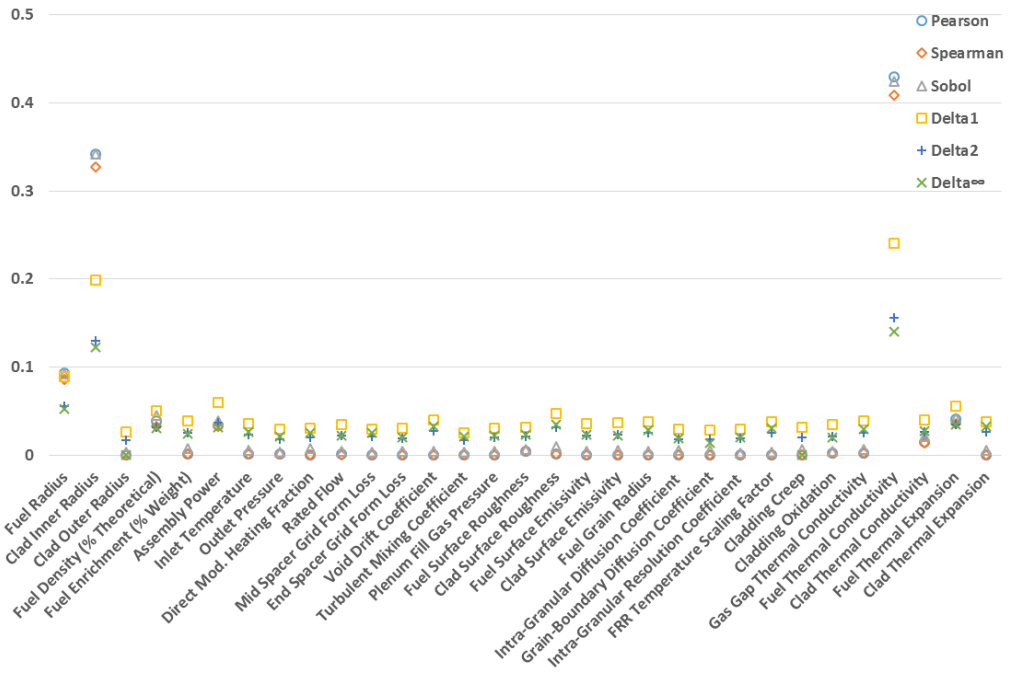

Fig. 6.8: Sensitivity Analysis Measures for MFCT at 0 Days.

The summation of Pearson measures for Fig. 6.8 is 1.01, indicating a linear system, thus all differences in SA measures stem from noise in partitioning methods and kernel

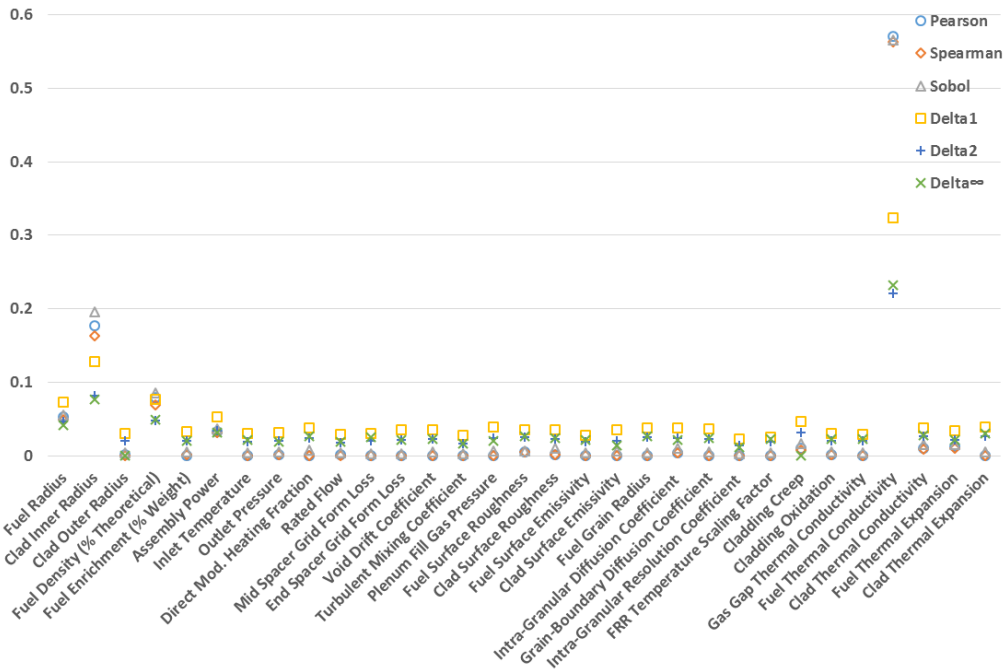

Fig. 6.9: Sensitivity Analysis Measures for MFCT at 348 Days.

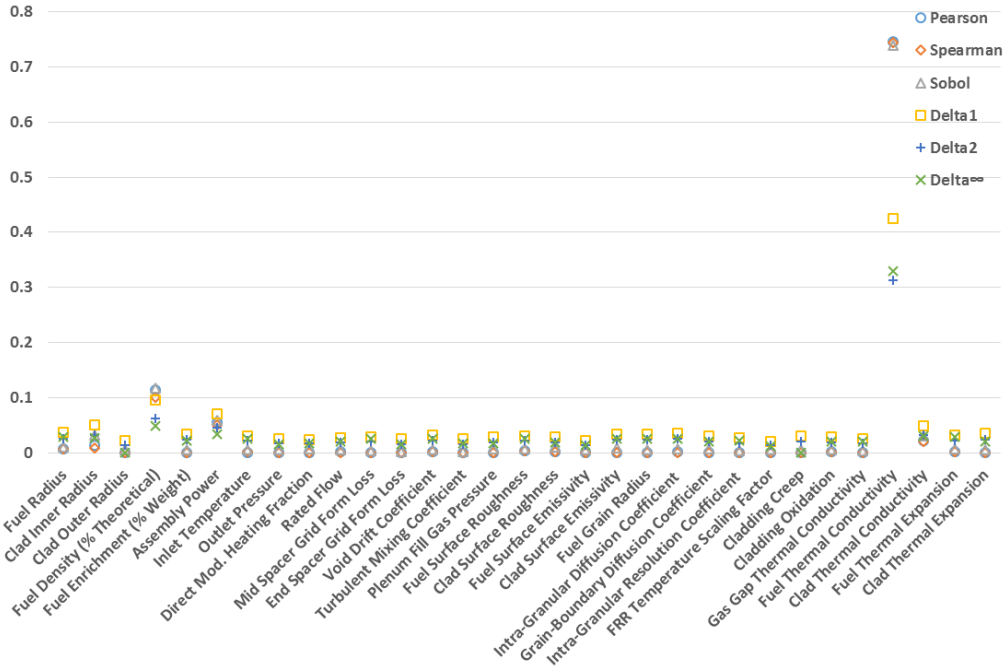

Fig. 6.10: Sensitivity Analysis Measures for MFCT at 448 Days.

density estimation. Fig. 6.8 shows that at the start of the fuel lifecycle, before burnup up has occurred, uncertainty primarily stems from fuel thermal conductivity due to its direct role in the gradients of temperature in the heat transfer calculation. Clad inner radius and fuel radius also contribute considerably due to their effects on gap width, which affects gap conductance. Note also that fuel thermal expansion has a slight impact due to its effect on gap width. Fuel density and core power also play a minor role due to their effect on burnup which affects fuel thermal conductivity. The SA measures remain relatively consistent between states and among each other in terms of rankings until the onset of contact, which is shown in Fig. 6.9.

Fig. 6.9 has a Pearson squared summation of 0.97 and shows a strong reduction in SA measures for gap dimensions in contrast to the pre-contact data of Fig. 6.8. This confirms intuition, since at this time many of the cases have transitioned from open to closed gap, resulting in a severely decreased dependency on gap dimension. As time progresses, eventually all cases contain closed gaps as shown in Fig. 6.10.

Pearson squared summation for Fig. 6.10 is 0.98, once again indicating most effects are linear. Fig. 6.10 shows that once most cases are in contact, nearly all uncertainty originates from fuel thermal conductivity with some effects from assembly power and fuel density due to their effect on burnup. This does not indicate that the MFCT is insensitive to assembly power, but rather that the MFCT uncertainty stemming from a 10% uncertainty in fuel thermal conductivity dwarfs the MFCT uncertainty arising from a 2% uncertainty in core power (see Table 6.2). Furthermore, the increase in SA measures on fuel thermal conductivity does not necessarily indicate an increased dependence of said input. Rather, it is more likely that the uncertainty stemming from gap width has ceased, causing a greater portion of the total uncertainty to originate from thermal conductivity.

Interestingly, at this state the fourth ranked input is clad thermal conductivity with a Pearson measure of 0.022, further emphasizing the near complete dependence on specific material properties once the gap is closed. The remainder of the life cycle shows little change in SA measures.

Sensitivity Analysis of Gap Conductance at Peak Power

Unlike MDNBR and MFCT, GCPP allows a showcasing of the higher order methods due to the presence of nonlinearities. The exclusively open and closed gap states are predominantly linear, however the intermediate states contain substantial nonlinearities due to the shifting between open and closed gap models as well as complexities stemming from fission gas generation. SA measures for GCPP at the pre-burnup state and mixed open and closed gap state are shown in Fig. 6.11 and 6.12.

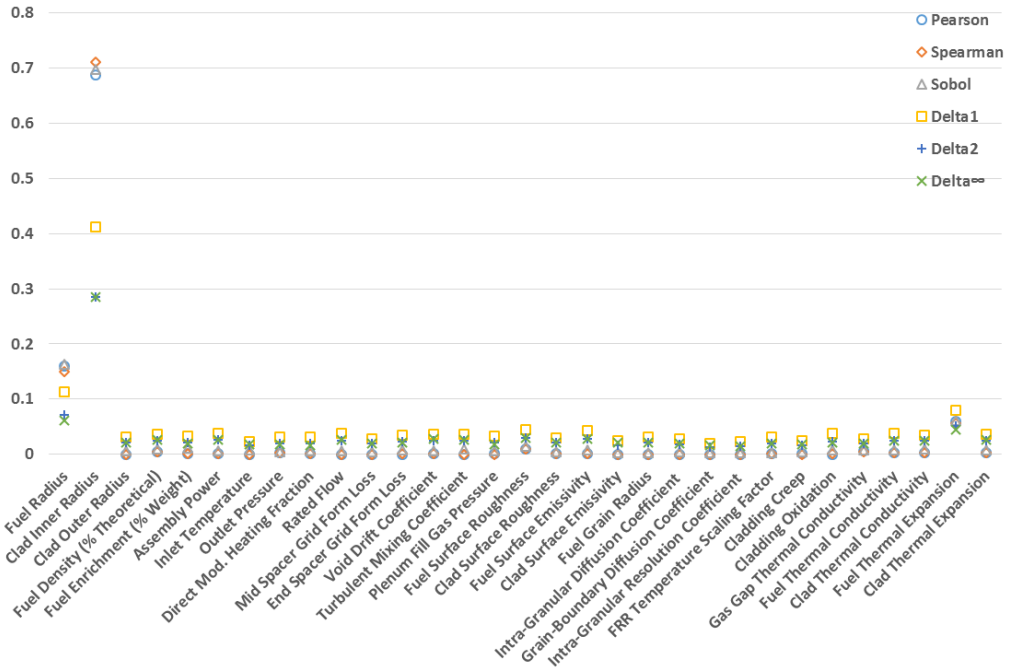

Fig. 6.11: Sensitivity Analysis Measures for GCPP at 0 Days.

Fig. 6.11 indicates that the clad inner radius and fuel radius are the largest contributors to GCPP uncertainty. This reaffirms that the GCPP is a strong function of gap dimensions. Note also that the third ranked input is the fuel thermal expansion due its direct effect on gap width. The Pearson squared summation is 1.01 indicating linear relations. The linearity of the data also creates consistent rankings among all measures.

Fig. 6.12 contains a Pearson squared summation of 0.60, indicating that while the

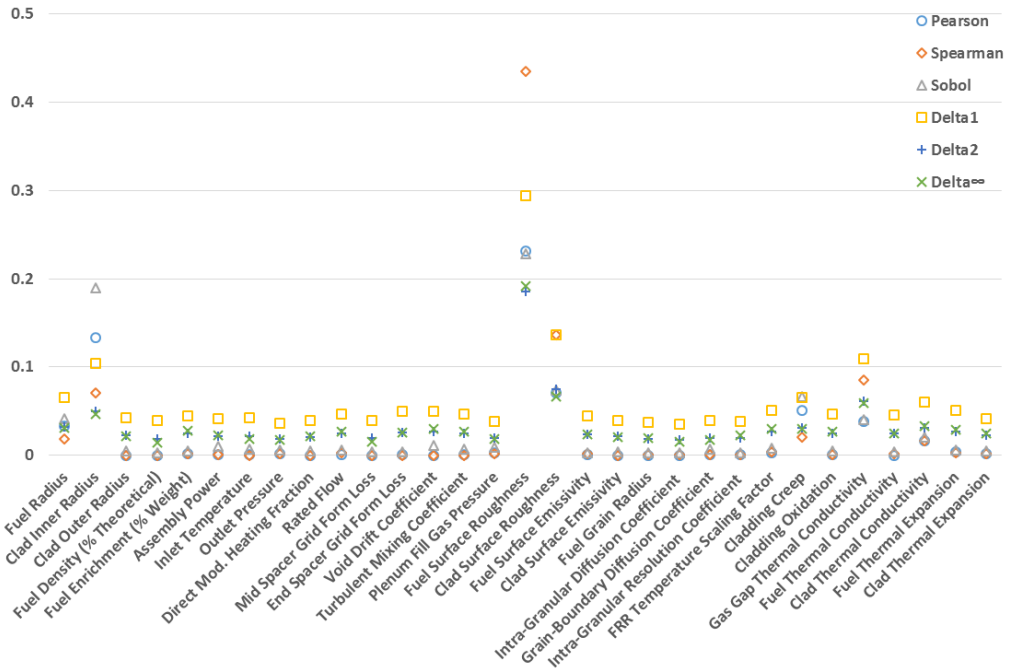

Fig. 6.12: Sensitivity Analysis Measures for GCPP at 448 Days.

majority of relations are still linear, 40% are nonlinear. These nonlinearities stem from the fact that while some cases still utilize the open gap models, the remainder have shifted to closed gap models. The presence of the open gap cases is evidenced by substantial SA measures for inner clad and fuel radii. Other cases have progressed to a complete independence from initial gap dimension, and a complete dependence on closed gap models. In such cases, GCPP is a strong function of fuel and clad roughness. This is due to BISON models treating closed gap cases as having finite thicknesses, which are highly dependent on fuel and cladding surface roughness.

Note that in Fig. 6.12, Spearman strongly detects the fuel and cladding surface roughness in comparison to Pearson. This ability is attributable to the Spearman measures superior ability to detect nonlinearities over Pearson. The fuel and surface roughness in particular are much larger with Spearman and Delta measures than Pearson and Sobol. This is likely due to the fact the perturbing of either roughness will only change GCPP for cases with small initial gap widths, and have next to no effect in instances with large initial

gaps. This behavior is highly nonlinear, specifically non-additive.

The variance based Sobol indices closely follows Pearson, but in fact underperforms Spearman in detection of surface roughness relations. This indicates nonlinearities of the roughness stem not from individual terms alone (i.e.) in which Sobol indices are effective, but rather from interactions between inputs (i.e.), which reaffirms that the model is non-additive.

It is worth noting that the GCPP uncertainty from the coupling of this work is more linear than the GCPP from past work with a VERA-CS and FRAPCON integration. This past work indicated that Pearson summations may be as low as 0.21 in mixed open and closed gap states [29]. Unfortunately a direct comparison between codes cannot be made at this time, as past FRAPCON work did not include the impactful fuel and cladding roughness as perturbed inputs. Nonetheless, the large increase in the summations of Pearson measures shows promise in establishing that within BISON, GCPP uncertainty behaves more linearly than its counterpart in FRAPCON due to more mechanistic models. This claim will be explored further in future work, by repeating a UQ/SA of VERA-CS/FRAPCON with the roughness inputs included.

Moving forward in the fuel lifecycle, Fig. 6.13 and 6.14 show GCPP SA measures at 548 days and 1644 days respectively.

The summation of Pearson measures for Fig. 6.13 indicates that roughly 86% of uncertainties come from linear effects. The linearity is further evidenced by strong agreement between SA measures. Note a complete independence from fuel and cladding radii, indicating all cases are independent of initial gap dimensions at this state. The increase in SA measure for gap gas thermal conductivity is likely due to the small gap dimension used by BISON for closed gap model. Since gap gas conductance is calculated as the gas thermal conductivity over the gap width, smaller gap dimensions cause changes in gas gap thermal conductivity to be magnified.

The Pearson summation decreases to 0.81 for Fig. 6.14. This increase in nonlinearity can be explained by the increase in SA measures for all fission gas release inputs, namely

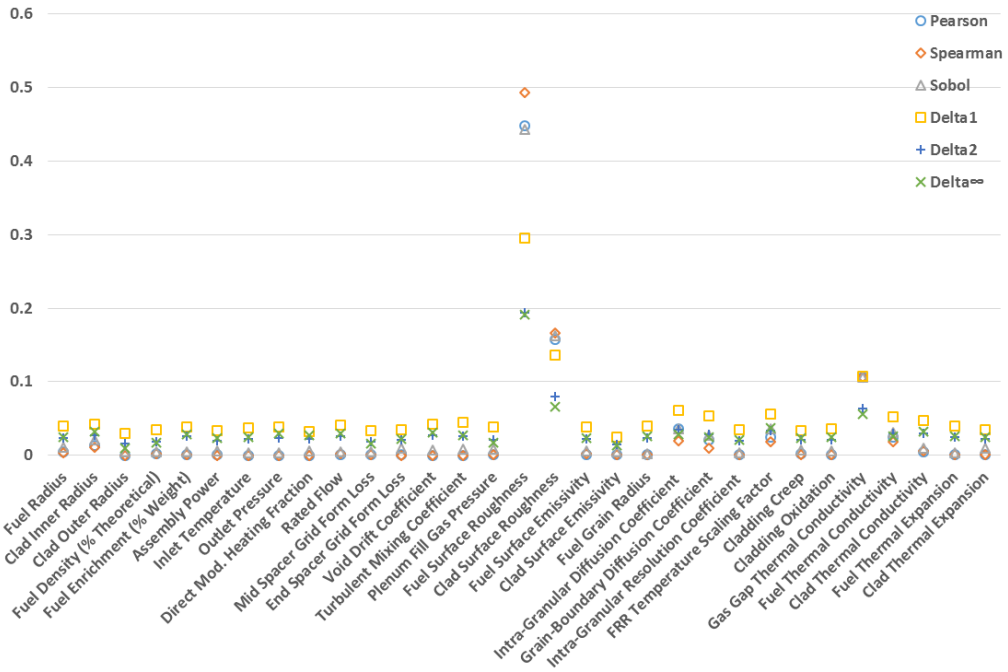

Fig. 6.13: Sensitivity Analysis Measures for GCPP at 548 Days.

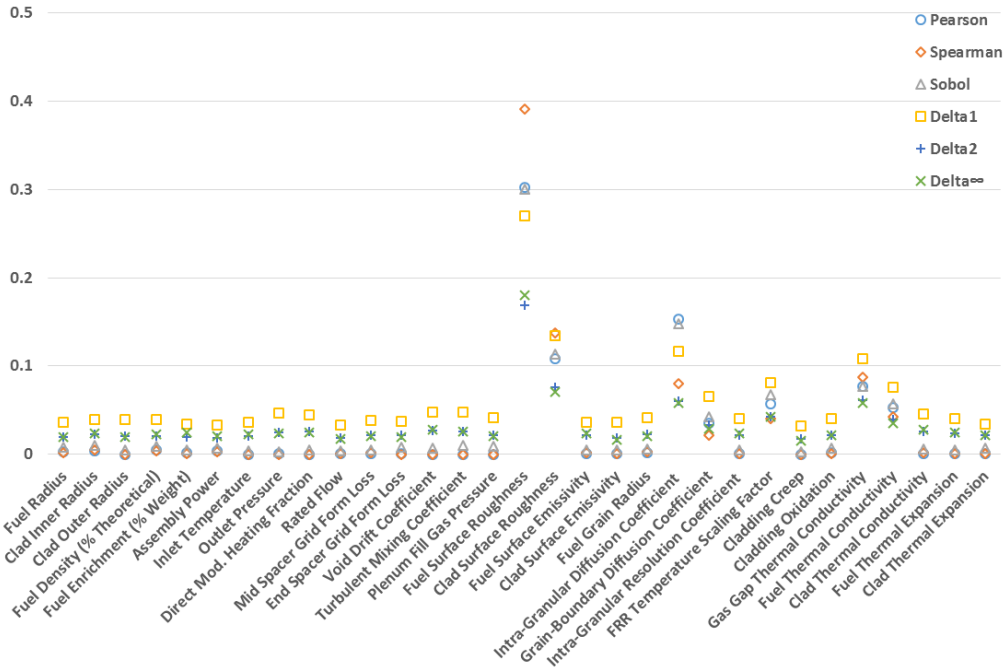

Fig. 6.14: Sensitivity Analysis Measures for GCPP at 1643 Days.

the intra-granular and grain boundary diffusion coefficients as well as fission gas release temperature biasing. This indicates that at higher states, sufficient fission gas release has occurred to the point of altering gap gas thermal conductivity. The models associated with fission gas release are extremely complex, and the perturbation range of the diffusion coefficients is very large (see Table 6.2). Thus the increase in nonlinearities from Fig. 6.13 to Fig. 6.14 is likely due to the increased role of fission gas products on GCPP at higher burnup.

6.7 Conclusions

LOTUS is a multiphysics environment which allows for the integration of the VERA-CS code with the fuel performance code BISON. All model inconsistencies are documented and either deemed negligible or given plans for future work. A successful Monte Carlo sampling with a direct data flow between the codes was used with a sample size of 2,500 VERA-CS cases and an equal number of BISON runs for the highest power pin at the final state.

Results provide UQ for MDNBR, MFCT, and GCPP for a 3 fuel cycle depletion case for a single assembly. Furthermore SA shows MDNBR to be linear, with little variation throughout the fuel cycle and a large dependence on assembly power and thermal hydraulic boundary conditions. MFCT also contains linear results, but shifts from a dependency on fuel thermal conductivity and gap dimensions, to almost exclusively fuel thermal conductivity after contact between fuel and cladding. Lastly, GCPP begins with linear relations and a strong dependence on gap dimension, followed by a nonlinear state dependent on gap dimension and surface roughness, followed by a predominantly linear state sensitive to surface roughness and fission gas release related inputs.

The SA results provide a path forward to decrease uncertainty for the FOM of this work. For instance, in the case of MFCT at the end of the fuel life cycle, SA indicates that over 80% of uncertainty at higher burnup stems from fuel thermal conductivity alone. Thus if a decrease in MFCT uncertainty at this state is desired, the primary focus must be on increasing the fidelity of fuel thermal conductivity models.

The UQ and SA results of MFCT and GCPP provide insights into the magnitude and

behavior of the uncertainty associated with rod internal energy and gap conductance in general, both of which are significant inputs in LB-LOCA simulations. Future LB-LOCA based work aimed at reducing operation margins will use the aforementioned SA results as a means of selecting relevant inputs. The incorporation of rigorous UQ and SA methods into integrated high-fidelity simulations of VERA-CS and BISON can better inform experiments to substantially accelerate the qualification of new fuel design concepts such as accident tolerant fuel and higher burnup fuel.

6.8 Acknowledgements

We would like to thank the BISON team at INL for their extensive work in developing BISON. This work is supported by the U.S. Department of Energy, under DOE Idaho Operations Office Contract DE-AC07-05ID14517. Accordingly, the U.S. Government retains a nonexclusive, royalty-free license to publish or reproduce the published form of this contribution, or allow others to do so, for U.S. Government purposes.

REFERENCES

[1] Blakely, C., Zhang, H., Folsom, C., Ban, H., and Szilard, R., "Application of regression, variance, and density based global sensitivity methods to integrated VERA-CS and BISON simulations," *Nuclear Engineering and Design*, Vol. 332, 2018, pp. 186 – 201.

[2] http://frapcon.labworks.org, Accessed: 2018.

[3] Sloan, B., McCorkle, D., and Bryden, K., "An Overview of Computational Environments for Engineering," *Proc. 51st AIAA Aerospace Sciences Meeting including the New Horizons Forum and Aerospace Exposition*, Jan 2013.

[4] https://www.casl.gov/, Accessed: 2018.

[5] Gaston, D., Newman, C., Hansen, G., and Lebrun-Grandié, D., "MOOSE: A parallel computational framework for coupled systems of nonlinear equations," *Nuclear Engineering and Design*, Vol. 239, No. 10, 2009, pp. 1768 – 1778.

[6] Todorova, N. K. and Ivanov, K. N., "Investigation of spatial coupling aspects for coupled code application in PWR safety analysis," *Annals of Nuclear Energy*, Vol. 30, No. 2, 2003, pp. 189 – 209.

[7] Sjenitzer, B. L., Hoogenboom, J. E., Escalante, J. J., and Espinoza, V. S., "Coupling of dynamic Monte Carlo with thermal-hydraulic feedback," *Annals of Nuclear Energy*, Vol. 76, 2015, pp. 27 – 39.

[8] Holt, L., Rohde, U., Seidl, M., Schubert, A., Uffelen, P. V., and Macián-Juan, R., "Development of a general coupling interface for the fuel performance code TRANSURANUS Tested with the reactor dynamics code DYN3D," *Annals of Nuclear Energy*, Vol. 84, 2015, pp. 73 – 85.

[9] Hales, J., Tonks, M., Gleicher, F., Spencer, B., Novascone, S., Williamson, R., Pastore, G., and Perez, D., "Advanced multiphysics coupling for LWR fuel performance analysis," *Annals of Nuclear Energy*, Vol. 84, 2015, pp. 98 – 110.

[10] Porter, I., Knight, T. W., and Raynaud, P., "Potential Impacts of Modeling Full Reactor Cores Using Combined Fuel Performance and Thermal Hydraulics Codes," *Nuclear Technology*, Vol. 190, No. 2, 2015, pp. 174–182.

[11] https://bison.inl.gov/, Accessed: 2018.

[12] Folsom, C. P., Jensen, C. B., Williamson, R. L., Woolstenhulme, N. E., Ban, H., and Wachs, D. M., "BISON Modeling of Reactivity-Initiated Accident Experiments in a Static Environment," *Proc. Top Fuel 2016*, Sept. 2016, Idaho National Laboratory, INL/CON-16-37614.

[13] Magedanz, J., Avramova, M., Perin, Y., and Velkov, A., "High-fidelity multi-physics system TORT-TD/CTF/FRAPTRAN for light water reactor analysis," *Annals of Nuclear Energy*, Vol. 84, 2015, pp. 234 – 243.

[14] Chang, G. S., "MCWO - Linking MCNP And ORIGEN2 For Fuel Burnup Analysis," *Proc. The Monte Carlo Method: Versatility Unbounded In A Dynamic Computing World*, April 2005, Idaho National Laboratory, INEEL/CON-04-02085.

[15] Leppänen, J., Pusa, M., Viitanen, T., Valtavirta, V., and Kaltiaisenaho, T., "The Serpent Monte Carlo code: Status, Development and Applications in 2013," *Annals of Nuclear Energy*, Vol. 82, 2015, pp. 142–150.

[16] Swiler, L. P., Lefebvre, R. A., Langley, B. R., and Thompson, A. B., "Integration of Dakota into the NEAMS Workbench," 2017, Sandia National Laboratories, SAND2017-7492.

[17] Bowman, S. M., "SCALE 6: Comprehensive Nuclear Safety Analysis Code System," *Nuclear Technology*, Vol. 174, No. 2, 2011, pp. 126–148.

[18] Boyack, B., Catton, I., Duffey, R., Griffith, P., Katsma, K., Lellouche, G., Levy, S., Rohatgi, U., Wilson, G., Wulff, W., and Zuber, N., "Quantifying reactor safety margins part 1: An overview of the code scaling, applicability, and uncertainty evaluation methodology," *Nuclear Engineering and Design*, Vol. 119, No. 1, 1990, pp. 1 – 15.

[19] Marcum, W. and Brigantic, A., "Applying uncertainty and sensitivity on thermal hydraulic subchannel analysis for the multi-application small light water reactor," *Nuclear Engineering and Design*, Vol. 293, 2015, pp. 272 – 291.

[20] Ikonen, T., "Comparison of global sensitivity analysis methods Application to fuel behavior modeling," *Nuclear Engineering and Design*, Vol. 297, 2016, pp. 72 – 80.

[21] Ikonen, T. and Tulkki, V., "The importance of input interactions in the uncertainty and sensitivity analysis of nuclear fuel behavior," *Nuclear Engineering and Design*, Vol. 275, 2014, pp. 229 – 241.

[22] Swiler, L. P., Gamble, K. A., Schmidt, R. C., , and Williamson, R. L., "Sensitivity Analysis of OECD Benchmark Tests in BISON," 2015, Sandia National Laboratories, SAND2015-8808.

[23] Pastore, G., Swiler, L., Hales, J., Novascone, S., Perez, D., Spencer, B., Luzzi, L., Uffelen, P. V., and Williamson, R., "Uncertainty and sensitivity analysis of fission gas behavior in engineering-scale fuel modeling," *Journal of Nuclear Materials*, Vol. 456, 2015, pp. 398 – 408.

[24] Talbot, P. W., Gamble, K. A., Rabiti, C., Wang, C., Alfonsi, A., Cogliati, J., Mandelli, D., and Prinja, A., "Time-Dependent Sensitivity Analysis of OECD Benchmark using BISON and RAVEN," *Transactions of the American Nuclear Society*, Vol. 115, 2016.

[25] Brown, C. and Zhang, H., "Uncertainty quantification and sensitivity analysis with CASL Core Simulator VERA-CS," *Annals of Nuclear Energy*, Vol. 95, 2016, pp. 188 – 201.

[26] Brown, C., Zhang, H., Kucukboyaci, V., and Sung, Y., "Best estimate plus uncertainty analysis of departure from nucleate boiling limiting case with CASL core simulator VERA-CS in response to PWR main steam line break event," *Nuclear Engineering and Design*, Vol. 309, 2016, pp. 8 – 22.

[27] Dinh, N., "CIPS Validation Data Plan," March 2012, Idaho National Laboratory, INL/EXT-12-25347.

[28] Williams, M. L. and Rearden, B. T., "SCALE-6 sensitivity/uncertainty methods and covariance data," *Nuclear Data Sheets*, Vol. 109, No. 12, 2008, pp. 2796 – 2800.

[29] Blakely, C., Zhang, H., and Ban, H., "Sensitivity analysis of VERA-CS and FRAPCON coupling in a multiphysics environment," *Annals of Nuclear Energy*, Vol. 111, 2018, pp. 683 – 701.

[30] Borgonovo, E., "A new uncertainty importance measure," *Reliability Engineering and System Safety*, Vol. 92, No. 6, 2007, pp. 771 – 784.

[31] Zhai, Q., Yang, J., Xie, M., and Zhao, Y., "Generalized moment-independent importance measures based on Minkowski distance," *European Journal of Operational Research*, Vol. 239, No. 2, 2014, pp. 449 – 455.

[32] Kochunas, B., Collins, B. S., Jabaay, D., Kim, K. S., Graham, A., Stimpson, S., Wieselquist, W. A., Clarno, K. T., Palmtag, S., Downar, T., and Gehin, J. C., "VERA Core Simulator Methodology for PWR Cycle Depletion," *Proc. ANS MC2015*, April 2015, Oak Ridge National Laboratory (ORNL); Oak Ridge Leadership Computing Facility (OLCF); Consortium for Advanced Simulation of LWRs (CASL).

[33] Rempe, K. R., Smith, K. S., and Henry, A. F., "SIMULATE-3 Pin Power Reconstruction: Methodology and Benchmarking," *Nuclear Science and Engineering*, Vol. 103, No. 4, 1989, pp. 334–342.

[34] Stimpson, S. G., Clarno, K. T., Powers, J. J., Collins, B. S., Pawlowski, R., Toth, A., Gardner, R., Novascone, S. R., Hales, J. D., and Pastore, G., "Demonstration of Coupled Tiamat Single Assembly Calculations," 2017, Oak Ridge National Laboratory, CASL-U-2017-1357-000.

[35] Williamson, R., Hales, J., Novascone, S., Tonks, M., Gaston, D., Permann, C., Andrs, D., and Martineau, R., "Multidimensional multiphysics simulation of nuclear fuel behavior," *Journal of Nuclear Materials*, Vol. 423, No. 1, 2012, pp. 149 – 163.

[36] Bai, X.-M., Tonks, M. R., Zhang, Y., and Hales, J. D., "Multiscale modeling of thermal conductivity of high burnup structures in UO2 fuels," *Journal of Nuclear Materials*, Vol. 470, 2016, pp. 208 – 215.

[37] Schwen, D., Aagesen, L., Peterson, J., and Tonks, M., "Rapid multiphase-field model development using a modular free energy based approach with automatic differentiation in MOOSE/MARMOT," *Computational Materials Science*, Vol. 132, 2017, pp. 36 – 45.

[38] Bratton, R. N., Jessee, M. A., and Wieselquist, W. A., "Rod internal pressure quantification and distribution analysis using Frapcon," *Proc. 2016 Conference on Physics of Reactors*, May 2016, pp. 2588–2602, ORNL/TM-2015/557.

[39] Stimpson, S., Powers, J., Gardner, R., Clarno, K., and Pawlowski, R., "Effect of Clad Fast Neutron Flux Distribution on Quarter-Core Fuel Performance Calculations with BISON," *Proc. 2017 Water Reactor Fuel Performance Meeting*, Sept. 2017, Idaho National Laboratory.

[40] Croff, A. G., "ORIGEN2: A Versatile Computer Code for Calculating the Nuclide Compositions and Characteristics of Nuclear Materials," *Nuclear Technology*, Vol. 62, No. 3, 1983, pp. 335–352.

[41] Lassmann, K., "TRANSURANUS: a fuel rod analysis code ready for use," *Journal of Nuclear Materials*, Vol. 188, 1992, pp. 295 – 302.

[42] Siefken, L. J., E. W. Coryell, E. A., Harvego, and Hohorst, J. K., "MATPRO - A Library of Materials Properties for Light-Water-Reactor Accident Analysis," 2001, Rev. 2, NUREG/CR-6150.

[43] Harding, B., Tremblay, C., and Cousineau, D., "Standard errors: A review and evaluation of standard error estimators using Monte Carlo simulations," *Tutorials in Quantitative Methods for Psychology*, Vol. 10, No. 2, 2014, pp. 107 – 123.

[44] Plischke, E., "An adaptive correlation ratio method using the cumulative sum of the reordered output," *Reliability Engineering and System Safety*, Vol. 107, 2012, pp. 149 – 156, SAMO 2010.

[45] Herman, J. and Usher, W., "SALib: An open-source Python library for Sensitivity Analysis," *The Journal of Open Source Software*, Vol. 2, No. 9, jan 2017.

[46] Plischke, E., Borgonovo, E., and Smith, C. L., "Global sensitivity measures from given data," *European Journal of Operational Research*, Vol. 226, No. 3, 2013, pp. 536 – 550.

[47] Botev, Z. I., Grotowski, J. F., and Kroese, D. P., "Kernel density estimation via diffusion," *Ann. Statist.*, Vol. 38, No. 5, 10 2010, pp. 2916–2957.

[48] http://pyqt-fit.readthedocs.io/en/latest/, Accessed: 2018.

aiaa

CHAPTER 7

Transition to Integration of PHISICS with FRAPCON and RELAP

Having performed UQ and SA studies of multiphysics of quasi-steady state depletion cases, the next natural progression was to begin exploring transient failure scenarios. The following chapter details the foundation for an integration between the nuetronics code PHISICS and RELAP5-3D, both of which were developed at INL, and FRAPCON. This integration is used to model a large break- loss of coolant accident (LB-LOCA).

PHISICS and FRAPCON are used in conjunction to supply initial core conditions to RELAP5-3D, after which RELAP5-3D handles all LB-LOCA modeling. The data transfer between the three codes is extensive, thus the primary focus of this work is the LOTUS framework itself, with a relatively simple UQ study performed using Wilks' method. Later work will include a Monte Carlo based UQ of the integration with an accompanying sensitivity analysis with higher order methods.

Perhaps most importantly, this work establishes the foundation for an HDF5 based LOTUS framework which allows for a plug and play environment. The data created from this work is extensive but compressed, and may be accessed by future integrations. All future works with LOTUS will include this framework, which will greatly streamline the integration process.

CHAPTER 8

DEMONSTRATION OF LOTUS MULTIPHYSICS BEPU ANALYSIS FRAMEWORK FOR LB-LOCA SIMULATIONS[1]

This chapter contains a reformatted version of an article which was submitted to the journal *Annals of Nuclear Energy* in April of 2018.

8.1 Abstract

The LOCA Toolkit for U.S. light water reactors (LOTUS) currently under development at Idaho National Labs (INL) is a plug and play, multiphysics environment to be used in support of system level plant transient analysis. New proposed rule changes in LOCA safety regulations (10 CFR 50.46c) require the inclusion of cladding hydrogen content in the evaluation of equivalent cladding reacted (ECR) and peak cladding temperature (PCT). This rule change would require new evaluation tools, specifically the union of neutronics, system analysis, and fuel performance codes within a framework allowing for uncertainty quantification (UQ). A demonstration of LOTUS capabilities to address this potential need is performed with an integration of the neutronics code PHISICS, the fuel performance code FRAPCON, and the system analysis code RELAP5-3D. UQ is performed via Wilks method to compute the one sided 95/95 confidence values of the aforementioned safety metrics. Results demonstrate the benefits of the Multiphysics Best Estimate Plus Uncertainty (MP-BEPU) methodology and provide useful visualization of the limiting cases.

8.2 Introduction

Mathematical modeling of light water reactors (LWR) requires capturing the effects of multiple, interconnected physical phenomena. Lately, the needed computational models for LWR simulations are being placed in computational environments. The word environment

[1] Coauthors: Hongbin Zhang, Ronaldo Szilard, Aaron Epiney, Rodolfo Vaghetto, and Heng Ban

is amorphous [1], however in this work it is taken to define a computational space in which programs are treated as modules by which large amounts of data can be created, exchanged, and processed.

A number of multiphysics environments are being developed within the nuclear community by a variety of different groups. Instances include MOOSE at Idaho National Laboratory (INL) [2], VERA by the Consortium of Advanced Simulation of Light Water Reactors (CASL) [3], and the Nuclear Energy Advanced Modeling and Simulation (NEAMS)s Workbench [4]. It is worth noting that many others have created multiphysics couplings between codes which may be considered environments. However for the sake of brevity, only relatively recent multiphysics environments intended to be platforms for a plethora of future studies in nuclear energy are listed here.

Current work at INL includes the building of a new multiphysics environment known as the LOCA Toolkit for U.S. Light Water Reactors (LOTUS). The LOTUS environment is unique in the use and size of HDF5 databases [5], allowing for a flexible plug and play environment. The focus of this work is to use LOTUS to build an integration of codes capable of enhancing system level plant transient analysis during large break loss of coolant accident (LB-LOCA) conditions.

As a demonstration, LOTUS is used to evaluate new LOCA safety metrics under U.S. Nuclear Regulatory Commission (NRC)s proposed 10 CFR 50.46c new rulemaking [6]. LOTUS would be adept at analyzing these new metrics as they require integrated core design, fuel performance, and systems analysis calculations. Pending approval by the U.S. NRC, the new rules (10 CFR 50.46c) would require taking cladding hydrogen content into account in the evaluation of peak cladding temperature (PCT) and the equivalent cladding reacted (ECR). The PCT and ECR limits as functions of cladding hydrogen content in weighted parts per million (wppm) are shown in Fig. 8.1.

ECR and PCT can be calculated within the well-established systems analysis code RELAP5-3D. However, cladding hydrogen content can only be obtained from fuel performance simulations of the fuel depletion preceding the LOCA event. This work seeks to

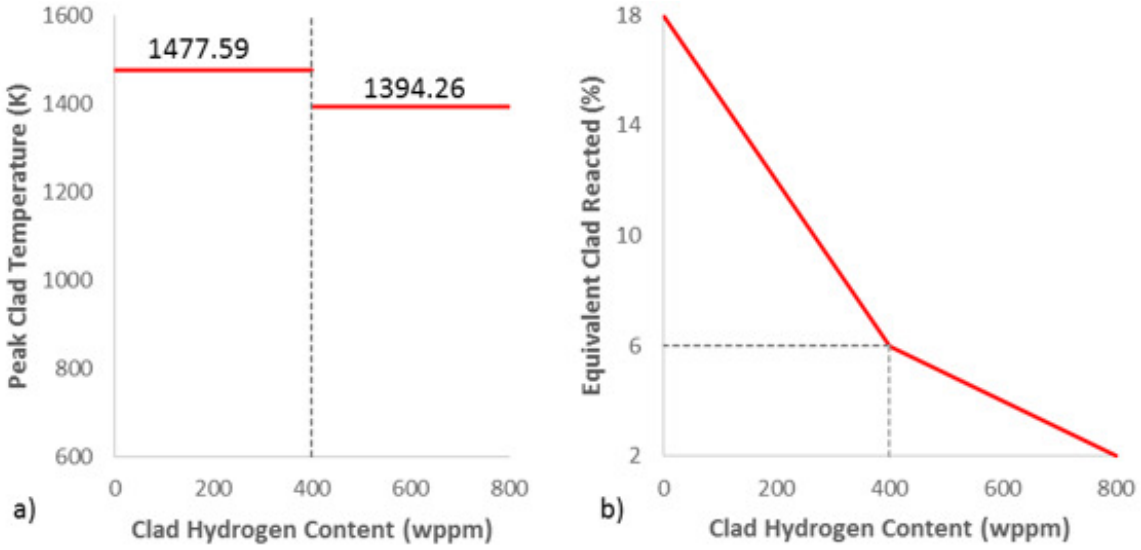

Fig. 8.1: a) PCT and b) ECR Limit as Functions of Cladding Hydrogen Content.

resolve this issue by using LOTUS to integrate RELAP5-3D [7] with the fuel performance code FRAPCON [8].

The integration of system analysis codes with fuel performance codes has been performed in the past. A foundational work has been performed for the generic, semi-implicit coupling of RELAP5-3D with COBRA, CONTAIN, as well as computational fluid dynamic CFD codes [9]. Integration of a past version of RELAP (RELAP4) with FRAPCON has also been performed [10].

Notable thermal hydraulic coupling with FRAPCON includes a coupling between a customized version of FRAPCON and the thermal hydraulic code TRACE for a quasi-steady state depletion case [11]. FRAPTRAN has also been coupled with the thermal hydraulic code COBRA-TF and the neutronics code TORT-TD [12]. A comparison of a FRAPCON/COBRA-TF/TORT-TD coupling to a COBRA-TF/TORT-TD coupling (with COBRA-TF handling the fuel performance) was also conducted [13]. Recent work at INL has focused on the modeling of Reactivity Insertion Accidents (RIA) using a coupling of RELAP5-3D with the new fuel performance code BISON [14].

LOTUS also supplies FRAPCON and RELAP5-3D with power profiles from the neutronics code PHISICS as previously outlined in past work [15]. The coupling methodology

of PHISICS to RELAP5-3D is well documented [16].

Noteworthy multiphysics studies involving RELAP5-3D with specialized neutronics calculations include a coupling with the SIMULATE-3K code [17]. Fuel performance codes have also been coupled with a variety of neutronics codes in the past. Examples include a coupling of FRAPCON with SCALE [18] and BISON with DeCART [19], SERPENT [20], and RATTLESNAKE [21].

In comparison to the aforementioned multiphysics studies, this work is unique in two aspects. Firstly, it focuses on the evaluation of ECR and PCT with respect to limits based on cladding hydrogen content. Secondly it performs uncertainty quantification (UQ) on the outputs of interest. In any mathematical model intended to be reflective of reality, all calculations and inputs have uncertainties. Due to the vast number of inputs and calculations within a multiphysics environment, it is particularly important to quantify the cumulative effects of uncertainties. UQ is essential in complying with the industry standard of best estimate plus uncertainty (BEPU) methodology. BEPU ensures that decisions makers are always privy to the corresponding level of confidence for all calculated values of concern.

The incorporation of BEPU methods within a multiphysics environment is known as multiphysics best estimate plus uncertainty (MP-BEPU) methodology. MP-BEPU is superior to standard BEPU in that more inputs and calculation biases may be concurrently perturbed. Furthermore, MP-BEPU may also allow for less conservative estimates of safety metrics. These improved estimates have the potential to decrease plant safety margins, thereby allowing higher operation power and/or greater flexibility during power maneuvers.

Within this work, only FRAPCON and RELAP5-3D input decks are subject to perturbations. The MP-BEPU methodology implemented in this work is focused on fuel performance and systems analysis. Thus while the PHISICS code is given proper attention, the primary emphasis is on the FRAPCON and RELAP5-3D codes. Future work will fully incorporate neutronics within the MP-BEPU methodology.

The primary objectives of this work are to describe the unique benefits of the LOTUS framework, and provide UQ of PCT and ECR measures using Wilks method for a large

break loss of coolant accident (LB-LOCA). The figures of merit (FOM) are to be evaluated for a LB-LOCA for an equilibrium cycle of a generic four-loop pressurized water reactor (PWR) at the beginning of cycle (BOC), and end of cycle (EOC) as well as 100 days, 200 days, 300 days, 400 days, and 500 days into the cycle. From the sample, the limiting case with respect to each FOM is presented and analyzed.

8.3 LOTUS Description

As shown in Fig. 8.1, LOTUS will provide an environment for the integration of multiple codes within the disciplines of Core Design Automation (CD-A), Fuel Performance (FP), Systems Analysis (SA), and Core Design Optimization (CD-O). LOTUS will also include Uncertainty Quantification (UQ), Sensitivity Analysis (SA), and Risk Assessment (RA).

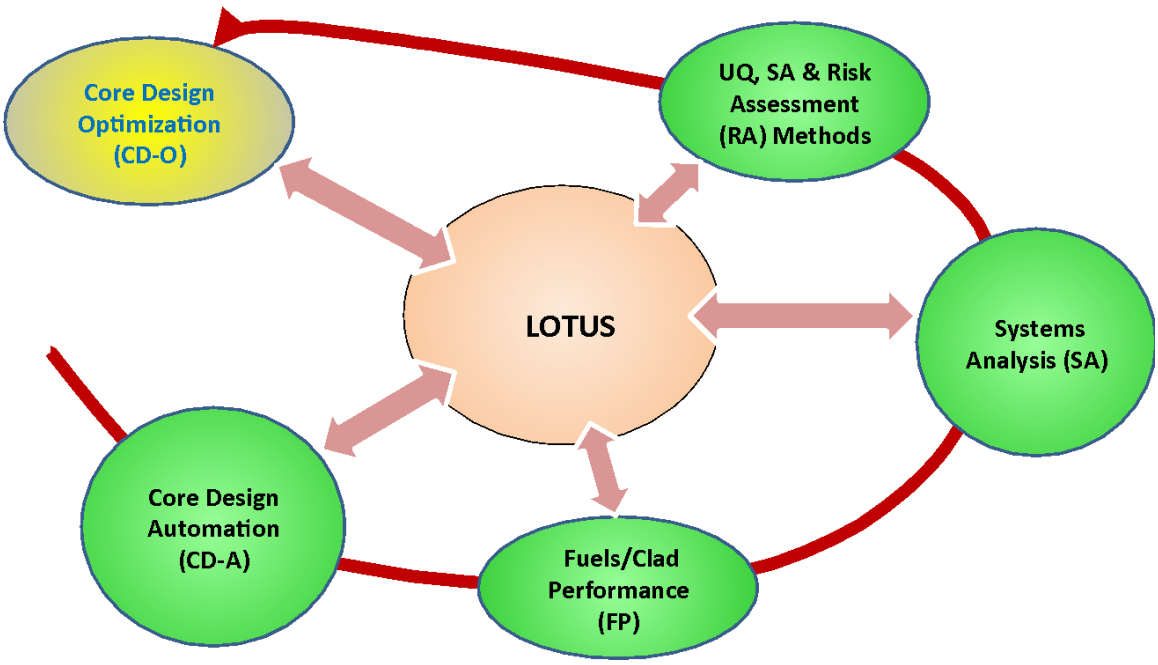

Fig. 8.2: Conceptual Schematic of LOTUS Capabilities.

The integration presented in this work demonstrates CD-A using the PHISCS code, fuel performance using the FRAPCON code, and system analysis using the RELAP5-3D

code in conjunction with UQ software, which is only a portion of eventual capabilities. As Fig. 8.2 suggests, LOTUS will eventually entail additional codes. LOTUS stores all data within HDF5 databases (see section 8.4). This method of storage allows the results of past cases to be accessed by later works, thereby avoiding redundancies in future code integrations.

8.3.1 Code Descriptions

This section contains descriptions of PHISCIS, FRAPCON, and RELAP5-3D as well as a section detailing code discrepancies.

PHISICS

The PHISICS (Parallel and Highly Innovative Simulation for the INL Code System) code toolkit is being developed at the Idaho National Laboratory [22, 23]. This package is intended to provide a modern analysis tool for reactor physics investigations. It is designed to maximize the accuracy for a given availability of computational resources and to give state-of-the-art tools to the nuclear engineer.

Several different algorithms and meshing approaches are implemented among which the user can choose in order to optimize the computational resources and accuracy needs. The software is completely modular in order to simplify independent development of modules and maintenance by different teams. The different modules currently available in the PHISICS package are a nodal and semi-structured transport core solver (INSTANT), a depletion module (MRTAU), a time-dependent solver (TimeIntegrator), a cross section interpolation and manipulation framework (MIXER), a criticality search module (CRITICALITY) and a fuel management and shuffling component (SHUFFLE).

PHISICS can be run in parallel to take advantage of multiple computer cores (10 to 100 cores). Due to the homogenization of neutronics and thermal hydraulic calculations, PHISICS has a largely reduced computational expense in comparison to pin resolved codes. PHISICS output files contain the core power distribution for three dimensional core geometries at a variety of states.

FRAPCON

FRAPCON [8] is a fuel performance code developed by Pacific Northwest National Laboratories over the course of forty years. FRAPCON is a mature technology with extensive experimental validation for quasi-steady state depletion cases. The code is 1 dimensional, meaning the equations are solved in an axisymmetric fashion, with only the radial direction fully solved. The code includes axial effects such as axial power peaking factors, and a single channel enthalpy rise model for the coolant. Furthermore, fission gas release and plenum pressure are computed based off of the cumulative effects of all axial locations.

FRAPCON simulations are very numerically stable and fast for PWR problems, with run times of roughly two seconds per case. FRAPCON often relies upon empirical relations in areas where more recent codes use more mechanistic models. While this limits the robustness of the code for new fuel and reactor designs, it is advantageous in performance and accuracy for PWR cases involving traditional materials.

RELAP5-3D

RELAP5-3D [7] is a simulation tool that allows users to model the behavior of the reactor coolant system and the core for various operational transients and postulated accidents that might occur in a nuclear reactor. RELAP5-3D (Reactor Excursion and Leak Analysis Program) can be used for reactor safety analysis, reactor design, simulator training of operators, and as an educational tool by universities. RELAP5-3D is developed and maintained at INL. It is able to model the behavior of the plant system (heat exchangers, steam generators, pumps, valves, etc.) and the thermal-hydraulics of the reactor core. The code was specifically designed for simulations of light water reactor (LWR) transients such as loss of coolant (LOCA), anticipated transients without scram, and operational transients such as loss of feed-water, etc.

RELAP5-3D input decks allow considerable user control. The structure of the code permits users to assign values to a vast number of material and performance parameters, as well as bias many individual thermal hydraulic calculations (i.e. the estimation of heat transfer coefficients). This flexibility allows for extensive input perturbations as shown in

the list of perturbed inputs of this work (see section 8.5.3).

8.3.2 Model Inconsistencies

Differences between PHISICS, FRAPCON, and RELAP5-3D fall into one of three categories, the domain of the code, phenomena modeled, and numerical discretization.

Code Domain

In terms of domain, PHISICS models a full reactor core while FRAPCON models individual fuel rods within an idealized single coolant subchannel. RELAP5-3D models a set of heat structures representing the full core, as well as the entire primary and secondary coolant loops and the Emergency Core Coolant System (ECCS). Essentially PHISICS and FRAPCON model a small subspace of the full RELAP5-3D domain. The largest discrepancies stemming from these domain differences are in the form of boundary conditions.

FRAPCON and PHISICS specify a core inlet temperature, outlet pressure, and mass flow rate or flux, all of which are not boundary conditions within RELAP5-3D as there are no domain boundaries at the core inlet and outlet. In the interests of minimizing the discrepancy to the extent possible, the PHISICS values and FRAPCON nominal values of mass flux and outlet pressure were selected based off the results of the nominal case of RELAP5-3D. Also the nominal FRAPCON inlet nominal temperature was selected based on the supplied input to PHISICS.

Phenomena Modeled

The phenomenological differences between PHISICS, FRAPCON, and RELAP5-3D are vast. FRAPCON and RELAP5-3D have evolved separately over forty years to solve very different types of problems, while PHISICS is a modern code relying on more recently developed methods. As a result there are large variations in the specific phenomena modeled as well as in the sophistication and numerical accuracy of the individual models involved.

For instance, RELAP5-3D has extensive empirical relations for coolant heat transfer coefficients while FRAPCON only utilizes two relations (one for forced film convection and

the other for nucleate boiling). Conversely FRAPCON contains dynamic gap conductance models which take into account material deformation, fission gas release, pellet cladding mechanical interaction and irradiative effects, while the dynamic gap conductance model of RELAP5-3D uses simplified gap deformation models in conjunction with the ideal gas law (constant gas composition assumed).

The elimination of the majority of these phenomenological discrepancies is either not reasonable, beyond the scope of this work, and/or of little benefit. In most cases, extensive validation has established that the simplifications within each code are appropriate for specific problems they encounter. Within the context of this work, PHISICS and FRAPCON may be thought of as initialization modules within the RELAP5-3D framework.

PHISICS provides power histories to FRAPCON and the core power shapes at the time of LB-LOCA to RELAP5-3D. FRAPCON solves a quasi-steady state depletion problem, which RELAP5-3D is not equipped to model. Fuel performance data from FRAPCON is then supplied to RELAP5-3D as means to potentially enhance the fidelity of the RELAP5-3D. RELAP5-3D then executes a LB-LOCA simulation, which FRAPCON is incapable of performing. The integration of these codes within LOTUS, while not an all-encompassing model of true reactor physics, is an improvement over more compartmentalized approaches.

Discretization

For steady state simulations of the fuel rods, both the FRAPCON and RELAP5-3D codes use finite difference approximations which solve the heat conduction equation in the radial direction alone, but allow for axial variation in linear heat rates. This is referred to as 1 D in FRAPCON documentation. While there are phenomenological differences in the computation of thermal conductivity, the numerical methods themselves do not contain significant discrepancies.

Within this work, the number of radial and axial nodes differs between code input files. FRAPCON has 17 radial elements in the fuel and 5 in the cladding while RELAP5-3D has only 5 in the fuel and 2 in the cladding. The PHISICS and FRAPCON input files have 15 axial elements within the fuel rod while RELAP5-3D uses 6 axial elements in the interests

of maintaining reasonable run times. Thus within this work, FRAPCON and PHISICS use greater spatial discretization as compared to the heat structures of RELAP5-3D. Once again it is stressed that FRAPCON and PHISCS can be seen as modules used for the initialization of the core within the RELAP5-3D structure. Thus numerical approximations within RELAP5-3D do not affect FRAPCON or PHISICS, and potential improvements in numerical estimates within PHISICS and FRAPCON serve only to enhance traditional RELAP5-3D studies.

8.4 LOTUS Structure

LOTUS retrieves all values of interest from output files and stores them in a more compact manner. The data is also easily accessible for other codes. Provided that the needed data was calculated and stored, any arbitrary codes can be added into the LOTUS structure in an ad-hoc manner and access previously generated data. This flexibility in storage allows for a plug and play environment. The data flow structure of this work is shown in Fig. 8.3 .

For this specific work which includes a nominal case and 93 perturbed cases at each selected cycle exposure point (see section 8.5.4), the entire HDF5 database uses 4.4 G as opposed to 1.2 TB if all PHISICS, FRAPCON, and RELAP5-3D files were to be stored. This compression in data will be essential in later works involving Monte Carlo analysis with sample sizes on the order of thousands.

It is worth noting that the codes within this work are integrated, not coupled. While some sources would consider the data flow shown in Fig. 8.3 to be an one-way or even loose coupling, within this work the term coupling indicates feedback between codes. Plans for future work include a tight coupling of transient fuel performance and systems analysis codes for increased fidelity in LOCA simulations.

Critical to MP-BEPU is consistent uncertainty propagation. The output of any code has a level of uncertainty. In cases where the frequency of code executions is limited by hardware constraints, more computationally expensive codes are executed a limited number of times. The resultant sample size is then used to create an estimated probability density

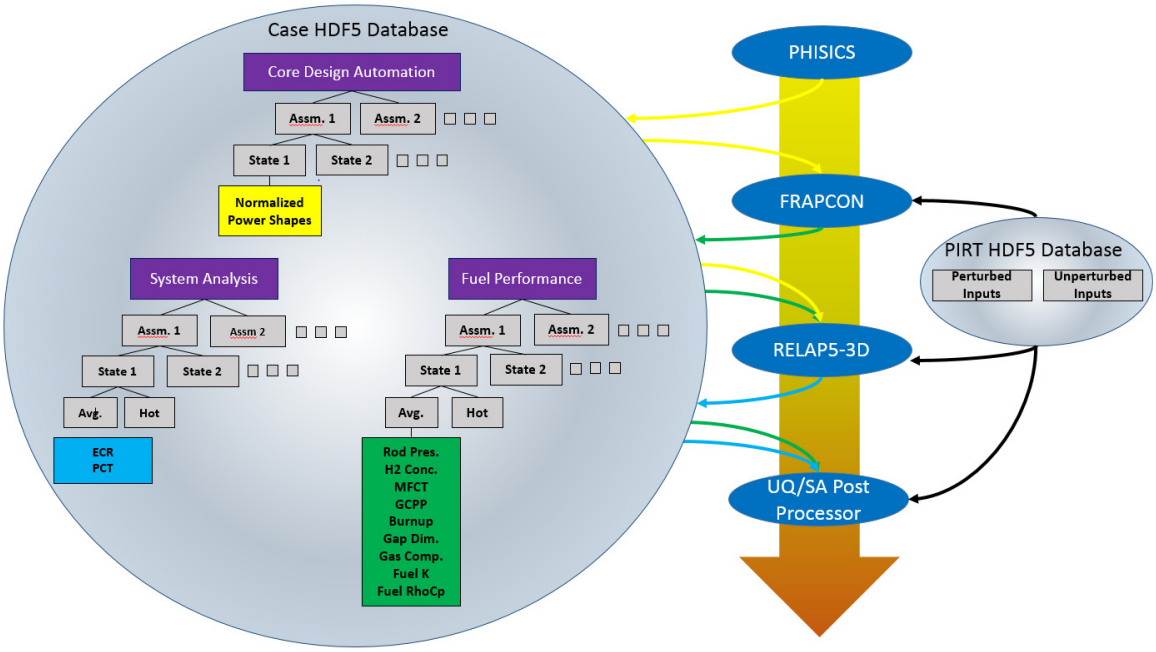

Fig. 8.3: LOTUS Data Flow Structure for a Single Instance of Monte Carlo Sampling. Colors of Arrows Connecting Case HDF5 Database to Codes Correspond to HDF5 Database Group.

function (PDF) for outputs of interest. A large sample size is then generated from these PDFs, which can then be used by less expensive codes.

Fortunately due to the mere 93 runs required by Wilks method (see section 8.5.4) and the large computational resources available at INL, a more preferable direct connection method is possible. In this method, the data is passed directly between codes for each instance of the sample. Essentially, the combination of the codes is treated by the UQ routines as a single code. This direct connection method is preferable as it eliminates the aforementioned multiple samplings and is more numerically accurate as PDF estimation is not required.

As shown in Fig. 8.3, no perturbed values are passed to PHISICS input files. The output data from PHISICS, which is essentially the core power distribution at several states of interest, is treated as a constant. A sample of perturbed PHISICS output files was not generated due to run time concerns. It is again emphasized that this work serves as a foundation, by which later work will include MP-BEPU analysis with fully incorporated

neutronics.

8.4.1 PHISICS Data Exchange

PHISICS output data contains core power shapes for each assembly at a large variety of states. The data set of each state contains coordinates for finite elements with their corresponding portion of the total core power. From this data, the core power shapes for 18 states of interest within an 18 month equilibrium fuel cycle are extracted. LOTUS also crops the data to the domain of the fuel rods. The axial power profile is then assigned to a group within an HDF5 database. The name of this group is based upon user supplied text files which relate Cartesian coordinates in the core to assembly name notation within PHISICS and RELAP5-3D. In the LOTUS build used in this work, no data is supplied to PHISICS from HDF5 databases.

8.4.2 FRAPCON Data Exchange

FRAPCON obtains axial power peaking profiles and axial averaged heat rates from LOTUS. The axial averaged power peaking profiles were obtained by first extrapolating the elemental averaged power portions of PHSICS to the normalized, nodal linear heat rates required by FRAPCON. Safeguards are put in place to assure that any negative values from the extrapolation are replaced with zero (Eq. 8.1). The nodal values are then normalized by the rod average value as shown in Eq. 8.2,

$$q_i'^N = max\left(w_{i-1}\frac{\Delta Q_{i-1}/Q}{L_{i-1}} + w_i\frac{\Delta Q_i/Q}{L_i}, 0\right)Q \tag{8.1}$$

$$\widetilde{q_i'^N} = \frac{q_i'^N}{\frac{1}{2L_{rod}}\sum_j^{nElem}\left(q_{j-1}'^N + q_j'^N\right)L_j} \tag{8.2}$$

where index i corresponds to axial locations within individual rods, $\Delta Q_i/Q$ is the ratio of the power generated within an element (ΔQ_i) to the total core power (Q), w_i represents the weightings used for extrapolation, L_i and L_{rod} are elemental and total rod lengths respectively, $q_i'^N$ is the nodal linear heat rate, and $\widetilde{q_i'^N}$ is the rod normalized nodal linear

heat rate or rod power peaking profile.

The axial averaged heat rate is calculated according to Eq. 8.3 for the highest power or hot rod in an assembly. Eq. 8.4 calculates the heat rate for a representation of the average of the remaining rods in the assembly. Since the PHISICS code only calculates the assembly homogenized powers and it does not provide pin powers, the hot and average rod relations were defined based on the assumption that the hot rod produces 3% more power than the average rod.

$$\overline{q'_{hot}} = \left(\sum_{i}^{nElem} \Delta Q_i / Q \right) \left(\frac{1.03}{263 + 1.03} \right) \frac{Q}{L_{rod}} \tag{8.3}$$

$$\overline{q'_{avg}} = \left(\sum_{i}^{nElem} \Delta Q_i / Q \right) \left(\frac{1}{263 + 1.03} \right) \frac{Q}{L_{rod}} \tag{8.4}$$

where $\overline{q'_{hot}}$ and $\overline{q'_{avg}}$ are the axial averaged heat rates for hot and average rods respectively. $\overline{q'}$ and $\widetilde{q'^{N}_{i}}$ are then supplied to FRAPCON for consecutive sets of states, which form power history. The composition of the power history is dependent on the time of the LB-LOCA and the shuffling scheme. For instance, a twice burned assembly subject to LB-LOCA at 300 days, will be supplied the full power histories for the previous two location of the assembly, as well as the first 300 days of the current location.

Lastly it is not assumed that the hot rod location is consistent between fuel cycles. For this reason, the heat rates of the average rods are supplied to the power histories of hot rods for the previous cycles of once and twice burned assemblies, after which the 3% power increase is applied to the current cycle.

LOTUS also transfers the appropriate perturbed inputs (see Table 8.4) to each FRAPCON inputs file. The data transferred from FRAPCON to the HDF5 databases is shown in Table 8.1. Note that not all data stored is used by RELAP5-3D. Many of the values such as stored internal energy and heat flux are stored in anticipation for later code integrations within LOTUS.

Table 8.1: Stored data from single FRAPCON case.

Name of Data Stored	Description of Data
Axial Mesh (Nodal Locations)	Array of Floats (nAxial+1)
Axially Averaged Burnup	Single Float
Burnup	Array of Floats (nAxial)
Fuel Centerline Temperature	Array of Floats (nAxial)
Maximum Centerline Temperature	Single Float
Gap Conductance	Array of Floats (nAxial)
Gap Conductance at Peak Power	Single Float
Gas Compositions	Array of Floats (nSpecies)
Hydrogen Concentrations	Array of Floats (nAxial)
Heat Flux	Array of Floats (nAxial)
Inner Clad Displacement	Array of Floats (nAxial)
Outer Clad Displacement	Array of Floats (nAxial)
Outer Fuel Displacement	Array of Floats (nAxial)
Outer Clad Diameter	Single Float
Oxide Layer Thickness	Single Float
Rod Internal Pressure	Single Float
Stored Rod Internal Energy	Array of Floats (nAxial)
Clad Thickness	Single Float
Gap Thickness	Single Float

8.4.3 RELAP5-3D Data Exchange

RELAP5-3D receives power profiles from the data stored from PHISICS. The PHISCIS and RELAP5-3D core heat structure meshes were selected such that each of the six RELAP5-3D axial elements is an aggregate of multiple PHISICS elements. Thus no interpolation is needed, only a direct summation. The RELAP5-3D input deck contains two heat structures for each assembly, one representing 263 average fuel rods and the other a single hot rod. Both the average and hot heat structures require the portion of the power deposited within the fuel as well as the direct moderator heating portion. The power data supplied to RELAP5-3D are shown in Eqs. 8.5-8.8,

$$(\Delta Q_j/Q)^{Hot,Fuel}_{RELAP} = \left(\sum_{i\in j}(\Delta Q_i/Q)_{PHISICS}\right)\left(\frac{1.03}{263+1.03}\right)\left(1-F^{DMH}\right) \tag{8.5}$$

Table 8.2: Fuel performance for each assembly heat structure within RELAP5-3D.

Name of Data Stored	Description of Data
Rod Internal Pressure	Single Float
Fuel Displacements	Array of Floats (nAxial)
Inner Cladding Displacements	Array of Floats (nAxial)
Initial Fuel Radius	Single Float
Initial Inner Cladding Radius	Single Float
Initial Outer Cladding Radius	Single Float
Fuel Thermal Conductivity	Temperature Dependent Table
Fuel Volumetric Thermal Capacity	Temperature Dependent Table
Gas Composition	Species Dependent Table

$$(\Delta Q_j/Q)^{Hot,DMH}_{RELAP} = \left(\sum_{i\in j}(\Delta Q_i/Q)_{PHISICS}\right)\left(\frac{1.03}{263+1.03}\right)F^{DMH} \tag{8.6}$$

$$(\Delta Q_j/Q)^{Avg,Fuel}_{RELAP} = \left(\sum_{i\in j}(\Delta Q_i/Q)_{PHISICS}\right)\left(\frac{263}{263+1.03}\right)(1-F^{DMH}) \tag{8.7}$$

$$(\Delta Q_j/Q)^{Avg,DMH}_{RELAP} = \left(\sum_{i\in j}(\Delta Q_i/Q)_{PHISICS}\right)\left(\frac{263}{263+1.03}\right)F^{DMH} \tag{8.8}$$

Where F^{DMH} is the direct moderator heating fraction, subscripts $RELAP5$ and $PHSICS$ indicate the code to which the data corresponds, superscripts Avg and Hot indicate the type of RELAP5-3D heat structure, superscripts $Fuel$ and DMH indicate fuel power deposition and direct moderator heating respectively, and $i \in j$ indicates the set of PHISICS indices i which reside in a specific RELAP5-3D index j. Table 8.2 contains the fuel performance data transferred for each assembly heat structure (both hot and average).

The temperature dependent tables for fuel thermal conductivity and volumetric heat capacity vary among heat structures based upon burnup. The tables are generated by first obtaining the axially averaged burnup of each heat structure. These burnup values and a set or expected fuel temperatures are then supplied to Uranium Dioxide material modules from FRAPCON, thereby generating separate temperature dependent material properties

for each heat structure. The fuel volumetric heat capacities also conserve mass by altering fuel density in inverse proportion to volumetric changes. The incorporation of these tables to create rudimentary burnup dependent fuel properties is an improvement in accuracy over traditional RELAP5-3D input decks.

The gas composition tables contain all present species and their corresponding mole fraction. LOTUS also transfers the perturbed inputs specific to RELAP5-3D (see Table 8.4). The data transferred from RELAP5-3D to HDF5 databases are the maximum PCT and ECR encountered during the LB-LOCA for each assembly.

8.5 MP-BEPU Analysis with LOTUS

In the section, LB-LOCA analyses of a generic four-loop PWR is performed using multiphysics best estimate plus uncertainty (MP-BEPU) methodology within the LOTUS framework.

8.5.1 Problem Description

The problem of interest is a four-loop PWR with 3853 MW rated thermal power. The number of fuel assemblies is 193 with 17x17 fuel rod design with 264 fuel rods and 25 non-fuel locations. The active core height is 4.2672 m (14 ft.).

Core Design Automation

The core simulation strategy employed to generate the data needed by the subsequent LOCA analysis is schematically shown in Fig. 8.4. The first step of the strategy is to generate homogenized neutron cross sections. The lattice code HELIOS-2 [24] is used to compute the cross sections for different geometrical conditions and different reactor states in the core. In this manner, a cross section library can be generated that captures effects like control rods, burnable poisons, etc. as well as different fuel temperatures, moderator densities, boron concentrations and burn-up levels. The PHISICS reactor physics package coupled to the thermal-hydraulic system code RELAP5-3D is used in a second step, in order to compute 3D assembly power distributions, burn-ups, etc. needed as initial conditions

for the subsequent LOCA analysis. Depending on the available data base to initiate the calculation, (core and fuel geometry description, burn-up maps, reloading pattern, power distributions, etc.), the PHISICS package can, in addition to solve the 3D core, also burn the core to the desired burn-up level, shuffle and reload the core and search for critical control rod positions or boron concentrations.

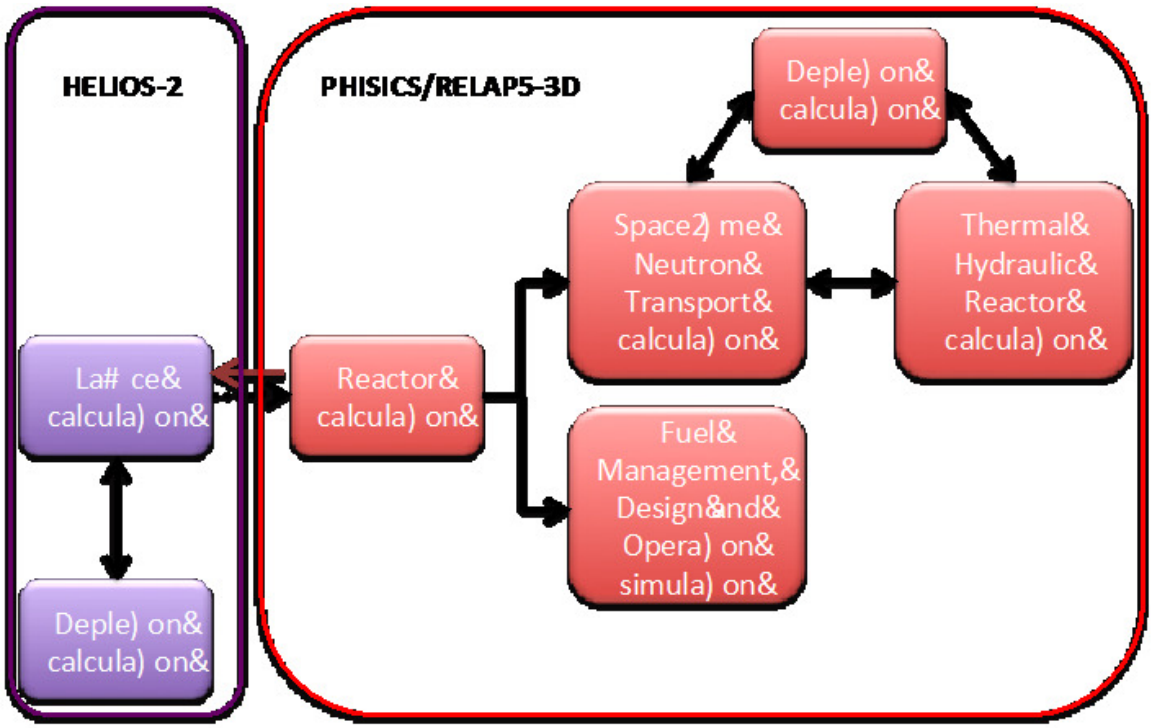

Fig. 8.4: LOTUS Demonstration: Core Simulation Strategy.

In this work, the LB-LOCA accident scenario is initiated from equilibrium cycle conditions to assess the compliance of the existing power plants to the proposed rule. From a loading point of view, the equilibrium cycle can be considered as the cycle from which the fuel reload pattern is almost constant (i.e. same composition and spatial loading of the fuel batches). In this work an equilibrium cycle is reached by following several operational cycles to achieve high burn-up, low radial power peaking and flat axial power profiles, i.e. somewhat realistic core conditions that represent a current PWR core. The loading pattern for the equilibrium cycle is shown in Fig. 8.5. The numeric numbers on the loading

map indicate the number of the Integral Fuel Burnable Absorber (IFBA) rods which are normal fuel rods that have a boron absorber coating sprayed on the cladding in the fresh fuel assemblies. The two enrichments found in order to reach, at the equilibrium, a cycle length of 18 months are 4.2% and 4.6%. The fuel rods contain a low enriched zone at the top and bottom. The keff at BOC has been found to be 1.10462 and the cycle ends when the keff falls below 1.0. Assuming a realistic boron worth of 10pcm/ppm, the maximum boron concentration in the core at BOC is expected be 1000ppm which is in the range of boron concentrations reported in the open literature. The quasi-steady state power profiles calculated by PHISICS for the equilibrium cycle are stored in the HDF5 database for subsequent fuel performance and LB-LOCA analyses.

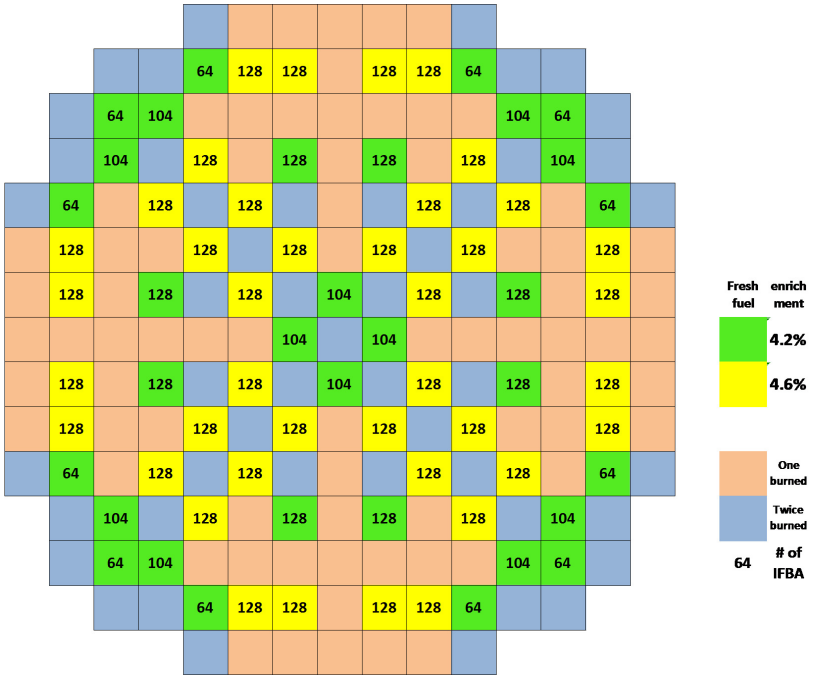

Fig. 8.5: Equilibrium Cycle Reload Pattern, Fresh Fuel Enrichment and Number of Burnable Absorber (BA) Pins in the Fresh Fuel Assemblies.

Fuel Performance

Fuels performance calculations are performed for a representation of the hot rod and

Table 8.3: FRAPCON code parameters.

Parameter	Value
Fuel Height	4.2672 m (14 ft.)
Pin Pitch Ratio	0.496
Plenum Height	0.1778 m (7 in.)
Pellet Material	Uranium Dioxide
Plenum Fill Gas	Helium
Cladding Material	ZIRLO
Pellet Height	9.8299 mm (0.387 in.)
Pellet Dish Height	0.3353 mm (0.0132 in.)
Limit On Swelling Fraction	0.05
Increase In Pellet Density	150 kg/m3

average rod (see section 8.4.3) for each fuel assembly. Each case is modeled with a single channel enthalpy rise model. Enrichments were inputted according to assembly locations (see Fig. 8.5). The supplied power histories of each rod include the effects of core shuffling (see section 8.4.2). The code constant parameters of FRAPCON are given in Table 8.3.

System Analysis

The RELAP5-3D input deck describes a typical four-loop Pressurized Water Reactor (PWR). The reactor system is simulated using one-dimensional components and includes all the main reactor features of importance when simulating LOCA scenarios. This includes a detailed representation of the primary system (reactor vessel and internals, four independent loops with cold and hot legs, primary coolant pumps, and steam generators), pressurizer, and Emergency Core Cooling Systems. The reactor core is simulated with six vertical pipe components (radially connected through cross-junctions) and six axial nodes. Six heat structures are included for each assembly in the model to represent different power regions of the reactor core, and connected individually to the core hydrodynamic pipe components. Each heat structure contains two sub-structures, one representing 263 average fuel rods and the other a single hot rod. The secondary loop includes the secondary side of the four steam generators up to the main steam isolation valves. The model is equipped with control logic to simulated automatic signals, and manual operating procedures adopted during LOCA. A simplified representation of the RELAP5-3D model of the reactor system is shown in Fig.

8.6. The parameters within the RELAP5-3D input deck are vast and are not included here for the sake of brevity.

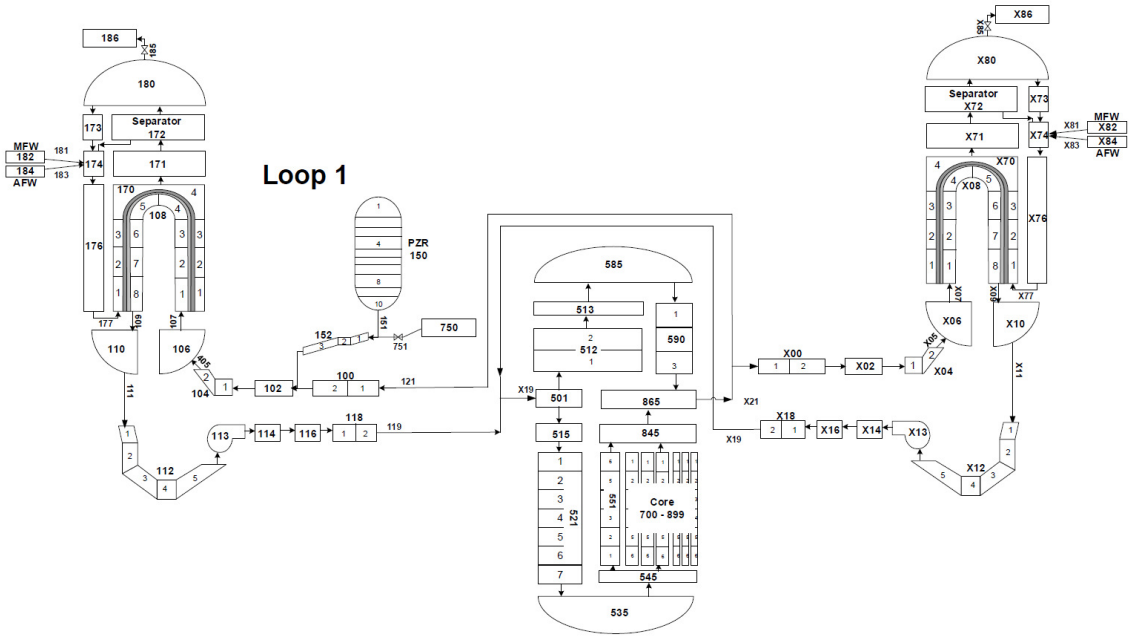

Fig. 8.6: RELAP5-3D PWR Nodalization Diagram.

8.5.2 Figures of Merit

The peak cladding temperatures (PCT) is of critical importance in evaluating plant safety under LOCA conditions. PCT is the highest cladding temperature encountered during a LB-LOCA. Excessive PCT leads to cladding rupture as well as excessive cladding oxidation.

Evaluation of equivalent cladding reacted (ECR) is also essential. ECR is the percentage of the cladding which has been oxidized. Cladding oxidation is an exothermic reaction which increases in rate at higher coolant temperatures. Thus as more cladding is oxidized, the coolant temperature rises further, causing greater oxidation. This runaway reaction has the potential to create vast quantities of hydrogen within the reactor core, leading to a potentially combustible scenario.

In order to evaluate PCT and ECR with respect to their cladding hydrogen content based limits (see Fig. 8.1), it is proposed that the figures of merit (FOM) be the ratios of PCT and ECR to their respective limits. The peak cladding temperature ratio (PCTR) and equivalent cladding reacted ratio (ECRR) are expressed in Eq. 8.9 and Eq. 8.10 respectively,

$$PCTR = \frac{PCT}{PCT_{Limit}\,(H_2Conc.)} \tag{8.9}$$

$$ECRR = \frac{ECR}{ECR_{Limit}\,(H_2Conc.)} \tag{8.10}$$

The functions of the limits of PCT and ECR are shown in Fig. 8.1. The PCT is a simple step function of hydrogen concentration while the ECR limit is a pricewise continuous function whose value may decrease by an order of magnitude when comparing fresh fuel to highly irradiated fuel.

If we define $PCTR_{max}$ and $ECRR_{max}$ as the maximum values of PCTR and ECRR within a core at a given state, then the acceptance criteria for the safety metrics are the following:

$$1)\ PCTR_{max} < 1$$

and

$$2)\ ECRR_{max} < 1$$

Using the above criteria, the limiting fuel rods can be identified as the fuel rods with $PCTR_{max}$ or $ECRR_{max}$. It is worth noting that the limiting rods frequently change location within the perturbed samples.

The nature of ECRR in particular prevents a reliable method for predicting the assemblies of greatest concern a priori. This is due to high cladding hydrogen content being correlated with high burnup and high ECR corresponding to large local linear heat rates. Since higher burnup fuel has lower neutron cross sections and thus lower linear heat rates, there is no reasonable method to determine the ECRR limiting assembly without modeling

each assembly in both FRAPOCN and RELAP5-3D.

8.5.3 Uncertainty Parameters and Random Sampling

The uncertainty ranges and distributions of relevant parameters were generated from past UQ/SA work on fuel performance [25], coupled thermal hydraulics and neutronics [26], and system analysis [27]. It should be noted that many of the ranges of the perturbed inputs exclusive to RELAP5-3D were selected based off of common practices for expected uncertainties within thermal hydraulics (i.e. 30% uncertainty in heat transfer coefficients).

The * in Table 8.4 indicates that the perturbed input of that row strongly influences the program of the corresponding column despite it not being a direct input. For instance, the initial plenum fill gas pressure of FRAPCON is not inputted to RELAP5-3D. However the plenum gas pressure at various states, which are highly dependent on the initial pressure, are included in RELAP5-3D input decks. The direct moderator heating fraction is also not directly supplied, however LOTUS scripts use the fraction in determining the portion of the core power to be placed in direct moderator heating within RELAP5-3D. Lastly in the nominal value column, a -entry indicates that a continually varying value within the code is biased by a specified amount, thus a nominal value does not exist.

8.5.4 Wilks' Uncertainty Quantification Method

Wilks method was introduced in 1941 by its namesake [28]. Wilks method entails finding tolerance limits for a population based off of a limited sample size. The method may be used for any output probability distribution function so long as it is continuous. While this is not technically true of floating point numbers, it is nevertheless a very fair assumption to treat code outputs as continuous variables.

To calculate a confidence interval, it is convenient to first state the probability β that at least one value of a sample of size N lies outside portion γ of the population, as shown in Eq. 8.11,

$$\beta = 1 - \gamma^N \tag{8.11}$$

Table 8.4: List of common uncertain parameters with corresponding uncertainty ranges.

Parameter	Nominal	Range (+/-)	Distribution	FRAP.	RELAP
Fuel Radius	0.40956 cm	0.001 cm	Trunc. Norm.	X	X
Clad Outer Radius	0.47498 cm	0.002 cm	Trunc. Norm.	X	X
Clad Thickness	0.05715 cm	0.002 cm	Trunc. Norm.	X	X
Plenum Fill Gas Pressure	3.0 MPa	0.08 MPa	Trunc. Norm.	X	*
Percent Theoretical Density	94.50%	1.60%	Trunc. Norm.	X	X
Fuel Thermal Conductivity	-	10%	Trunc. Norm.	X	X
Core Power	3.85 GW	2%	Trunc. Norm.	X	X
Direct Moderator Heating	0.02	10%	Trunc. Norm.	X	*
Decay Heat Multiplier	1	0.06	Uniform		X
Accum. Pressure	606 psi	10%	Trunc. Norm.		X
Accum. Liquid Temperature	126	25	Uniform		X
Accum. Liquid Volume	1250 ft3	8	Uniform		X
Pump Side Sub-Cooled CFM	1	0.2	Uniform		X
Pump Side Two-Phase CFM	1	0.2	Uniform		X
Pump Side Super-Heated CFM	1	0.2	Uniform		X
Vessel Side Sub-Cooled CFM	1	0.2	Uniform		X
Vessel Side Two-Phase CFM	1	0.2	Uniform		X
Vessel Side Super-Heated CFM	1	0.2	Uniform		X
Turbulence HTM	1	0.3	Uniform		X
Nucleate Boiling HTM	1	0.3	Uniform		X
Critical Heat Flux Multiplier	1	0.3	Uniform		X
Transition Boiling HTM	1	0.3	Uniform		X
Film Boiling HTM	1	0.3	Uniform		X
Condensation HTM	1	0.3	Uniform		X
Natural Convection HTM	1	0.3	Uniform		X
Laminar HTM	1	0.3	Uniform		X
Fuel Enrichment	2.6/4.2/4.6	0.003%	Trunc. Norm.	X	
Fuel Roughness	2.0 m	0.33333 m	Trunc. Norm.	X	
Clad Roughness	1.0 m	0.2 m	Trunc. Norm.	X	
Fuel Thermal Expansion	-	15%	Trunc. Norm.	X	
Fission Gas Release Biasing	-	+200% -67%	Trunc. Norm.	X	
Fuel Swelling	-	20%	Trunc. Norm.	X	
Clad Creep	-	30%	Trunc. Norm.	X	
Clad Axial Growth	-	50%	Trunc. Norm.	X	
Clad Oxidation	-	40%	Trunc. Norm.	X	
CladH2Pickup	-	80 ppm	Trunc. Norm.	X	
Outlet Pressure	2275 psi	2%	Trunc. Norm.	X	
Inlet Mass Flux	2605453 lb/hr-ft2	2%	Trunc. Norm.	X	

* Indicates inputs supplied to code are directly affected by perturbed value of row.

In order to find a one sided 95/95 confidence value, the question can be asked, given that $\gamma = 0.95$, what is the minimal N for which $\beta \geq 0.95$? By setting N to 59, there is 95.15 probability that at least one value is greater than the 95th percentile of the population. Thus by performing any set of perturbed calculations 59 times, the highest obtained value serves as a conservative bound for a 95/95 confidence interval.

This process has been expanded to determine the confidence intervals based upon upper and lower bounds for arbitrary ranks [29]. The probability that a lower bound of rank r and upper bound of rank s bound portion is given by Eq. 8.12,

$$\beta = \sum_{j=0}^{s-r-1} \left(\begin{array}{c} N \\ j \end{array} \right) \gamma^j \left(1-\gamma\right)^{N-j} \tag{8.12}$$

Wilks method has been further expanded by Guba *et al.* for multiple outputs [29]. This is not to be misinterpreted that Eq. 8.11 and 8.12 are inadequate for simulations producing multiple outputs. Rather, if a decision maker desires to construct multidimensional bounds (i.e. rectangular bounds for two outputs), then the required sample sizes and ranks must be modified. For a problem of order p, the probability that ranks $r = 0$ and $s = N - p + 1$ bound portion γ of the population is given by Eq. 8.13,

$$\beta = \sum_{j=0}^{N-p} \left(\begin{array}{c} N \\ j \end{array} \right) \gamma^j \left(1-\gamma\right)^{N-j} \tag{8.13}$$

For evaluation of PCTR and ECRR ($p = 2$), Eq. 8.13 indicates that if a β of at least 0.95 is desired with no lower bounds ($r = 0$), and the highest and second highest values set as upper bounds for the first and second output respectively ($s = N - p + 1$), then a sample size of at least 93 is required. In order to ensure outputs are treated equally, it has become a common practice in the nuclear safety community to take the highest rank of all outputs as bounds [30]. While this is more conservative, it still qualifies as bounding 95% or more of the population with *at least* 95% confidence.

Table 8.5: Statistical PCTR information from Wilks study.

Time of LB-LOCA	Nominal $PCTR_{max}$	One Sided 95/95 $PCTR_{max}$
BOC	0.589958	0.713493
100 Day	0.59126	0.63767
200 Day	0.606401	0.670105
300 Day	0.6346	0.72091
400 Day	0.645763	0.847698
500 Day	0.626262	0.704844
EOC	0.648437	0.732429

8.6 Results

LB-LOCA scenario simulations are run at a variety of states throughout the equilibrium fuel cycle (BOC, 100 days, 200 days, 300 days, 400 days, 500 days, EOC). The results are divided into two sections. The first containing the nominal and one sided 95/95 confidence values determined via the Wilks method (section 8.6.1). The second section includes the ECR, PCT, hydrogen content, and burnup information for the limiting cases of the Wilks sample (section 8.6.2).

8.6.1 Uncertainty Quantification Results

The nominal and one sided 95/95 confidence values for $PCTR_{max}$ are given in Table 8.5.

The $PCTR_{max}$ values within Table 8.5 show sporadic fluctuation between the times for LB-LOCA for both nominal values (less than 11.6% variation) and 95/95 values (less than 12.9% variation). The changes in $PCTR_{max}$ from state to state stem from two factors. The first factor is the PCTR being a strong function of assembly power and axial peaking profiles. The second factor is the PCT limit changing from 1477.59 K to 1394.26 K when the cladding of higher burnup has hydrogen content in excess of 400 wppm (see Fig. 8.1), resulting in a 6% PCTR increase. Thus PCTR fluctuations do not follow a specific trend when comparing the time of LB-LOCA. The results for $ECRR_{max}$ is given in Table 8.6.

The $ECRR_{max}$ values in general shows an increasing trend as the LB-LOCA occurs later in the fuel cycle. This behavior is attributable to the ECR limit being a strong function of hydrogen content (see Fig. 8.1). At the EOC, the hydrogen content can be in excess of

Table 8.6: Statistical ECRR information from Wilks study.

Time of LB-LOCA	Nominal $ECRR_{max}$	One Sided 95/95 $ECRR_{max}$
BOC	0.00423	0.033925
100 Day	0.003184	0.007207
200 Day	0.006262	0.026219
300 Day	0.014913	0.078752
400 Day	0.021398	0.128074
500 Day	0.026144	0.133754
EOC	0.038685	0.134973

650 wppm (see Fig. 8.15) causing the ECR limit to be as much of a factor of 5 less than the limit for fresh fuel.

Table 8.5 and 8.6 highlight the benefits of the MP-BEPU methodology. The inclusion of the uncertainty in the calculation results in as much as a 31.2 % increase in $PCTR_{max}$ estimates and over an 8 fold increase in $ECRR_{max}$ estimates. The drastic differences in $ECRR_{max}$ are due to the limiting cases having far more cladding oxidation then the nominal cases. When oxide forms, heat is released causing coolant temperatures increases, which in turn causes more oxidation. This unstable relation causes ECRR to behave as a threshold variable, meaning a variable which changes drastically once a threshold is passed. This behavior in particular demonstrates the need for decision makers to be supplied with data obtained through MP-BEPU methodologies.

8.6.2 Limiting Cases

Fig. 8.7 through 8.13 show the core maps of PCT and ECR for the limiting cases for an LB-LOCA occurring at seven separate states. The specific limiting case for $PCTR_{max}$ often differs from that of $ECRR_{max}$. Furthermore, the limiting cases also vary from state to state. The data of Fig. 8.7 through 8.13 originated from the hot pin heat structures of RELAP5-3D, with no data coming from the average pin fuel structures.

Not surprisingly, the highest PCT values always coincide with fresh assembly locations (compare reload pattern in Fig. 8.5) due the increased neutron fission cross sections, and thus assembly power. It is for this same reason that the PCT values of fresh assemblies are often largest for higher enrichment fresh fuel (compare fresh fuel enrichments in Fig. 8.5).

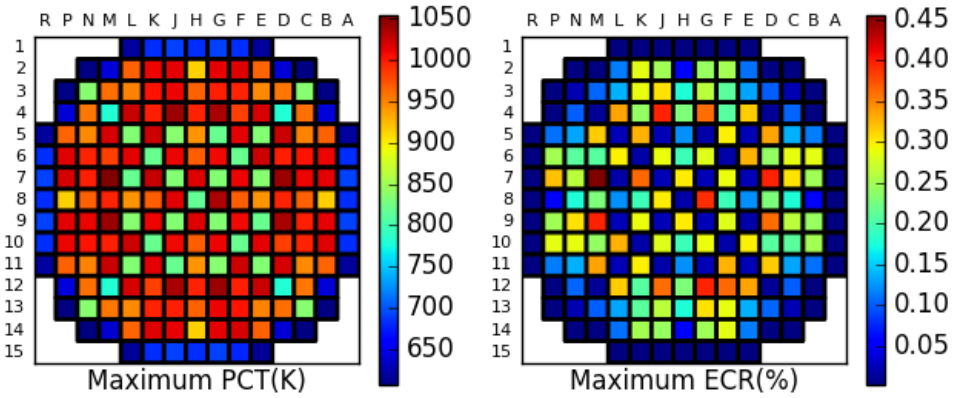

Fig. 8.7: PCT and ECR Core Map for Limiting Case at BOC.

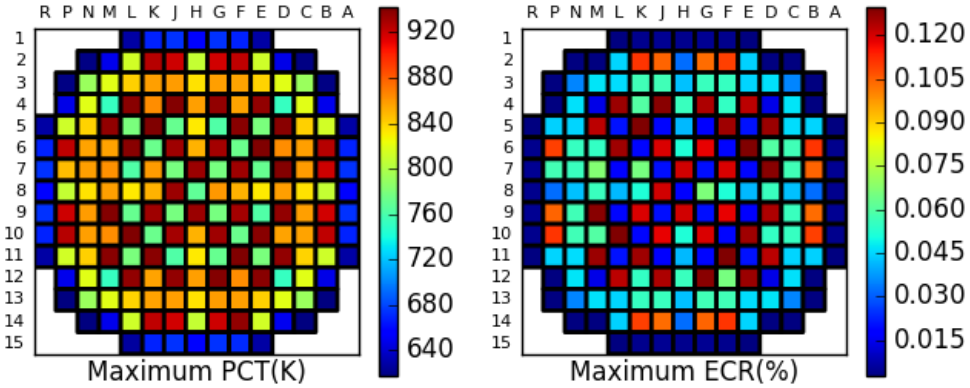

Fig. 8.8: PCT and ECR Core Map for Limiting Case at 100d.

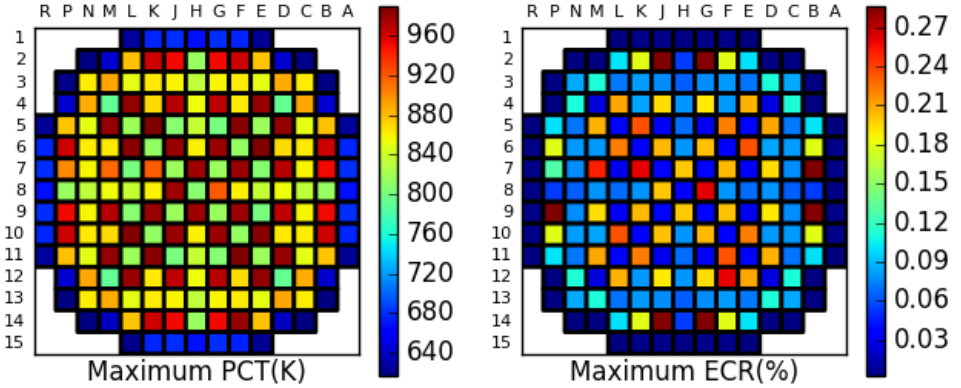

Fig. 8.9: PCT and ECR Core Map for Limiting Case at 200d.

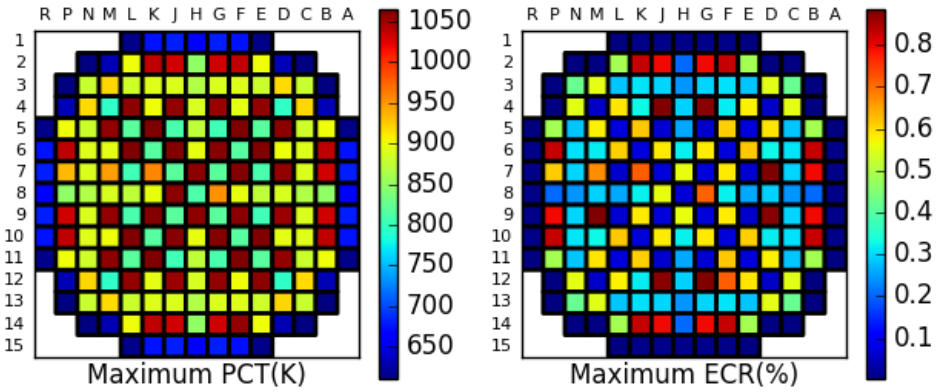

Fig. 8.10: PCT and ECR Core Map for Limiting Case at 300d.

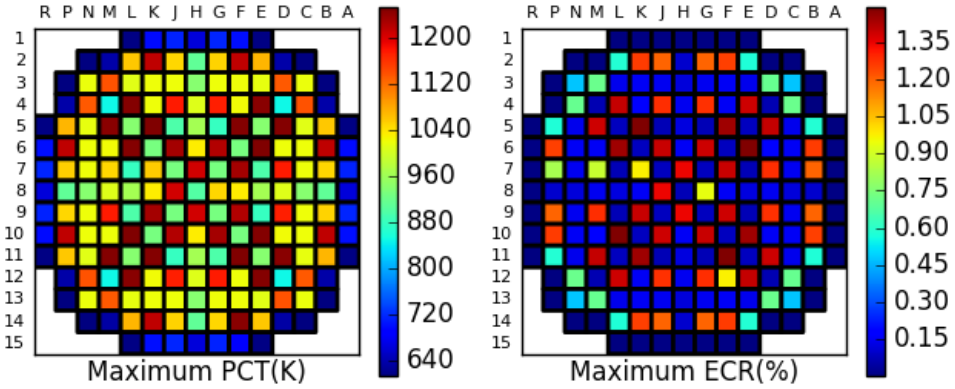

Fig. 8.11: PCT and ECR Core Map for Limiting Case at 400d.

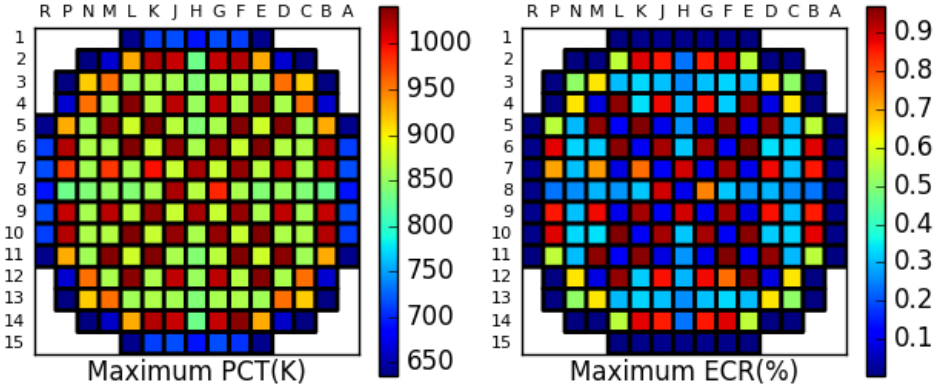

Fig. 8.12: PCT and ECR Core Map for Limiting Case at 500d.

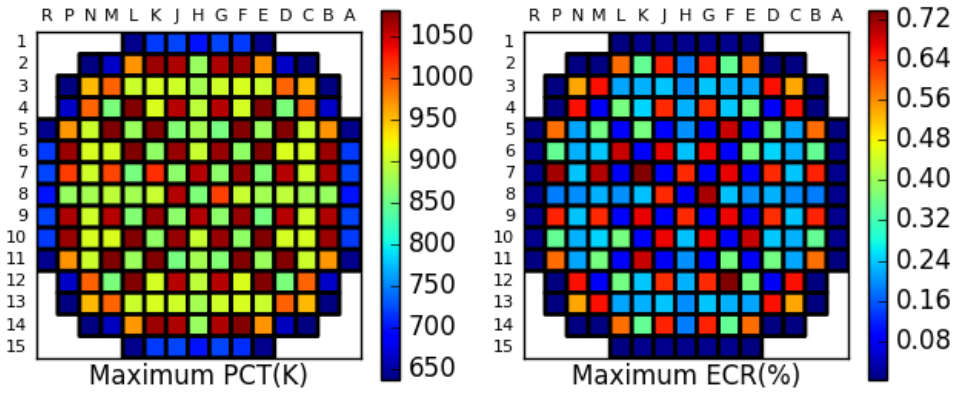

Fig. 8.13: PCT and ECR Core Map for Limiting Case at EOC.

The high PCT fresh assemblies vary from state to state, however the distribution is roughly symmetrical with high enrichment assemblies not in proximity to the core boundary being the most limiting.

The ECR values behave less predictably. While the limiting assemblies all contain fresh fuel, the specific location among fresh fuel assembly does not follow a specific trend. Furthermore, the ECR distributions are asymmetrical. This asymmetry can be traced back to minor difference (roughly 2%) in the PHISICS generated power shapes for supposedly symmetric locations. As discussed in section 8.6.1, due to ECR being a threshold variable, minor differences may cause radically different results.

Fig. 8.14 contains the PCT data for the assemblies in the limiting cases for a LB-LOCA occurring at the aforementioned states. The data includes PCT vs hydrogen content for each assembly in addition to the PCT limit as a function of hydrogen content. Fig. 8.14 also contains a similar plot for PCT vs fuel burnup. As indicated by the legend, colors red, yellow, and green respond to fresh, once burned, and twice burned assemblies respectively. Fig. 8.15 contains an analogous set of plots for ECR data. Note that the ECR limit as a function of cladding hydrogen content was not plotted due to all ECR values being far below said limit. As before, all data within Fig. 8.14 and 8.15 was generated from the hot pin heat structures within RELAP5-3D.

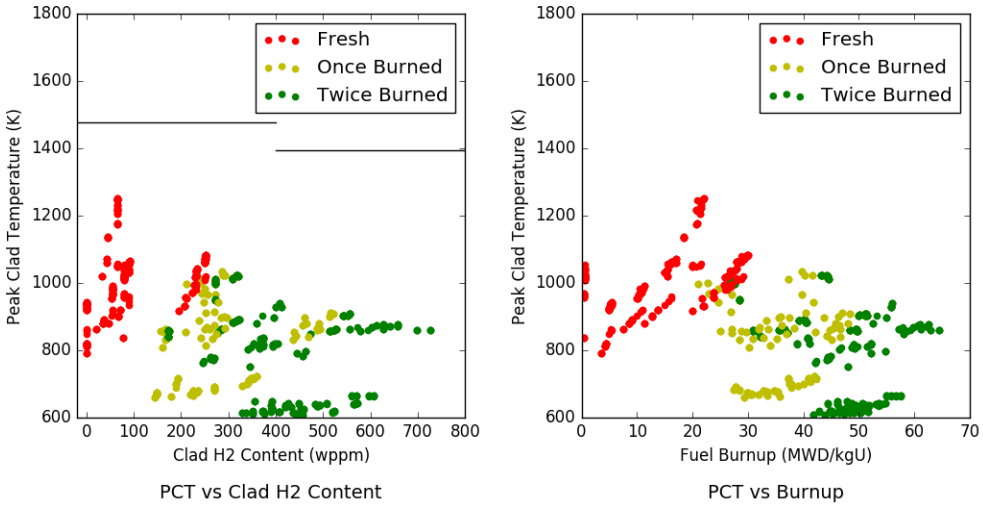

Fig. 8.14: PCT and PCT Limit vs Cladding Hydrogen Content and PCT vs Fuel Burnup for the PCTR Limiting Cases at each State of Interest (BOC,100 days, 200 days, 300 days, 400 days, 500 days, EOC).

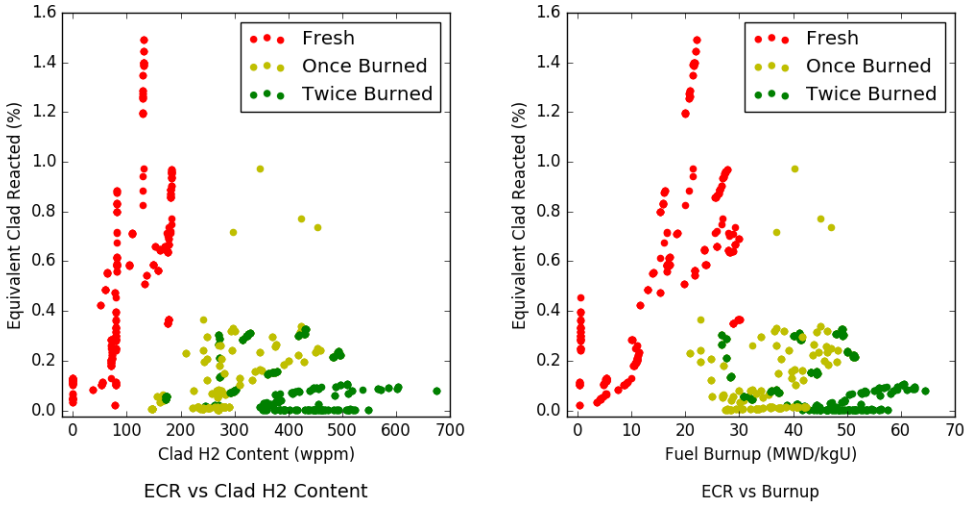

Fig. 8.15: ECR vs Cladding Hydrogen Content and ECR vs Fuel Burnup for the ECRR Limiting Cases at each State of Interest (BOC,100 days, 200 days, 300 days, 400 days, 500 days, EOC)

Fig. 8.14 indicates that the PCT fluctuations within assemblies is larger than the PCT limit reduction occurring at 400 ppm. As a result, from the PCTR perspective, the assemblies of greatest concerns are the fresh fuel assemblies with high assembly power. Fig. 8.15 shows a number of outliers in the once burned fuel with values of roughly 1/2 to 2/3 the maximum ECR, but with reduced ECR limits which may be as low as a 1/3 of the fresh fuel ECR limit. Therefore a small number of once burned assemblies are the most limiting in terms of .

Fig. 8.15 in particular establishes the benefits of using MP-BEPU methodology, specifically the multiphysics aspect. If the fuel performance and system analysis calculations were performed separately, then ECRR may have been evaluated with the limiting value of ECR from RELAP5-3D and the limiting value of cladding hydrogen content from FRAPCON. However, Fig. 8.15 indicates that high ECR assemblies have low cladding hydrogen content, and assemblies with high cladding hydrogen content have low ECR. In reality, the true limiting assembly ($ECRR_{max}$) contains neither the core maximum of ECR nor hydrogen content. Thus MP-BEPU methodology helps to avoid a needlessly conservative estimate of $ECRR_{max}$.

8.7 Conclusions

LOTUS utilizes HDF5 databases to create a flexible plug and play environment capable of UQ. LOTUS was used to integrate the neutronics codes PHISCS, fuel performance code FRAPCON, and systems analysis code RELAP5-3D. This integration provides MP-BEPU for systems level plant transient analysis. LOTUS allows for the cladding hydrogen content based evaluation of PCT and ECR in accordance with the U.S. NRCs proposed rulemaking in 10 CFR 50.46c.

The Wilkss one sided 95/95 confidence values for the FOM were dramatically higher than their corresponding nominal values, thus demonstrating the necessity of following MP-BEPU methodology. Core maps of PCT and ECR for the limiting case for seven separate states were presented. Further visualization of the limiting cases included plots of PCT and ECR with respect to cladding hydrogen content and fuel burnup. Results reaffirmed the

need to model all core assemblies with both fuel performance and systems analysis codes in order to obtain the true limiting assembly for a given case.

8.8 Acknowledgements

This work is supported by the U.S. Department of Energy, under DOE Idaho Operations Office Contract DE-AC07-05ID14517. Accordingly, the U.S. Government retains a nonexclusive, royalty-free license to publish or reproduce the published form of this contribution, or allow others to do so, for U.S. Government purposes. This work was also supported by consultations and contributions from Cliff Davis and Paul Bayless.

REFERENCES

[1] Sloan, B., McCorkle, D., and Bryden, K., "An Overview of Computational Environments for Engineering," *Proc. 51st AIAA Aerospace Sciences Meeting including the New Horizons Forum and Aerospace Exposition*, Jan 2013.

[2] Gaston, D., Newman, C., Hansen, G., and Lebrun-Grandié, D., "MOOSE: A parallel computational framework for coupled systems of nonlinear equations," *Nuclear Engineering and Design*, Vol. 239, No. 10, 2009, pp. 1768 – 1778.

[3] https://www.casl.gov/, Accessed: 2018.

[4] Swiler, L. P., Lefebvre, R. A., Langley, B. R., and Thompson, A. B., "Integration of Dakota into the NEAMS Workbench," 2017, Sandia National Laboratories, SAND2017-7492.

[5] The HDF Group, "Hierarchical data format version 5," http://www.hdfgroup.org/HDF5, Accessed: 2018.

[6] U.S. Nuclear Regulatory Commission, "Establishing Analytical Limits for Zirconium-Alloy Cladding Material," 2014, Regulatory Guide 1.224, DG-1263.

[7] The RELAP5-3D Code Development Team, "The RELAP5-3D Code Manual Volume I: Code Structure, System Models, and Solution Methods," 2012, Rev. 4, Idaho National Laboratory, INEEL-EXT-98-00834.

[8] http://frapcon.labworks.org, Accessed: 2018.

[9] Weaver, W., Tomlinson, E., and Aumiller, D., "A generic semi-implicit coupling methodology for use in RELAP5-3D," *Nuclear Engineering and Design*, Vol. 211, No. 1, 2002, pp. 13 – 26.

[10] Marra Neto, A., Silva, A., Sabundjian, G., and Conti, T., "Link of FRAP-T, FRAPCON and RELAP-4 codes for fuel rod behaviour analysis under transient and accident

conditions in light water reactors," *Proc. 7th National Meeting of Reactor Physics and Thermohydraulic*, Vol. 2, 1989, p. 358.

[11] Porter, I., Knight, T. W., and Raynaud, P., "Potential Impacts of Modeling Full Reactor Cores Using Combined Fuel Performance and Thermal Hydraulics Codes," *Nuclear Technology*, Vol. 190, No. 2, 2015, pp. 174–182.

[12] Magedanz, J., Avramova, M., Perin, Y., and Velkov, A., "High-fidelity multi-physics system TORT-TD/CTF/FRAPTRAN for light water reactor analysis," *Annals of Nuclear Energy*, Vol. 84, 2015, pp. 234 – 243.

[13] Yilmaz, M. O., Avramova, M. N., and Andersen, J. G., "Multi-physics code system with improved feedback modeling," *Progress in Nuclear Energy*, Vol. 98, 2017, pp. 94 – 108.

[14] Folsom, C. P., Jensen, C. B., Williamson, R. L., Woolstenhulme, N. E., Ban, H., and Wachs, D. M., "BISON Modeling of Reactivity-Initiated Accident Experiments in a Static Environment," *Proc. Top Fuel 2016*, Sept. 2016, Idaho National Laboratory, INL/CON-16-37614.

[15] Epiney, A. S., Parisi, C., Alfonsi, A., Zhang, H., and Szilard, R., "RISMC Industry Application #1 (ECCS/LOCA) Core Characterization Automation: Reference PWR designs for IA #1," *Transactions of the American Nuclear Society*, Vol. 116, June 2017, Idaho National Laboratory.

[16] Strydom, G., Epiney, A. S., Alfonsi, A., and Rabiti, C., "Comparison of the PHISICS/RELAP5-3D Ring and Block Model Results for Phase I of the OECD/NEA MHTGR-350 Benchmark," *Nuclear Technology*, Vol. 193, No. 1, 2016, pp. 15–35.

[17] Judd, J., Grandi, G., and Redwine, J., "A best-estimate coupled code for reactor safety analyses using SIMULATE-3K and RELAP5-3D," *Proc. of Advances in Nuclear Fuel Management IV*, April 2009.

[18] Bratton, R. N., Jessee, M. A., and Wieselquist, W. A., "Rod internal pressure quantification and distribution analysis using Frapcon," *Proc. 2016 Conference on Physics of Reactors*, May 2016, pp. 2588–2602, ORNL/TM-2015/557.

[19] Hales, J., Tonks, M., Gleicher, F., Spencer, B., Novascone, S., Williamson, R., Pastore, G., and Perez, D., "Advanced multiphysics coupling for LWR fuel performance analysis," *Annals of Nuclear Energy*, Vol. 84, 2015, pp. 98 – 110.

[20] Wu, X., Kozlowski, T., and Hales, J. D., "Neutronics and fuel performance evaluation of accident tolerant FeCrAl cladding under normal operation conditions," *Annals of Nuclear Energy*, Vol. 85, 2015, pp. 763 – 775.

[21] Gleicher, F. N., Williamson, R. L., Ortensi, J., Wang, Y., Spencer, B. W., Novascone, S. R., Hales, J. D., and Martineau, R. C., "The coupling of the neutron transport application RATTLESNAKE to the nuclear fuels performance application BISON under the MOOSE framework," *Proc. PHYSOR 2014*, Oct. 2014, Idaho National Laboratory, INL/CON-14-31079.

[22] Epiney, A., Rabiti, C., Alfonsi, A., Wang, Y., Cogliati, J., and Strydom, G., "PHISICS multi-group transport neutronic capabilities for RELAP5," *Proc. ICAPP 2012*, June 2012, Idaho National Laboratory.

[23] Rabiti, C., Alfonsi, A., and Epiney, A., "New Simulation Schemes and Capabilities for the PHISICS/RELAP5-3D Coupled Suite," *Nuclear Science and Engineering*, Vol. 182, No. 1, 2016, pp. 104–118.

[24] Wemple, C., Gheorghiu, H., Stammler, R., and Villarino, E., "The HELIOS-2 lattice physics code," *Proc. 18th AER Symposium on VVER Reactor Physics and Reactor Safety*, Oct. 2008.

[25] Ikonen, T., "Comparison of global sensitivity analysis methods Application to fuel behavior modeling," *Nuclear Engineering and Design*, Vol. 297, 2016, pp. 72 – 80.

[26] Brown, C. and Zhang, H., "Uncertainty quantification and sensitivity analysis with CASL Core Simulator VERA-CS," *Annals of Nuclear Energy*, Vol. 95, 2016, pp. 188 – 201.

[27] Zhang, H., Szilard, R., Epiney, A., Parisi, C., Vaghetto, R., Vanni, A., and Neptune, K., "Industry Application ECCS / LOCA Integrated Cladding/Emergency Core Cooling System Performance: Demonstration of LOTUS-Baseline Coupled Analysis of the South Texas Plant Model," 2017, Idaho National Laboratory, INL/EXT-17-42461.

[28] Wilks, S. S., "Determination of Sample Sizes for Setting Tolerance Limits," *The Annals of Mathematical Statistics*, Vol. 12, No. 1, 1941, pp. 91–96.

[29] Guba, A., Makai, M., and Pál, L., "Statistical aspects of best estimate method−I," *Reliability Engineering and System Safety*, Vol. 80, No. 3, 2003, pp. 217 – 232.

[30] Frepoli, C., "An Overview of Westinghouse Realistic Large Break LOCA Evaluation Model," *Science and Technology of Nuclear Installations*, Vol. 2008, 2008.

aiaa

CHAPTER 9

Conclusions

Uncertainty quantification (UQ) and Sensitivity Analysis (SA) have been performed on a variety of multiphysics environments. SA includes recently developed higher order measures which enhance analysis of nonlinear input and output uncertainty relations. The scope of this work includes both quasi-steady state depletions cases as well as modeling of transient large break-loss of coolant accidents (LB-LOCA).

Through the LOTUS environment, the first known integration of VERA-CS and FRAP-CON was developed for a quasi-steady state depletion case. MDNBR uncertainty was shown to behave linearly and to be temporally consistent, with the largest sources of uncertainty being thermal hydraulic boundary conditions of outlet pressure and inlet temperature as well as the core power. MFCT uncertainty was linear and time dependent, with open gap states dependent on gap dimensions and fuel thermal conductivity and closed gap states predominantly stemming from fuel thermal conductivity.

SA results for GCPP demonstrated the utility of higher order variance and density based measures. The uncertainty of open gap states was linear, and originating from mainly gap dimensions. In states where the Monte Carlo sampling was a mix of open and closed gap states, the uncertainty relations were highly nonlinear, with the most dominant input uncertainty being cladding corrosion due to its role in raising gap gas temperature and by extension, gap conductance. The uncertainty of later states with closed gaps stemmed from cladding inner radius, fuel swelling, and cladding creep due to their effect on gap interfacial pressure.

LOTUS was also used to perform the first known higher order SA for an integration of VERA-CS and BISON. SA Results were similar for MDNBR and MFCT. GCPP results differed due to the inclusion of fuel and cladding roughness in the input perturbations, both of which were impactful inputs for states contains closed gaps in the Monte Carlo sampling.

GCPP results also showed differences in the relative magnitude of SA measures for biasing of specific calculations (i.e. fission gas release coefficients).

The LOTUS environment has also been extended to conduct the first UQ of peak cladding temperature ratio (PCTR) and equivalent cladding reacted ratio (ECRR) from an integration of PHISICS, FRAPCON, and RELAP5-3D for a transient LB-LOCA case. UQ results revealed the threshold nature of ECRR, thus highlighting the need for the 95/95 confidence values. Furthermore, PCTR and especially ECRR required fuel performance and system analysis for each assembly in the core for proper analysis, thus establishing the benefits of multiphysics simulations.

The incorporation of HDF5 databases within the LOTUS structure in this research shows promise for streamlining future integrations and enhancing post processing analysis. This foundation will provide a flexible plug-and-play environment allowing for MP-BEPU methodology to be applied to a variety of safety metrics, thereby allowing for potential decreases in operational margins. LOTUS also shows potential for being a highly adaptable and informative tool for the simulation of new fuel design concepts.

In regards to future work, this work serves as part of the foundation of the LOTUS multihpysics environment developed at INL. Valuable insights have been gained, but LOTUS is still in its infancy, with the promise of exciting new integrations, couplings, and analysis capabilities to be implemented in the near future.

APPENDICES

APPENDIX A

Permission from Coauthors to Use Work in Dissertation

Permission to Use Journal Articles in Dissertation Inbox x

Blakely, Cole D <cole.blakely@inl.gov> Jun 28 (11 days ago)
to Hongbin

Hello Dr. Zhang,

In the interests of completing my doctorate at Utah State University I am submitting my dissertation which includes the following articles for which you are a coauthor:

1. Sensitivity Analysis of VERA-CS and FRAPCON Coupling in a Multiphysics Environment

2. Application of Regression, Variance, and Density Based Global Sensitivity Analysis Methods to Integrated VERA-CS and BISON Simulations

3. Demonstration of LOTUS Multiphysics BEPU Analysis Framework for LB-LOCA Simulations

May I have your permission to place said journal articles within my dissertation?

Thank you

Zhang, Hongbin Jun 28 (11 days ago)
to me

Yes

Fig. A.1: Permission from Dr. Hongbin Zhang to use Journal Articles in Dissertation.

Author is in a ongoing discussion with Rodolfo Vaghetto in regards to permission to use his work. Note that the article to which Rodolfo Vaghetto has contributed is in the review process and has yet to be published.

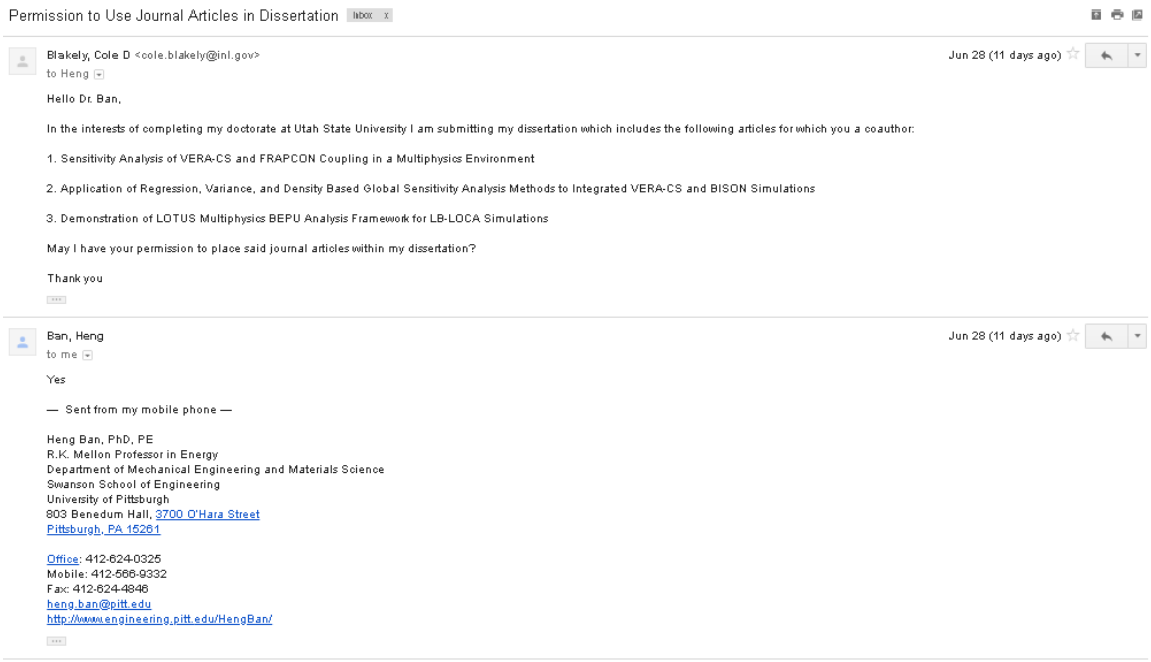

Fig. A.2: Permission from Dr. Heng Ban to use Journal Articles in Dissertation.

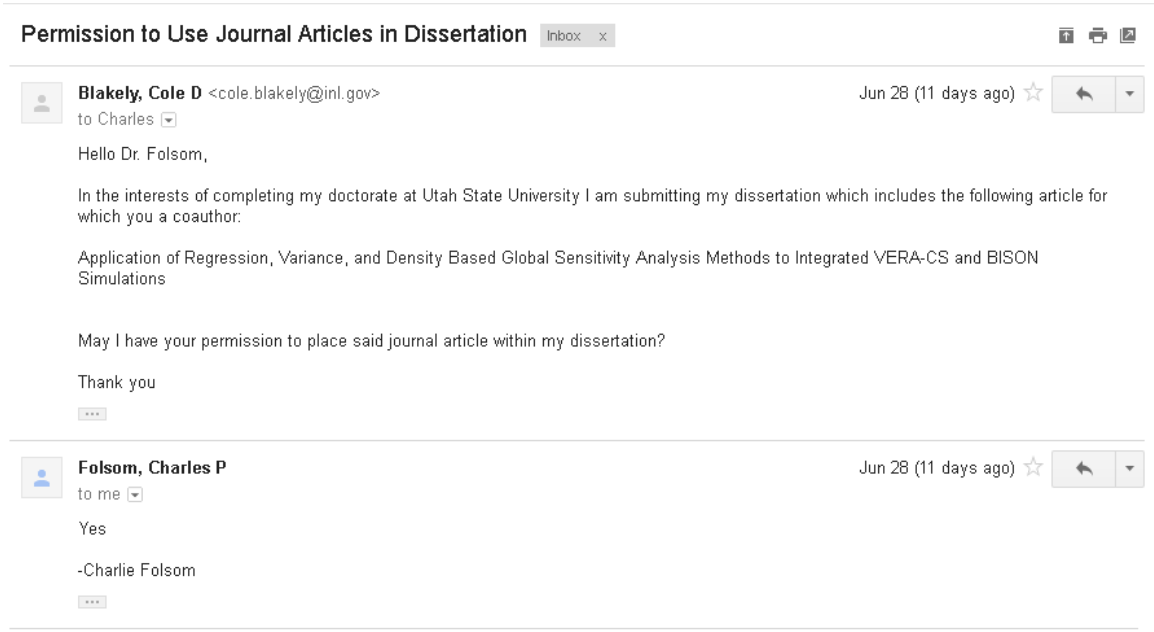

Fig. A.3: Permission from Dr. Charlie Folsom to use Journal Article in Dissertation.

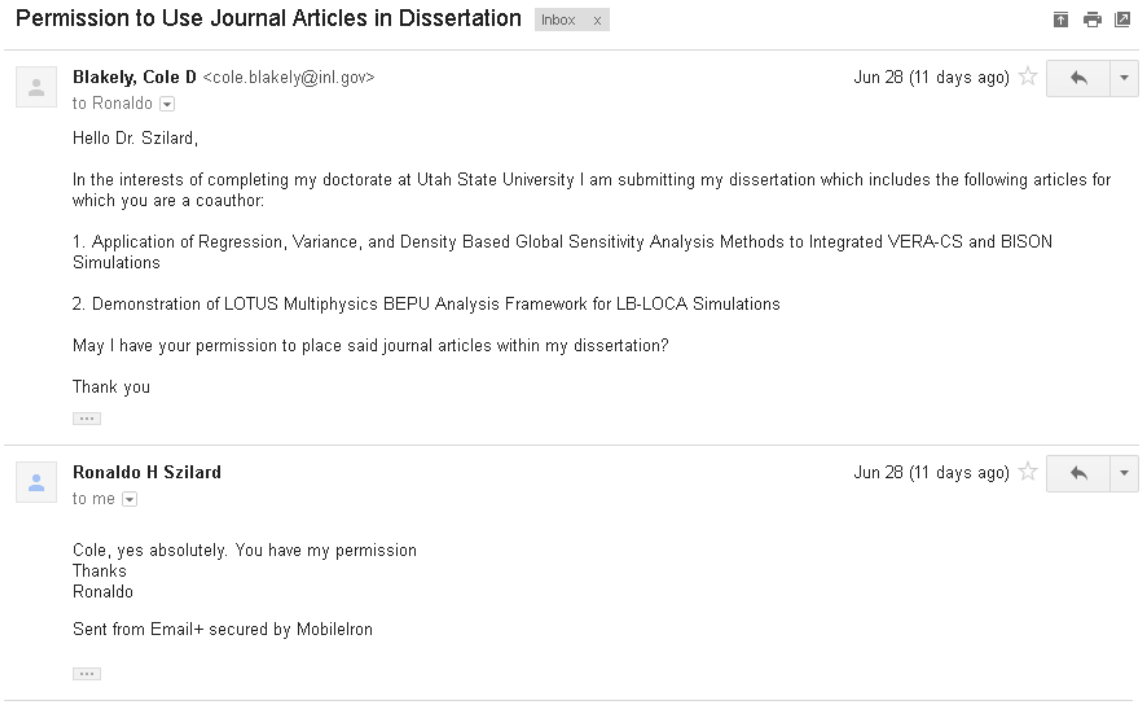

Permission to Use Journal Articles in Dissertation Inbox x

Blakely, Cole D <cole.blakely@inl.gov> Jun 28 (11 days ago)
to Ronaldo

Hello Dr. Szilard,

In the interests of completing my doctorate at Utah State University I am submitting my dissertation which includes the following articles for which you are a coauthor:

1. Application of Regression, Variance, and Density Based Global Sensitivity Analysis Methods to Integrated VERA-CS and BISON Simulations

2. Demonstration of LOTUS Multiphysics BEPU Analysis Framework for LB-LOCA Simulations

May I have your permission to place said journal articles within my dissertation?

Thank you

Ronaldo H Szilard Jun 28 (11 days ago)
to me

Cole, yes absolutely. You have my permission
Thanks
Ronaldo

Sent from Email+ secured by MobileIron

Fig. A.4: Permission from Dr. Ronaldo Szilard to use Journal Articles in Dissertation.

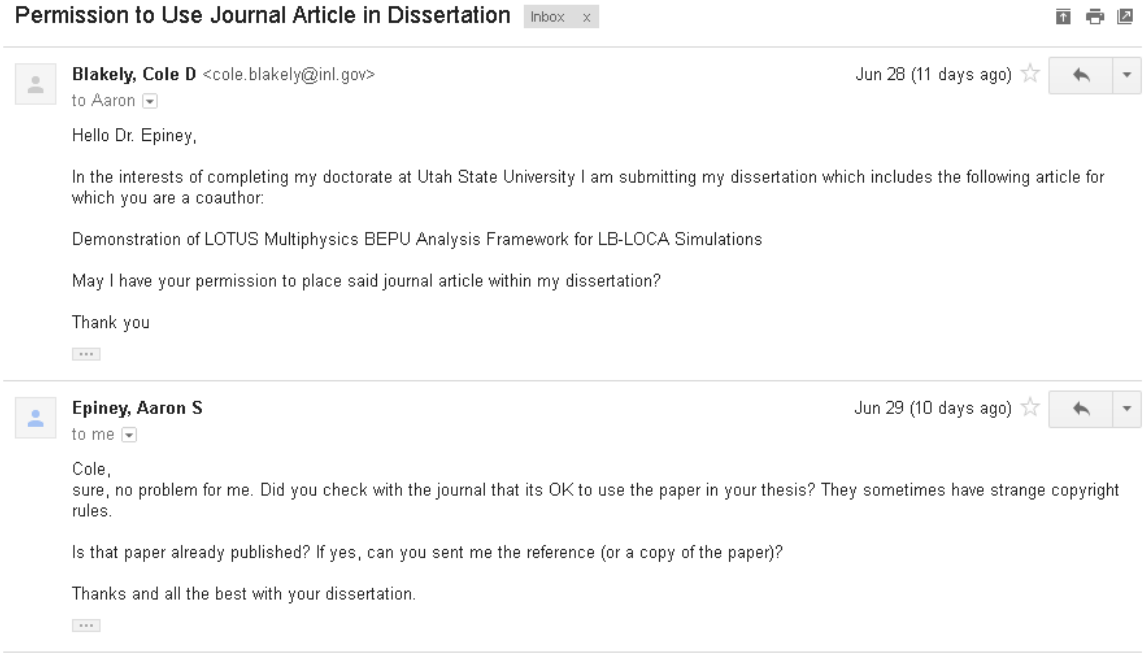

Permission to Use Journal Article in Dissertation Inbox x

Blakely, Cole D <cole.blakely@inl.gov> Jun 28 (11 days ago)
to Aaron

Hello Dr. Epiney,

In the interests of completing my doctorate at Utah State University I am submitting my dissertation which includes the following article for which you are a coauthor:

Demonstration of LOTUS Multiphysics BEPU Analysis Framework for LB-LOCA Simulations

May I have your permission to place said journal article within my dissertation?

Thank you

Epiney, Aaron S Jun 29 (10 days ago)
to me

Cole,
sure, no problem for me. Did you check with the journal that its OK to use the paper in your thesis? They sometimes have strange copyright rules.

Is that paper already published? If yes, can you sent me the reference (or a copy of the paper)?

Thanks and all the best with your dissertation.

Fig. A.5: Permission from Aaron Epiney to use Journal Article in Dissertation.

CURRICULUM VITAE

Cole Blakely

Journal Articles

- Multiphysics Environment, Uncertainty Quantification, Sensitivity Analysis, VERA-CS, FRAPCON, Cole Blakely and Hongbin Zhang and Heng Ban, *Annals of Nuclear Energy*, vol. 111, pp. 683 - 701.
- Application of Regression, Variance, and Density based Global Sensitivity Methods to Integrated VERA-CS and BISON Simulations, Cole Blakely, Hongbin Zhang, Charlie Folsom, Heng Ban, and Ronaldo Szilard, *Nuclear Engineering and Design*, vol. 332, pp. 186-201. 2002.
- Demonstration of LOTUS Multiphysics BEPU Analysis Framework for LB-LOCA Simulations, *Annals of Nuclear Energy*, *Submitted April 2018*.

Published Conference Papers

- Uncertainty Quantification and Sensitivity Analysis for Coupled VERA-CS and FRAPCON, Cole Blakely, Heng Ban, and Hongbin Zhang, in *Transactions of the American Nuclear Society, Vol. 116, San Francisco, California*, June 1115, 2017.
- Comparative Studies of Sensitivity Analyses for Coupled VERA-CS/FRAPCON and VERA-CS /BISONSimulations, Hongbin Zhang (INL) and Cole Blakely, *Proc. ICAPP*, April 8, 2018.
- High-Order Strand Grid Methods for Multi-species Reacting Flow, Cole Blakely, Oisin Tong, and Aaron Katz, *Proc. American Institute of Aeronautics and Astronautics Conference*, June 13-17 2016.

- Optimizing Vertical Mixing In Algal Raceways using Delta Wings, Cole Blakely, Justin Hunt, Jason Quinn, and Byard Wood *Algae Biomass Conference*, Sept. 29 -Oct. 2014.